SIMULATION OF THE EFFECT OF ATRIOVENTRICULAR BLOCK ON LEFT VENTRICULAR PERFORMANCE.

By

Stephen Jakuma Ojaj

A thesis presented to

Centre of Biomedical Engineering

Addis Ababa Institute of Technology

Addis Ababa University

In partial fulfilment

of the Requirements for the Degree of Master of Science in

Biomedical Engineering (Bioinstrumentation and Imaging)

Supervised by:

Dawit Assefa Haile (PhD)

Biruk Abraham (MSc)

October 2021

Certificate of Examination

This is to certify that the Master of science (MSc) thesis prepared by Jakuma Stephen Ojaj entitled **"SIMULATION OF THE EFFECT OF ATRIOVENTRICULAR BLOCK ON LEFT VENTRICULAR PERFORMANCE"** submitted in partial fulfillment of the requirement for the degree of Master of Science in Biomedical Engineering (Bioinstrumentation and Imaging) complies with regulation of the University and meets the accepted standards with respect to originality and quality.

Signed by the examining committee:

Examiner……Signature…….

Examiner……Signature…….

Chairperson……Signature…….

Advisor……Signature…….

Co-advisor……Signature……

……..

Chief of Department of Graduate program Coordinator

Declaration

I hereby declare that the work which is presented in this thesis entitled 'Simulation of the effect of Atrio-ventricular Block on Left Ventricular contraction' is an original piece of my own work, has not been presented for a degree in any other university; and that all sources of material used for the thesis have been acknowledged.

Candidate's name: **Jakuma Stephen Ojaj**

Signature: ……...Date: ……

This is to certify that the above declaration made by the candidate is correct to the best of my knowledge.

Supervisor's name: **Dawit Assefa Haile (PhD)**

Signature: ...……...Date: …….

Co-supervisor's name: **Biruk Abraham (MSc)**

Signature: ……Date: ……

Abstract

With the growing interests in multiscale computation studies in different fields in recent decades, its application in the biomedical field has been of great importance specially to analyse, process, design and diagnose different biological activities at both microscopic and macroscopic levels. This has resulted into improvement in medical technologies and disease management. Despite the continued efforts to improve computational interventions in biomedical studies, little has been done to understand the cardiovascular system (heart) in terms of its electrical behaviour in relation to its mechanical responses. This gap in computational knowledge especially in normal cardiac physiology and pathological conditions presents a problem to be tackled in order to improve diagnosis, and treatment of different cardio pathological conditions. This thesis investigates the effects of AVN block on left ventricular performance via an electromechanical coupled setup.

The cardiac electromechanical properties work on the principles that the electrical impulses from Sinoatrial node (SAN) in the atria via the AVN convey to the ventricles causing mechanical contraction and hence pumping of the blood. A 3D left ventricular model was developed on SOLIDWORKS and imported into COMSOL Multiphysics. Furthermore, through simulation using finite element (FE) analysis software COMSOL Multiphysics, a parametric study was performed on the effect of atrioventricular block on left ventricular function.

Based on the data adopted, the effects of varying the current stimulus as parameter were noted and discussed. From our model, observable and quantitative results were derived. The results obtained in this thesis allow the drawing of essential conclusions with regards to the left ventricular mechanical response to degrees of atrioventricular blockage which are essential to further computational studies. Also, in the simplified ventricular model the orthotropic nature of the myocardium, fiber orientations, and fluid mechanics were considered. The transmembrane chemical effects such as calcium handling, potassium, sodium concentration in the cytoplasm and mechano-electrical feed-back were neglected. The perturbations of the electrical impulses for the three AVN block cases resulted into variations in action potential durations (APDs). The variations were also noted on the myocardial voltage dependent stress during the simulations. Conclusively, the LV mechanical function was greatly affected by the variations of impulse stimulus due to AVN blockage.

Keywords: Heart tissue, Electromechanical model, Heart modeling, Heart diseases, COMSOL Multiphysics.

Acknowledgement

I would like to give thanks to God the Almighty for His unconditional favour towards me all my life. I am grateful to the African Biomedical Engineering Mobility (ABEM) Scheme in conjunction with Addis Ababa University for providing me with the scholarship for my MSc study. Appreciation to my advisors Dawit Assefa (PhD) and Biruk Abraham (MSc) for giving me an opportunity to work under their guidance to the accomplishment of this thesis by sharing their knowledge and experience with me. Without them, this thesis wouldn't be completed. Special thanks go to the Addis Ababa University and Centre of Biomedical Engineering lecturers for all the help rendered for the accomplishment of this MSc and this research in particular. I would also like to express my gratitude to my course mates and friends namely: Alex Favour, Agoreyo Sharon, Wafa Mohammed, Entwalu Emma, Wacoo Paul Alex, who have been believing in me and encouraging me to follow my dreams and aiding me in this research through time-to-time discussions that opened my mind to understand the subject matter. Finally, I would like to thank my lovely family who were always there standing by me through the good and bad times.

TABLE OF CONTENTS

List of Figures

List of tables

Nomenclature

Term	Meaning
Ach	Acetylcholine
APD	Action potential duration
AVN	Atrioventricular Node
Ca^{2+}	Calcium
CAD	Coronary Artery Disease
CHF	Congestive Heart Failure
CT	Computer Tomography
CVD	Cardiovascular disease
CVS	Cardiovascular system
DT-MRI	Diffusion Tensor Magnetic Resonance Imaging
ECG	Echocardiography
ECM	Extracellular Matrix
EDV	End Diastolic Volume
GB	Gigabytes
K^+, Na^+	Potassium, Sodium
LV	Left Ventricle
MRI	Magnetic Resonance Imaging
NE	Norepinephrine

Term	Meaning
PCG	Phonocardiogram
PDEs	Partial Differential Equations
RA	Right Atrium
RAM	Random Accessory Memory
SAN	Sinoatrial Node
SCD	Sudden cardiac death
SV	Stroke Volume
WHO	World Health Organization
3D	3 Dimensions

CHAPTER ONE

INTRODUCTION

1.1 Background

Cardiovascular diseases (CVDs) are a group of disorders of the heart and blood vessels and have been on increase worldwide in recent decades, with more deaths reported yearly across the whole globe as per report by the World Health Organization (WHO) in 2019, cardiovascular related conditions are number 1 cause of global deaths. This estimates 17.9 million deaths, hence making CVDs the highest predisposing factor among both communicable and non-communicable patients. Most of the deaths are sudden cardiac deaths which occur within a short period of time. Despite of a statistical decline in sudden cardiac deaths from the 1980s, it's still a health threat especially due to coronary heart diseases. Developing countries contribute to nearly three quarters of global CVDs deaths. Poor integrated health care programs in developing nations for early diagnosis and treatment of population with risk factors are the main contributing factors to the rise in these statistics compared to those in developed countries [1] [2]. Figure 1-1 illustrates the global burden of CVDs across time, location, cause and risk factors from 1990/2010 and 2019.

Sudden cardiac death being untimely in occurrence makes it 40% unpredictable hence posing a challenge in its clinical classification. Thus, the development of improved diagnose and treatment procedures thereof is of utmost importance. This, in turn, requires a better understanding of the actual functioning of the heart. Current experimental methods of studying the activity of the heart are often too invasive. For example, an electrophysiology study involves the percutaneous introduction of electrode catheters. Unsuitable catheters may lead to punctures in the wall tissue which could lead to internal bleedings. The procedure might also stimulate severe rhythm problems and may, rarely, cause the perforation of the heart. On the other hand, less invasive procedures do not provide the same level of detail. For instance, in electrocardiograms, the solution of an inverse problem is necessary in order to determine the actual activity of the heart [3],[4].

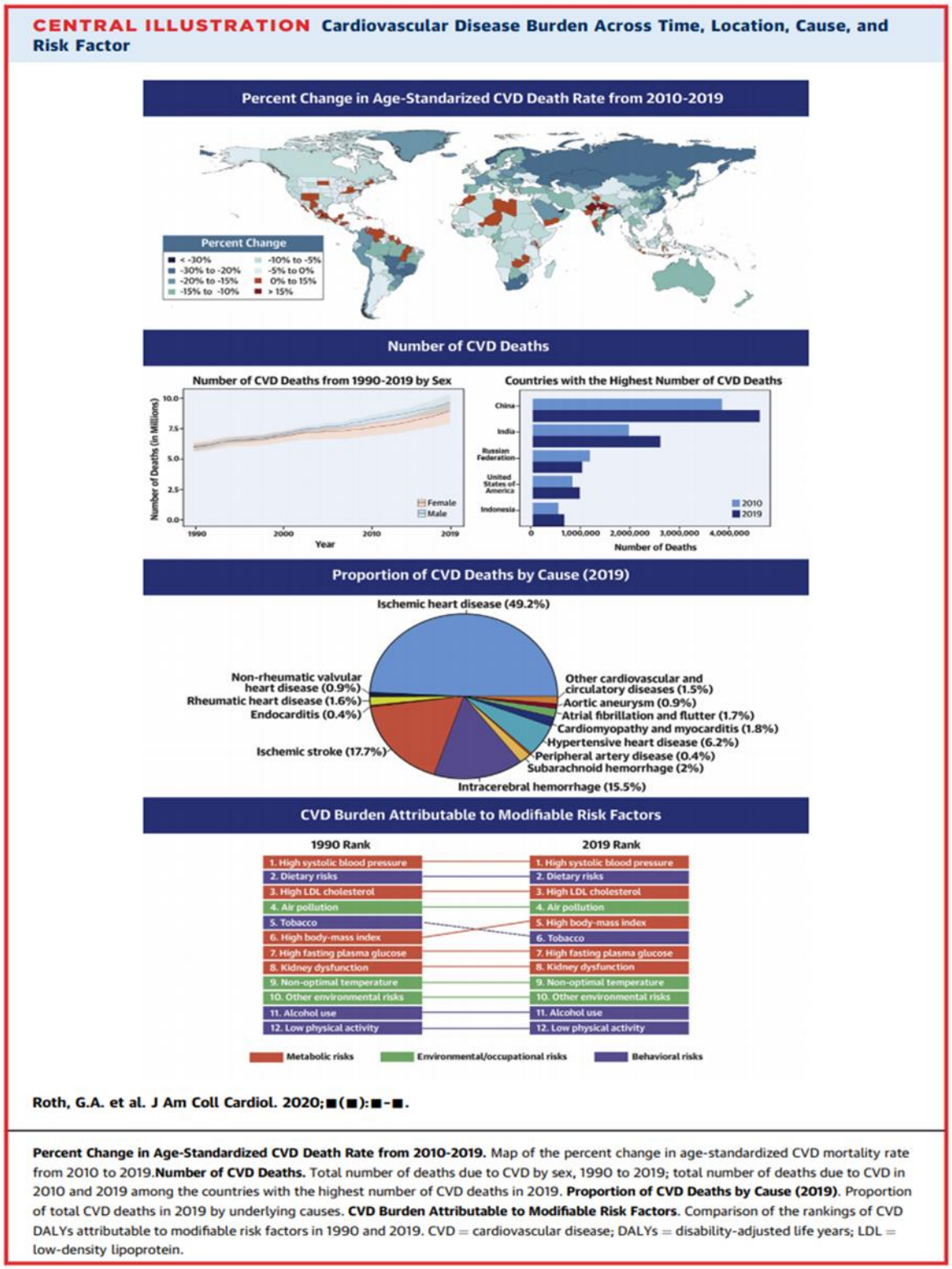

Figure 1-1: Global cardiovascular burden [5].

Cardiac MRI is recently taken as a novel “gold standard” in detecting warning signals of blockage in the heart by looking at both the structure and functioning of the heart. Cardiac MRI produces extremely detailed images and are regarded as superior in quality to ECG.

CVDs patients with low to moderate risk are being diagnosed using cardiac CT scan called cardiac calcium-score screening scan.

This is due to its ability to effectively find calcium deposits in plague of these patients resulting into early spotting of atherosclerosis prior to development of the symptoms. Increased coronary calcium levels indicate higher risk of CVDs in future.

Phonocardiogram (PCG) records the mechanical activity of the heart by digital stethoscope as a high-fidelity plot. The PCG signals are sound vibrations generated from the valves closure. PCG is a comparatively a novel metric in classifying and localizing the cardiac sounds. Different methods have been adopted in analyzing the PCG signals such as filtering, denoising, classification, feature extraction and, transform-based algorithm [6],[7],[8].

A mathematical model would help determine important physiological parameters by applying realistic physical constraints to the inverse problem. Computational models would not pose risks to the patients. Moreover, they are not subject to the ethics procedures that would be required for performing experiments on either people or animals. Additionally, even when experimental studies are carried out, they never provide measurements for all the functional elements of the heart. Computer simulations would help both in simulating unavailable events and also in understanding better the data acquired [9], [10].

The understanding of normal and pathophysiology of a system or an organ requires deep knowledge of interactions between organ structures and functions. With new measurement techniques, more data is available to describe the myocardium mathematical properties and this can be applied in simulating the myocardium behaviour. This has further been simplified and accelerated by improvements in computation capabilities lately where complex systems can be studied using simple models to predict tissue responses.

The rhythmic cardiac mechanical deformation is sustained by electrical impulses passing through the myocardium originating at cell level. The spread of the electrical activation on the cardiac muscle controls the myocardium contraction. Therefore, any alteration in the electrical conduction rhythm (atrioventricular block) can result in abnormality in myocardium contraction hence leading

to reduced contraction force and cardiac output. The block or delay is termed physiological if it originates from abnormally fast atrial rates or can be pathological when the atrial rates are normal. AV block is generally defined based on a regular atrial rhythm. Alteration in the cardiac electrical activity manifests due to numerous conditions and can result in death. As stated previously, several medical machines and methods are being developed by researchers to better understand the physiological dynamics of the heart in order to model it and further understand both the normal and diseased organ behaviours.

ECG parameters are also associated with an adverse outcome in cardiovascular disorders. First or second-degree atrioventricular (AV) block has been shown to be an independent risk factor in idiopathic dilated cardiomyopathy, particularly in combination with either reduced LVEF or frequent ventricular couplets [11]. Shamim et al [12] showed an increase in all cases caused mortality with progressive increase in the duration of the QRS complex. QRS duration was an independent variable on multivariate analysis, as were LVEF and peak oxygen consumption. Furthermore in 2002 this group demonstrated that the relative change in QRS duration over time was a more sensitive prognostic indicator than absolute values of QRS duration [13]. This correlated with echocardiographic markers of deterioration of ventricular systolic function and increased LV filling pressures. The PR interval was also significantly longer in non-survivors than in survivors. Therefore, there is a close relationship between electrical and haemodynamic components of cardiac function and clinical outcome.

Conduction delays are present in approximately 50% of patients with CHF [15] . Atrioventricular and intraventricular conduction delay produce adverse haemodynamic effects by their impact on AV synchrony and left ventricular contraction/relaxation respectively. A long PR interval predisposes to pre-systolic mitral regurgitation [16]. Multisite biventricular pacing techniques (also known as cardiac resynchronisation therapy (CRT)) improve cardiac function by synchronising ventricular contraction and relaxation [17]. Systolic function of the LV can be improved by preload optimisation by correct timing of AV delay[18]. Breithardt et al [19] demonstrated that optimum cardiac index and Doppler indices of LV filling occurred at AV delays between 80 and 120ms in patients with NYHA Class III-IV CHF. Thus, maximum improvement in LV performance requires both resynchronisation of AV conduction and optimisation of AV delay.

The models interplay between the myocardium anatomy and physiology have four organization levels: organ, tissue, cellular and molecular levels hence multiscale modeling [20]. The myocardium models attempt to demonstrate the myocardial electrical activation or the myocardial mechanics independently or coupling the electrical activation and the mechanical response of the myocardium via electromechanical activation at cellular and tissue level of integration, also known as multiscale cardiac modeling [10], [21].

Rapid electrical activation in the myocytes is due to the presence of gap junctions in the myocardium that in turn affects the ventricular ejection fraction. Electromechanical coupling has been used to narrow between cellular and tissue level models. Computing an activation impulse wavefront through a tissue block can be adopted in modeling different myocardial areas [22].

Cell to organ modeling of the cardiac electrical activity is paramount clinically since the first cardiac physiological assessment is at body surface due to organ to body modeling [7], [20].

The dynamic propagation can be represented by displaying an iso-surface of the transmembrane potential value. The complete propagation can be shown with the isochrones, where colors represent the different depolarization times [23][24]. To model the macroscopic characteristics of the myocardium, Aliev-Panfilov modification to the FitzHugh-Nagumo model is used which is also a reaction- diffusion based model, which represents a more realistic pattern of the cardiac action potential using spatial, temporal and fiber orientation parameters [25].

Complex interaction between pathophysiology and abnormal tissue structures that lead to arrhythmias can be studied using computation modeling tools. These computer-based models are very powerful in detecting various arrhythmic types ranging from ectopic beats to lethal fibrillation of the ventricles [3]. These could be due to overload of Na^{+} and Ca^{2+} at cellular level leading to metabolic changes, hence causing abnormal depolarization due to hyper influx of calcium in the cytoplasm. Re-entry is a major myocardial action potential conduction disorder that can lead to tachycardia and fibrillation. It causes continuous refractory tissue excitation as the action potential circulates. The occurrence of the re-entry is seen when a closed pathway of greater length than the product of the action potential duration (APD) and with existence of tissue conduction velocity. Few studies have been reported on re-entry using 3D computational models compared to the 2D [21].

Various cardiac disorders such as bundle branch block and, atrioventricular node (AVN) blocks can be simulated using the finite element based computational model by slight perturbation in the impulse conduction system. Reduced amplitude of action potential and conduction velocity within the myocardium causes myocardial infarction or ischemia [26]. The outcome of cardiac computational modeling is dependent on various tissue parameters, and one of the basic factors is the fiber orientation which is paramount in modeling electrical and mechanical properties of the myocardium. Personalized models demand for in vivo fiber direction measurements which is often inapplicable in humans due to invasive requirements. In recent years, a non-invasive technique of measuring myocardial fiber orientation has been invented using the diffusion tensor magnetic resonance imaging (DTMRI) [27],[28],[26].

The results from the animal experiment, cadaveric studies and MRI can be used to determine the direction of fibers in the myocardium [29]. Those studies show that the fiber directions in the left and right ventricular free wall, typically varies from -60^{o} at the epicardium to $+90^{o}$ at the endocardium, and a -90^{o} fiber angle is reported at the septal wall of inner surface of the right ventricle and $+80^{o}$ in the left ventricle [30].

Myocardial fiber orientation was considered in anatomical model design allowing the capture of anisotropic electromechanical behavior of the myocardium. Three structural axes can be located at any node on the wall of the ventricular models namely: fiber direction axes, axes perpendicular to myocardial fiber direction and lastly axes normal to the myocardial layer [10].

Tissue fibrosis within the myocardium greatly affects mechanical models both at cellular and macroscopic levels as the deformation tends to be unidirectional to fiber direction. The myocytes are responsible for contraction force development in the myocardium through sarcoma stretch and cytosolic calcium concentration. These parameters in addition to the excitation potential duration and excitation current are the major input values for cardiac modeling [31],[32],[33].

Modeling the myocardial contraction requires incorporation of coupled electromechanics in the constitutive law. The myocardium's constitutive rule is challenging to implement considering the inclusion of both an active and passive element representing contraction and elastic cardiac mechanics respectively regulated by the transmembrane potential [24]. Myocardial force development model has been recently reported to have 14 state variables embedded with three units' interplay: troponin, actin-myosin, and tropomyosin [26].

The holistic cardiac modeling approach considers electromechanical model as a coupled problem where the electrical component is used for simulating the electrical excitation wave of propagation leading into myocardial mechanical activity due to active forces.

1.2 Problem Statement

The incidences of cardiovascular diseases are on the rise across the world making CVDs number 1 cause of global deaths among communicable and non-communicable patients as reported by WHO, 2019 [1],[2]. With the low-to-middle income countries having majority of these deaths, [34] people aged >70 years contributing >50% of the deaths [35]. Furthermore, Sub-Saharan Africa reported nearly 1 million cardiovascular related mortalities in 2013, this tends to create more burden on the economy worldwide [36].

Different medical devices are used to detect variations in electromechanical patterns between the normal and failing heart [6] in addition to biological experiments and clinical studies which have been used in the past decades to study cardiac disorders. However, these methods have had their drawbacks in term of cost, time, tissue damage, limited control and access to certain variables and their interactions and the measurements obtained from experiments are limited to ethical issues. These limitations render computer-based simulations as a great alternative due to its cost-effectiveness, ability to solve complex system interactions despite its challenges such as mathematical model simplification [27], [37]. Multiscale modeling has been adopted as a one of the major computational tools in studying several cardiac disorders such as bundle blocks, arrhythmias, cardiac fibrillation especially using 1D, 2D models, however limited or no 3D computational finite element simulations have been reported on the AVN block in regards to its contribution to the function of the left ventricle [21].

The AVN being the main electrical conveyor bridge from the upper heart chambers to the lower chambers for myocardial contraction presents a major health problem yet there are limited experimental and multiscale computation information concerning its pathophysiology [29],[21].

This thesis was intended to bridge the knowledge gap in AVN pathologies by parametric simulations of the effects of different degrees of atrioventricular blocks on the left ventricular function as a fully coupled problem between the electrical activation and the mechanical behavior.

1.3 Research Objectives

This research work focused on 3D computational modeling of the parametric atrioventricular block effects on heart performance with electrical activation and electromechanical coupling in the myocardium

Specific objectives are:

i.) Anisotropic representation of fiber orientation within cardiac tissue.
ii.) Electrical activation and electro-mechanical coupling of the myocardium
iii.) Simulation of the atrioventricular block effect and on the heart contraction.

Research Scope

This thesis consists of parametric simulation of the AVN block and, an explicit coupling scheme between the 3D solid mechanics governing Partial Differential Equations (PDEs) and the electrophysiological formulation was used and, finite element platform (COMSOL Multiphysics environment) is utilized to solve the governing equations.

1.4 Significance of the Study

The simulation results from this research can be useful and added to the existing academic knowledge on the subject and improve technical aspects of the current computational models and apply them to new series of data sets from different heart conditions which can be utilized in clinical settings as well help in planning surgery and further heart modelling such as the prediction of the effect of pharmacological compounds (drug study) on cardiac rhythm.

1.5 Thesis Organization

The rest of the thesis has been organized as follow: Chapter 2 presents the literature review on cardiac electrophysiology, mechanics and some governing equations. The research methodology is presented in Chapter 3. In Chapter 4, the results obtained from the study are presented. Chapter 5, has discussions and analysis based on the results obtained. Finally, in Chapter 6, conclusion, limitations and future recommendations are provided.

CHAPTER TWO

LITERATURE REVIEW

This thesis focuses on myocardial modelling at macroscopic level based on differential equations and laws of continuum that determine the heart excitation and propagation process coupled with its mechanical contraction.

2.1 The heart and Atrioventricular node

Cardiovascular system is a major system component in the body with the heart as the main organ. The main functions of this system in addition to the lymphatic system are transportation of oxygen, nutrients, metabolic wastes, regulation of the hormones, temperature, and protection against microbes, toxins, blood loss and as needed by the body cell. The blood is the transportation medium through which the necessary materials are distributed to other cells of the body via the vessels [38].

Alteration in the functionality of the heart can cause serious cardiac disorders ranging from arrhythmia to lethal fibrillation of the ventricles. All those functions make the heart vital and computer simulations are useful for investigating the complex interaction between abnormal structures and functions that underlay the development of cardiac arrhythmias.

2.1.1 Anatomy of the atrioventricular junction

The atrioventricular node is the only normal electrical connection between the atria and the ventricles. The node lies in the lower atrial septum within the Triangle of Koch, bound superiorly by the tendon of Todaro, laterally by the orifice of the coronary sinus and inferiorly by the attachment of the septal leaflet of the tricuspid valve (Figure 2-1). The AV node has a multi-layered structure. The most superficial layer is the transitional zone between fast conducting atrial muscle (A zone) and the region of the compact AV node (N zone). Action potentials from the transitional zone (AN cells) are similar in character to atrial action potentials. The mid-nodal region describes the “compact node” or nodal (N) zone, an area of slow conduction and slow action potential upstrokes (N-cells). The deepest layer is a transitional zone between the N zone and the His bundle and exhibits so called “NH (nodal-His)” action potentials [39],[40].

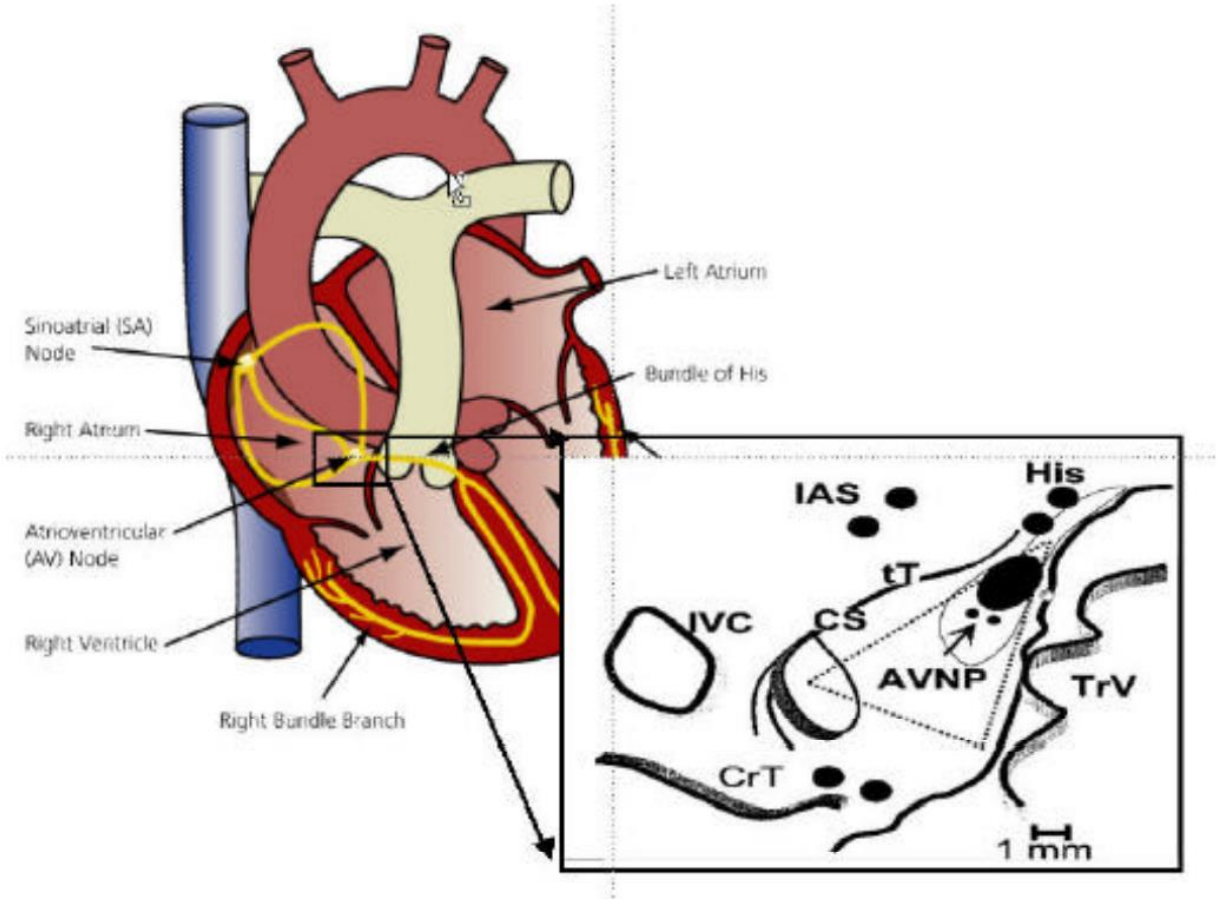

Figure 2-1: The Triangle of Koch. IAS – inter-atrial septum; IVC – inferior vena cava; CrT – Crista terminalis; tT – tendon of Todaro; TrV – tricuspid valve; CS – coronary sinus; His – His bundle; AVNP – AV nodal input pathways.

Anatomical and physiological studies of the AV node have been reported to indicating dual input pathways, providing the substrate for clinically important AV nodal re-entrant tachy-arrhythmias. This was first demonstrated in dog [41], where the authors observed an "echo" (non-stimulated) ventricular beat elicited when they delivered an appropriately timed ventricular premature beat to the heart. Further studies in human subjects some years later demonstrated similar finding. The findings in dog and human studies have been confirmed in studies of the rabbit AV node [42]. However, anatomical studies of humans with AV nodal re-entrant tachycardia or dual AV nodal pathways have shown that the AV node is structurally normal [43]. Therefore, dual AV nodal pathways are a functional rather than an anatomical problem, as demonstrated by Figure 2-2.

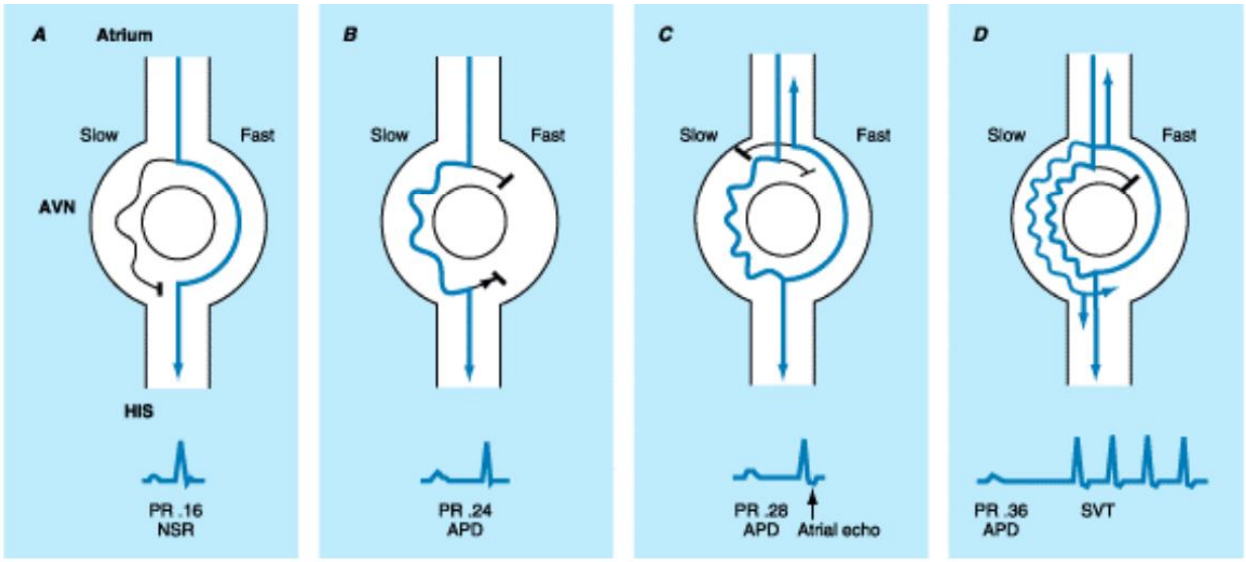

Figure 2-2: Dual AV nodal physiology.

The atrium, AV node (AVN), and His bundle are shown schematically. The AV node is longitudinally dissociated into two pathways, slow and fast, with different functional properties. In each panel of this diagram, blue lines denote excitation in the AV node, which is manifest on the surface electrocardiogram, while black lines denote conduction, which is concealed and not apparent on the surface electrocardiogram. A. During sinus rhythm (NSR) the impulse from the atrium conducts down both pathways. However, only conduction over the fast pathway is manifest on the surface ECG, producing a normal PR interval of 0.16 s. B. An atrial premature depolarization (APD) blocks in the fast pathway. The impulse conducts over the slow pathway to the His bundle and ventricles, producing a PR interval of 0.24 s. Because the impulse is premature, conduction over the slow pathway occurs more slowly than it would during sinus rhythm. C. A more premature atrial impulse blocks in the fast pathway, conducting with increased delay in the slow pathway, producing a PR interval of 0.28 s. The impulse conducts retrogradely up the fast pathway producing a single atrial echo. Sustained re-entry is prevented by subsequent block in the slow pathway. D. A still more premature atrial impulse blocks initially in the fast pathway, conducting over the slow pathway with increasing delay producing a PR interval of 0.36 s. Retrograde conduction occurs over the fast pathway and re-entry occurs, producing a sustained tachycardia (SVT). (Adapted from http://rezidentiat.3x.ro/)

2.2 Types of Atrioventricular block

Heart beats are controlled by the electrical impulses. The signals are conducted to the cardiac muscles to initiate contraction. The normal cardiac rhythm is generated from the SA node in the atria resulting into its contraction. The impulses are conveyed through to the ventricles, hence its contraction. When a heart block happens, the electrical conducting system from the upper chambers and lower chambers is interfered with, therefore leading to interference with ventricular contraction and slowing down the signals. The heart block can be categorized into three degrees, namely: first, second, and third.

- *First-degree AV block***.** This block condition is less severe though the impulses are slowed down as they travel from atria to ventricles un-interrupted. This type of block doesn't require medical treatment.
- *Second-degree AV block***.** In this case, the electrical conduction systems are intermittently interrupted as they travel between upper chambers and the lower chambers. Second-degree heart block is divided into two;
    - *Mobitz type I***.** Here the electrical conduction between the heart beats is slowed repeatedly.
    - *Mobitz type II***.** The conduction signals to the ventricles are on and off without progressive electrical delay. This type of AV block can lead to severe block.
- *Third-degree AVN block or complete cardiac block.* Full cardiac block is the most critical case of heart block. In this case there is no or little electrical conduction to the ventricles leading to severe slowing of impulse in presence of heart rate backup or no impulse [8].

The myocardial behavior can be studied in comparison to other muscles in the human body which comprise of smooth muscles, and skeletal muscles. Cardiac muscles have striated form and Z lines and also contain actin, tropomyosin and troponin proteins that are similar to those in skeletal muscles [44]. Unlike skeletal muscles, the myocytes have branched fibers. It has more mitochondria in the cells compared to other striated muscle cells but it has only one nucleus for each cell. The end of one muscle fiber lies adjacent to another fiber; those are connected to each other via gap junctions, which provide low-resistance bridges for the excitation propagation [38]. In Table 2.1, other properties of cardiac muscles are presented and compared to other muscle types.

Table 2-1 Comparison of structures and functions of different muscle types [44].

Structure/ Function	**Smooth muscle**	**Cardiac muscle (striated)**	**Skeletal muscle (striated)**
Motor end-plates	None	None	Yes
Fibers	Fusiform, short (-<0.2mm)	Branched	Cylindrical, long(-<15cm)
Mitochondria	Few	Many	Few (depending on muscle type)
Nucleus per fiber	1	1	Multiple
Sarcomeres	None	Yes, length -<2.6 μm	Yes, length -<3.65 μm
Electrical coupling	Some (single-unit type)	Yes, (functional syncytium)	No
Sarcoplasmic Reticulum	Little developed	Moderately developed	Highly developed
Calcium "switch"	Calmodulin/caldesmon	Troponin	Troponin
Pacemaker	Some spontaneous rhythmic activity ($1s^{-1}$–$1h^{-1}$)	Yes (Sinus nodes ca.$1s^{-1}$)	No (requires nerve stimulus)
Tetanizable	Yes	No	Yes
Work range	Length-force curve is variable	In rising length-force curve	At peak of length-force curve

Not only the muscle types but also the cardiac tissues themselves vary according to the function and spatial location of the cells. Different myocyte types in the heart are presented in Figure 2-3.

The gap junction orientation and density differ depending on the tissue. For example, the density of the gap junctions in the SA and AV nodes is less than the density in the ventricular myocardium [30]. Also, in the same tissue it differs in longitudinal orientation and transversal orientation. It can be said that density is larger in longitudinal direction. The average length of longitudinal gap junctions is smaller than the length of transversal gap junctions. Both circumstances lead to a macroscopic, anisotropic, electrical propagation. Response of the tissue to excitation also changes in those different cardiac cells; SA node, AV node, Purkinje fibers, and myocardial cells.

The main heart muscles consist of the myocardial cells. Those striated muscle cells also show anatomical and physiological differences due to anisotropy as also shown in the longitudinal and cross-sectional electron microscopy images shown in Figure 2-4.

Those longitudinal and cross-section images in Figure 2-4 represent cardiac muscle sheets. However, the anisotropy of the myocardium not only changes due to longitudinal and cross-sectional orientation of the cells. The anisotropy complexity begins with the embryonic heart tissue formation, when the heart begins to looping and bending on itself [45]. If the heart is unwrapped, the anisotropy of the tissue becomes more visible, which can be seen in Figure 2-5.

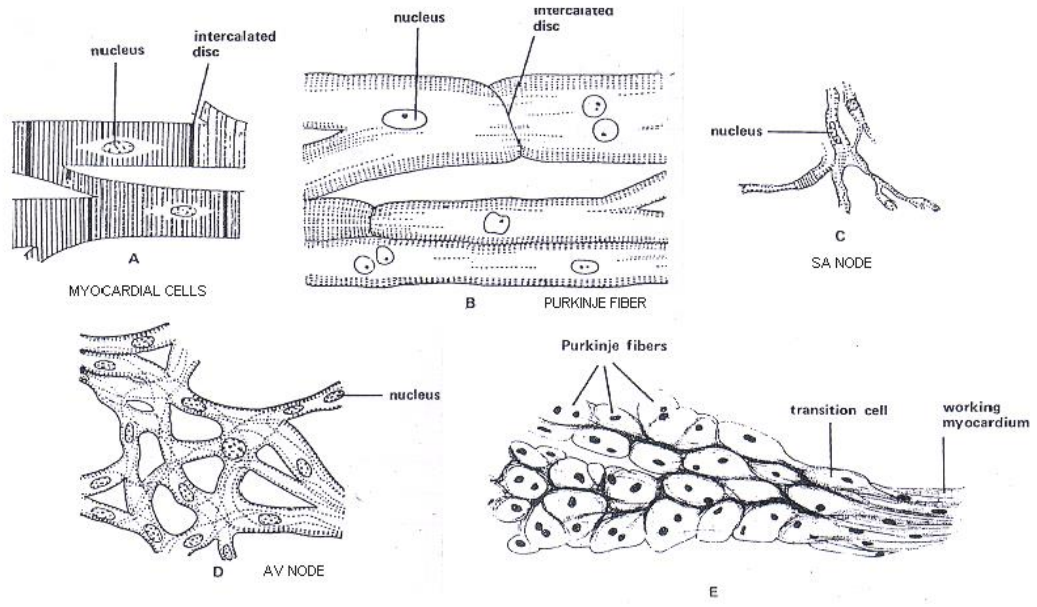

Figure 2-3: Illustrations of cardiac cells; (a) myocardial cells, (b) purkinje fibers, (c) SA node, (d) AV node, (e) transition cell [44].

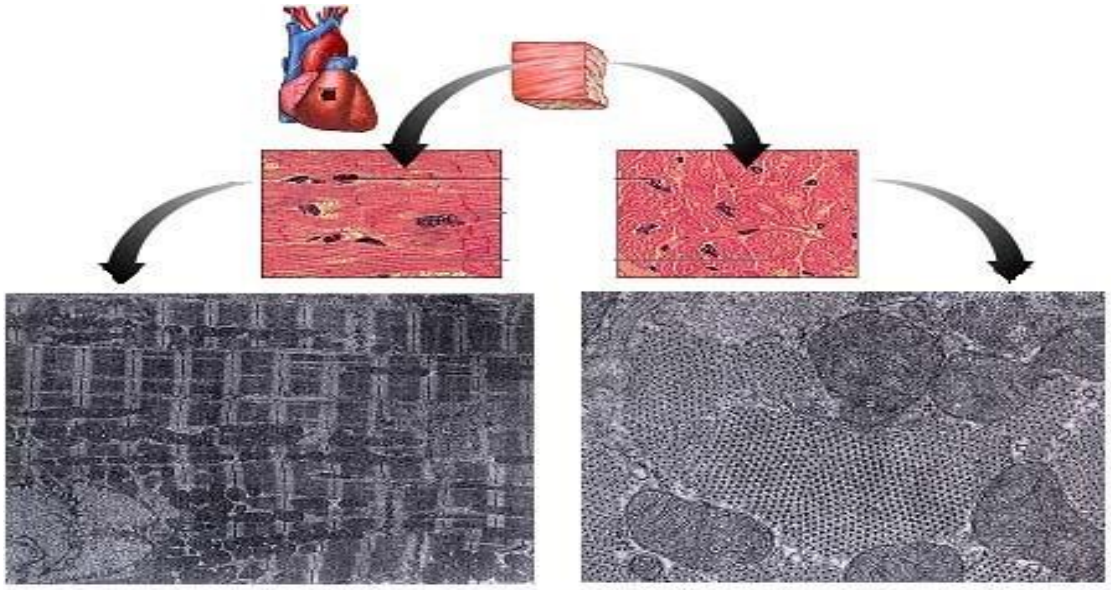

Figure 2-4: Human myocardium in longitudinal section (left) and cross section (right). Electron microphotograph of myocardial cells [44]

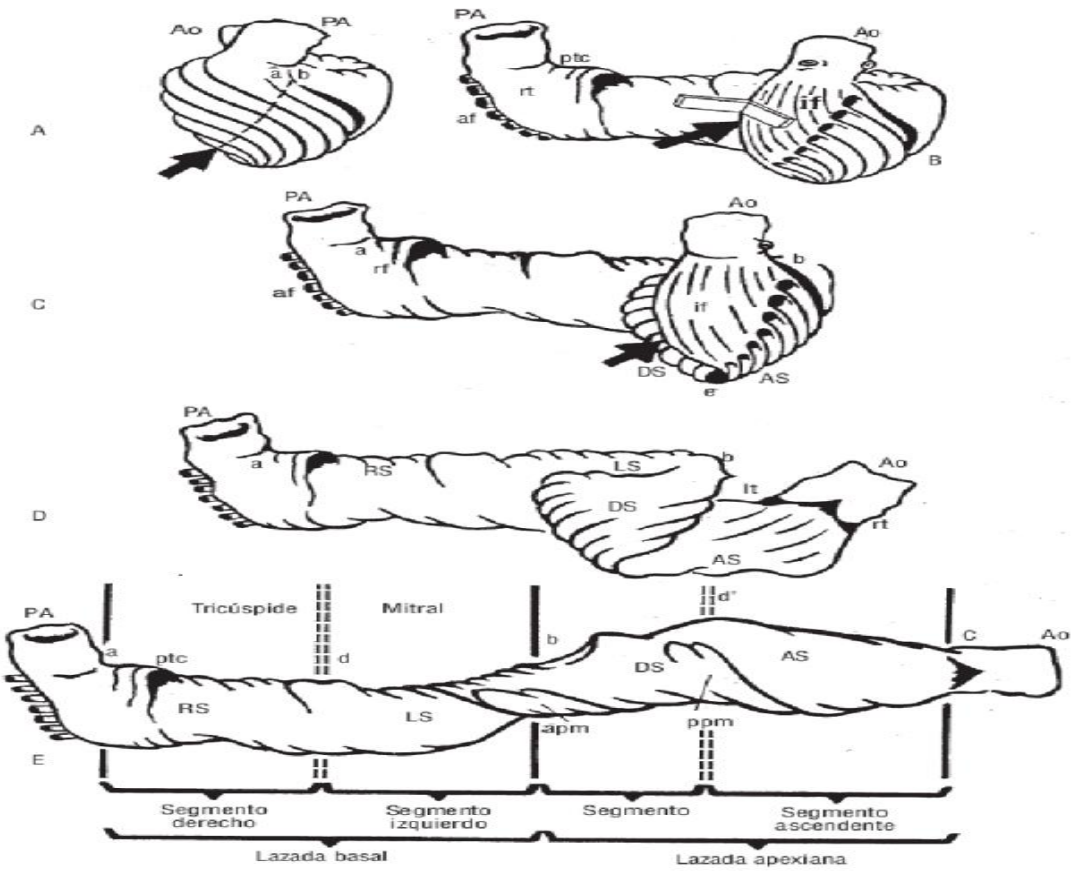

Figure 2-5 :Unwrapping the heart [46]

The fibers in the wall are not uniformly oriented throughout the wall. Instead, their orientation varies continuously so that stress and strain workload of the muscle fibers are homogeneous.

Some studies reported that a total fiber angle variation of 140 degrees from the outermost layer to the innermost layer of the heart [45]. The fiber orientation of the total heart tissue shows angular variation from endocardium to epicardium [20]. Figure 2-6 illustrates the fiber direction change in 100 μm width tissue for twenty separate sheets. Furthermore, fiber orientation, distribution of gap junctions and pathologies influence the activity of the heart, which leads to inhomogeneity in electromechanical properties of the heart.

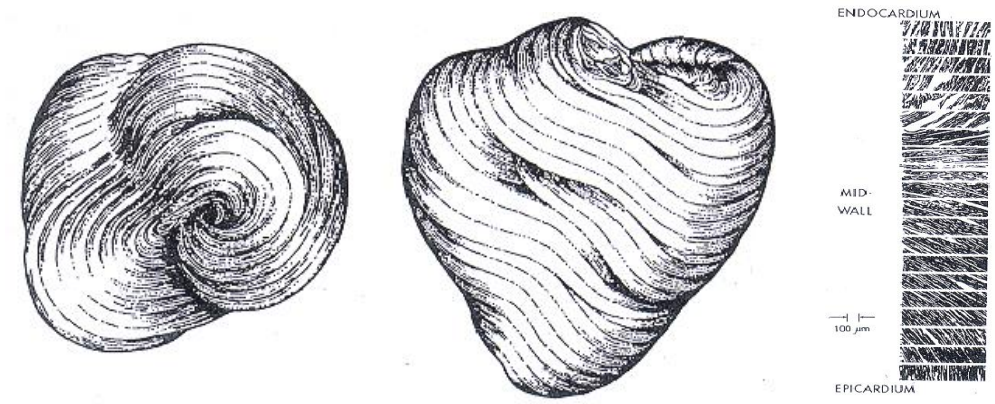

Figure 2-6: Fiber orientation distribution of the heart. View from apex, view from side and angular distribution from endocardium to epicardium [45].

2.3 Cardiac Physiology

The heart is subdivided into two halves by walls: interatrial and interventricular septa. Each of the septum controls one part of the circulatory system [38]. Basic diagram of cardiac and vascular system is illustrated in Figure 2-7. Both atria are blood filled and then contract simultaneously after which simultaneous contraction of the two ventricles follows, which pushes blood from the ventricles to the body and organs.

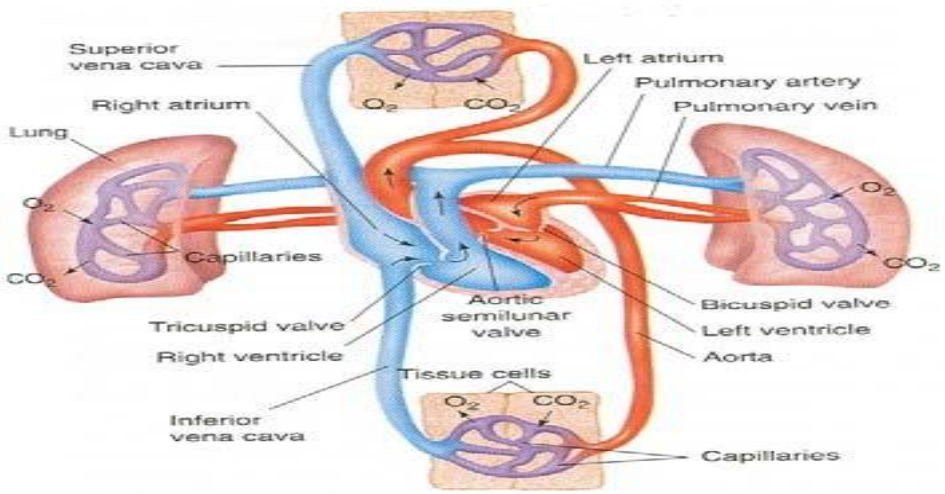

Figure 2-7: Circulation system diagram [38].

Blood is pumped from the LV to capillaries in the periphery via the arterial vessels of the systemic circulation and returns via the veins to the right heart. It is then expelled from the right lower chamber to the lungs via the pulmonary circulation and returns to the left heart [38].

Source of the pulmonary circulation is the right ventricle. The blood, which has low O_2 concentration, is pumped out of the right lower (ventricle) through pulmonary arteries and reaches the lungs where it will be oxygenated. Capillary blood absorbs oxygen from the air, while discharging carbon dioxide in the opposite direction. After this gas exchange, oxygen–rich blood reaches back to the left atrium of the heart through pulmonary veins [38].

Left lower chamber (ventricle) is the source of systemic circulation. The blood, which has oxygenated in the lungs, is pumped out of the left ventricle through the aorta, which is the largest and most elastic artery in the body and reaches to each living cell in the body. Oxygen, nitrites and hormones diffuse from the capillary blood to cells, and metabolic wastes are collected from cells

to blood. After this exchange, as a result of cellular respiration, the oxygen concentration of the blood decreases and carbon dioxide concentration increases in the blood. Through superior and inferior venae cavae the blood coming from organs will return to the right atrium of the heart [38].

The resting heart rate is 60–80 beats per minute. A cardiac cycle therefore, takes roughly 1 s. It's often categorized into four main phases:

a) Contraction phase
b) Ejection phase
c) Relaxation phase
d) Filling phase.

The contraction and ejection phases occur in systole while the relaxation and filling phases occur in diastole. The atria contract at the end of the filling phase. Electrical excitation of the atria and ventricles come before their contraction. The cardiac valves determine the direction of blood flow within the heart. All cardiac valves are closed during phases (a) and (c). Opening and closing of the valves is controlled by the pressures exerted on the two sides of the valves [38]

Near the end of ventricular diastole, the SA node emits an electrical impulse. This results in atrial contraction and is followed by ventricular excitation. The ventricular pressure then starts to rise until it exceeds the atrial pressure, causing the atrioventricular valves (mitral and tricuspid valves) to close, marking the end of diastole phase.

The mean end-diastolic volume (EDV) in the ventricle is now about 120 mL or, more precisely, 70 mL/m^2 body surface area. During the phase of isovolumetric contraction with all valves are closed, the ventricles now contract, producing the first heart sound, and the ventricular pressure increases rapidly. The semilunar valves (aortic and pulmonary valves) now open because left ventricular pressure exceeds that in the aorta at about 80 mmHg, and the right ventricular pressure exceeds that in the pulmonary artery at about 10 mmHg [38].

During the ejection period, the pressure in the left ventricle and aorta reaches a maximum systolic pressure (120 mmHg). In the early phase of ejection, a large portion of the stroke volume (SV) is rapidly ejected and the blood flow rate reaches a maximum. Myocardial excitation subsequently decreases and ventricular pressure decreases until it falls below that of the aorta or pulmonary artery, respectively. This leads to closing of the semilunar valves, producing the second hear

sound.

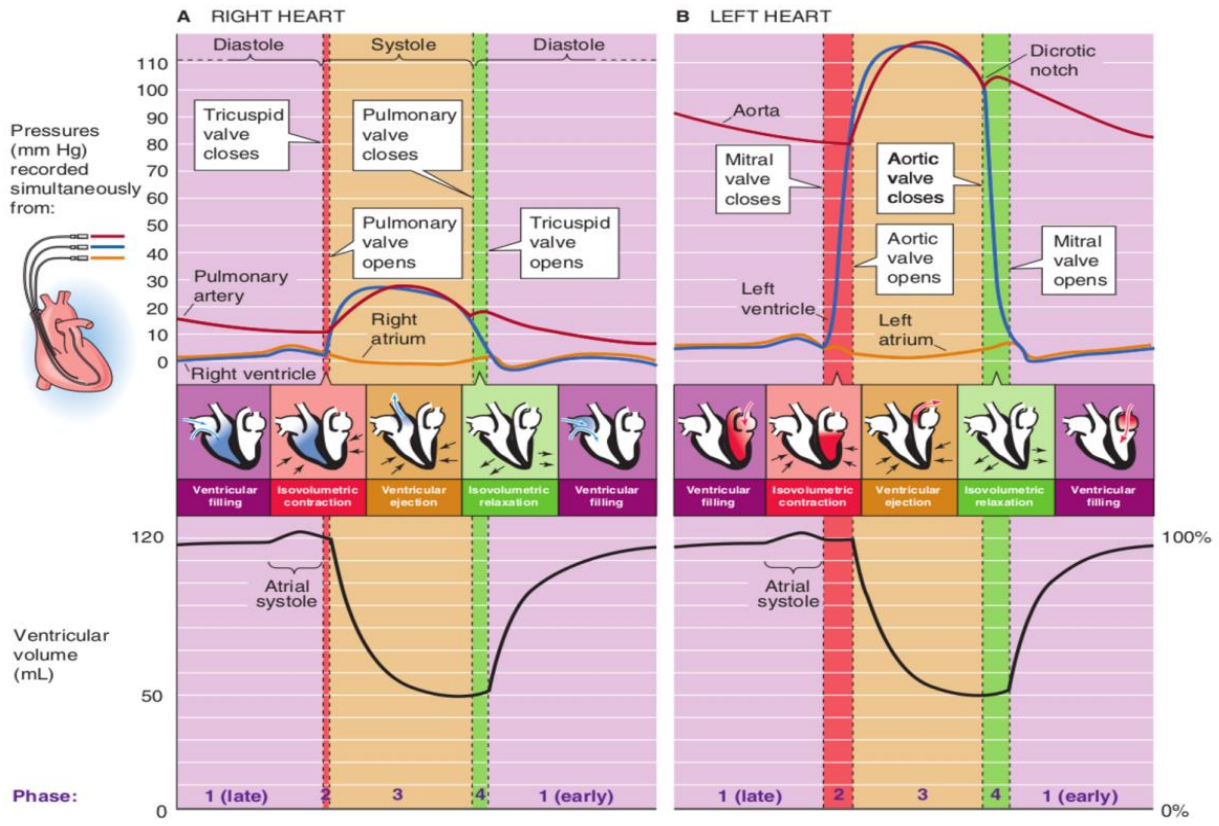

Figure 2-8 : Cardiac cycle (1) atrial systole, (2) isovolumetric ventricular contraction, (3) ventricular ejection, (4) isovolumetric ventricular relaxation, (5) ventricular filling [14].

In the first phase of ventricular diastole (isovolumetric relaxation), the atria have meanwhile refilled, mainly due to the suction effect created by the lowering of the valve plane during ejection. As a result, the central venous pressure decreases. The ventricular pressure now drops rapidly, causing the atrioventricular valves to open again when it falls short of atrial pressure.

The blood passes rapidly from the atria into the ventricles, resulting in a drop in central venous pressure at the filling phase. At a normal heart rate, the atrial contraction contributes about 15% to ventricular filling. When the heart beat increases, the cardiac cycle duration decreases mainly at the expense of diastole, and the contribution of atrial contraction to ventricular filling increases.

Pressure, volume and blood flow changes during the cardiac cycle can be followed from Figure 2-8. Duration of each cardiac cycle changes due to heart rate. The graph illustrated in Figure 2-9 shows the normal heart rate value which is taken as 75 beats per minute.

The amount of blood pumped out of each ventricle beat, is called stroke volume, and is about 80 mL in a resting man. The output of the heart in unit time is called cardiac output, which is approximately equal to 5.5 L/min in a resting man. Cardiac output can be affected by various conditions, which affect either the heart rate or the stroke volume, like excitement, exercise, drugs, and also arrhythmias, and heart diseases [14].

2.4 Cellular Electrophysiology of the AV node

Heterogeneity of ion channel and gap junction expression exists within the AV nodal architecture. Transitional cells of the AV node (AN and NH cells) have a relatively abundant sodium current (INa). There is a relative lack of expression of sodium channels in the ovoid type isolated cells (N cells), in which the main depolarising current is the L-type calcium current (ICa, L). This results in a relatively slow Phase 0 of the action potential and therefore a slow speed of conduction. In addition, there is an inwardly directed Na-Ca exchanger current (INa, Ca). Also, at potentials relevant to the diastolic potential during spontaneous activity in the majority of cells a small time-independent inward current is present (If). Some N cells also exhibit the dihydropyridine sensitive sustained inward current (Ist). There is generally no Phase 1 in nodal cells, and there is usually a very brief plateau phase. The main repolarising currents of the AVN are the transient outward K+ current (Ito) and the delayed rectifier K+ current (IKr). The cells of the sino-atrial and atrio-ventricular nodes have unstable resting potential unlike cells of the myocardium. Following repolarisation, the membrane potential undergoes spontaneous depolarisation (phase 4 depolarisation or the pacemaker potential). The interactions between the background current (Ib) and the delayed rectifier current (IKr) plus the hyperpolarisation activated (or “pacemaker” current), contribute to the generation of the pacemaker potential, and consequently to the automaticity of the N cells [47],[48].

Rate dependency of the action potential duration and effective refractory periods in isolated AV nodal and atrial cells

Rate-dependent periodicity has been demonstrated in single N cells isolated from the AV node as well as in intact node preparations [49]. Isolated AV nodal cells beat spontaneously at between 180 and 260 beats per minute (bpm) [50]. Repetitive stimulation of AV nodal cells at 300bpm results in a 1:1 response, but at rates of 480bpm, a 2:1 response is observed. At 400bpm, a progressive reduction in the Vmax of successive APs is observed, with subsequent increasing

latency. This results in failure of response to the 4th pulse and subsequent 3:2 response. This response is analogous to Wenckebach 2nd degree AV block in the intact heart. Atrial cells differ from AV nodal cells in that they sustain 1:1 activation even at pacing rates of 600 bpm. The effective refractory period (ERP) of the intact AV node lengthens at higher rates. AV nodal cells show significant shortening of ERP at low rates, but Workman et al found no effect on the ERP at higher rates[49], [50]. However, the exact region of the AV node from which the cells originated was not known and there is evidence of a differing contribution of different regions of the node to refractoriness.

2.5 Factors affecting conduction velocity through the AV node

Conduction through the AV node is relatively slow compared to conduction through the atria or ventricles, ensuring the sequential contraction of the atria followed by the ventricles. The AV node serves a protective function during arrhythmias such as atrial fibrillation by limiting the number of impulses transmitted to the ventricles. In contrast, the AV node plays a key role in the maintenance of other arrhythmias; for example, in supraventricular tachycardia the AV node is an integral part of the re-entrant conduction circuit.

i.) Ion channel conductance and membrane excitability. There are a number of determinants of conduction velocity. At the cellular level, conduction velocity is affected by the excitability of the cell membrane, i.e., by a reduction in K + conductance or by an increase in the current density of the depolarising current (Na+ or Ca2+) and by the degree of intercellular resistance [51].

ii.) Gap junctional channels Gap junctional channels (connexins) play a prominent role in AV conduction. The mammalian heart contains three main isoforms of gap junctional protein, namely connexins Cx43, 40 and 45. There is heterogeneous expression of all three isoforms within the tissue of the Triangle of Koch. Cx43 has a major role in cell-cell communication between ventricular and atrial myocytes. It has relatively low expression within the N region of the AV node, but is expressed more in the transitional zones (the AN and NH regions). The posterior nodal extension has been shown to have the lowest Cx43 mRNA and the most abundant HCN4 mRNA expression in keeping with its low conduction velocity and pacemaker activity [52]. Cx45 has been shown to be abundant in the compact node and both Cx40 and 45 in the NH region [53],[54].

iii.) Specific mutations in cardiac voltage gated ion channels. Recently mutations in the cardiac voltage gated Na+ channel Nav1.5 (SCN5A) have been associated with familial cases of AV conduction disorder [54]. Yoo et al [55] studied the expression of Na+ channel

isoforms at the AV junction in rat and found that Nav1.5 expression was abundant in atrial and ventricular myocardium and left bundle branch, reduced in the inferior nodal extension and transitional zone, but absent in the compact node and penetrating bundle. In contrast, Greener et al [52] studied the expression of Nav1.5 mRNA in rabbit AV junction and found it to be abundant in the compact node and penetrating bundle, but absent in the posterior nodal extension and the transitional region immediately adjacent to this. Despite these important species differences in the relative expression of Nav1.5 at the AV junction, mutations in or loss of this channel result in clinically important AV conduction disturbances and further research in human subjects is required to clarify the link.

iv.) Tissue architecture, macroscopically the architecture of the myocardial tissue may also determine conduction velocity. In 2001, Kucera et al [56] studied microscopic impulse propagation using multiple optical recordings of transmembrane voltage in conjunction with patterned growth cultures of neonatal rat ventricular myocytes. They observed a 70% reduction in conduction velocity by reducing excitability, but a 99% reduction by reducing electrical coupling (in the absence of structural discontinuities). Furthermore, they observed slowing of conduction velocities evoked by branching tissue geometries in the absence of electrical uncoupling. The conduction velocities observed in the latter were similar to those observed in the AV node. Histological sections of the AV node have demonstrated a highly complex tissue architecture consisting of numerous intermingled strands separated by connective tissue, and this may correlate with the prototype tissue structures used in the above cited study. Furthermore, in studies of aged hearts, micro fibrosis was found to result in a reduction in transverse conduction velocity in atrial and AV nodal tissues [57].

2.5.1 Autonomic modulation of AV nodal conduction

The AVN is richly innervated by the sympathetic and parasympathetic branches of the autonomic nervous system. There is reciprocal action of the two divisions of the autonomic nervous system, having different effects on the chronotropic, dromotropic and inotropic responses of the heart. Sympathetic innervation, Acetylcholine (ACh) is the predominant sympathetic preganglionic neurotransmitter; norepinephrine (NE) is the predominant post-ganglionic neurotransmitter. The arrival of an impulse at the nerve terminal in the AVN effects NE release, and this interacts with adrenergic receptors on the cardiac effector cell membrane. Increases in sympathetic activity raise intracellular levels of cyclic adenosine mono-phosphate (cAMP). This sets off a cascade of intracellular events culminating in changes in the conductivity of ion channels within AV nodal

conduction fibres. At rest, cardiac sympathetic activity occurs in rhythmic bursts synchronous with respiration. However, changes in heart rate and AV nodal conduction velocity do not follow the same pattern. The responses are slow, as are the recoveries of the responses to their basal level as a result of the slow removal and re-uptake of NE from the cardiac effector cell receptor and into the presynaptic nerve terminals respectively. AV conduction time depends on the interaction between the prevailing heart rate and the level of sympathetic tone, both of which exert opposite effects on AV conduction. If the heart rate is held constant by artificial pacing, sympathetic stimulation decreases AV conduction time. However, an increase in heart rate by atrial pacing prolongs AV conduction time.

Parasympathetic innervation, vagus nerve carries the efferent parasympathetic fibres to the heart. ACh is the predominant neurotransmitter released from both pre- and post-ganglionic vagus nerve terminals. The right vagus nerve has a much greater effect on AV conduction than the left. Vagal stimulation leads to reduction in the conduction velocity and prolongation of the refractory period of the AVN by hyperpolarisation of the AVN cell membrane and reduction of the amplitude and the upstroke velocity of the cardiac action potential (51;71). This results in prolongation of the AH interval by blocking conduction at the mid-nodal (N) and NH regions of the AVN. When the heart rate is held constant by atrial pacing vagal stimulation always prolongs the AV conduction time.

Other neural modulators of AV nodal function such as Adenosine are ubiquitous as it is involved in the metabolism and catabolism of adenosine tri-phosphate (ATP). ATP is packaged and co-released with ACh and NE, and serves as a source of adenosine to bind to cell membrane receptors and affect intracellular processes. Adenosine may signal conditions that are detrimental to the organism such as hypoxia. In hypoxia, adenosine reduces the myocardial oxygen demand by reducing sinus node automaticity and AV node conduction velocity. Furthermore, adenosine reduces AV nodal excitability by inactivation of ICa, L and activation of a time-dependent inwardly rectifying potassium current. The effects of adenosine may counteract the effects of adrenergic stimulation by inhibiting the activation of adenylyl cyclase. The renin-angiotensin system, via angiotensin II, has been implicated in the control of heart rate. 38 chronotropic effect when infused directly into the sinus node via the cannulated sinus node artery in the isolated canine heart [58] .

2.6 Cardiac conducting system

The heart muscle cells generate the impulse within the heart automatically, conduct and respond to electrical impulses. The frequency and regularity of pace making activity brings the heart rhythm. Myocardial tissue comprises a functional syncytium because the cells are connected by gap junctions. This also includes the atrioventricular junction. Thus, an impulse arising in any heart region leads to complete contraction of both ventricles and atria [59].

Cardiac contraction normally starts from the SA node, which is therefore called the primary pacemaker. The impulses are conveyed to the AVN from the atria. The bundle of His is the beginning of the specialized conduction system, including also the right and left bundle branches and the Purkinje fibers, which further transmit the impulses to the ventricular myocardium [14]. Conduction system and specialized myocardial cells are presented in Figure 2-9. Electrical activation propagation and contraction due to the activation of the muscles are illustrated in Figure 2-10. The cell potential in the SA node is a pacemaker potential.

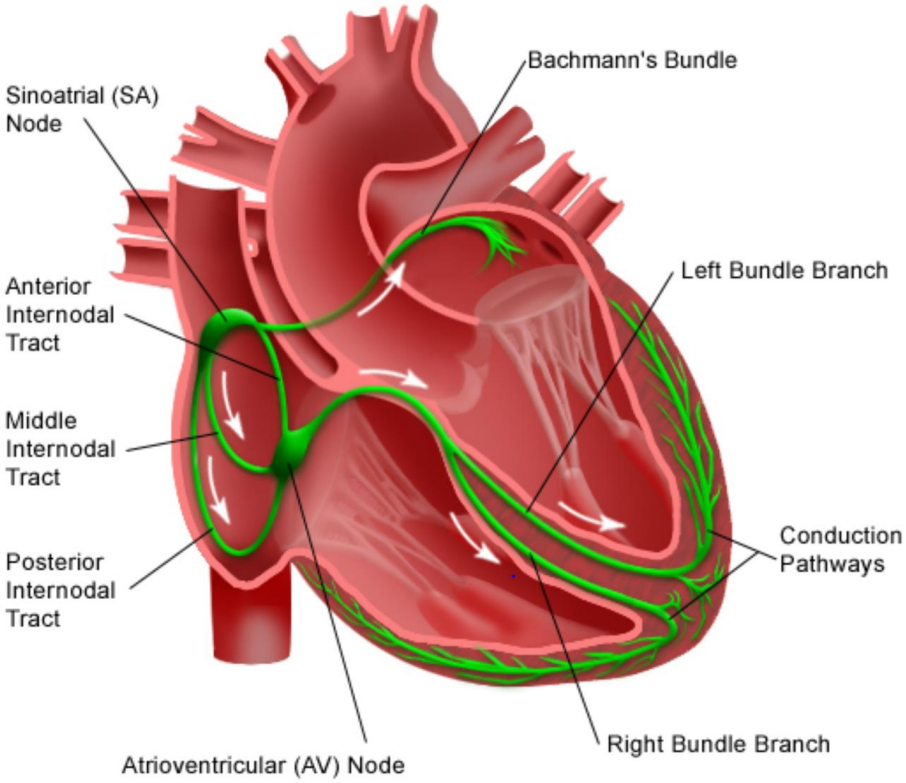

Figure 2-9: The cardiac electrical conduction system [38]

These cells do not have a constant resting potential. Instead, they slowly depolarize immediately after each repolarization, the most negative value of which is the maximum diastolic potential. The membrane potential begins at -60 mV and gradually depolarizes to -40 mV threshold, initiating an action potential (AP). Thus, each beat triggers another AP [14].

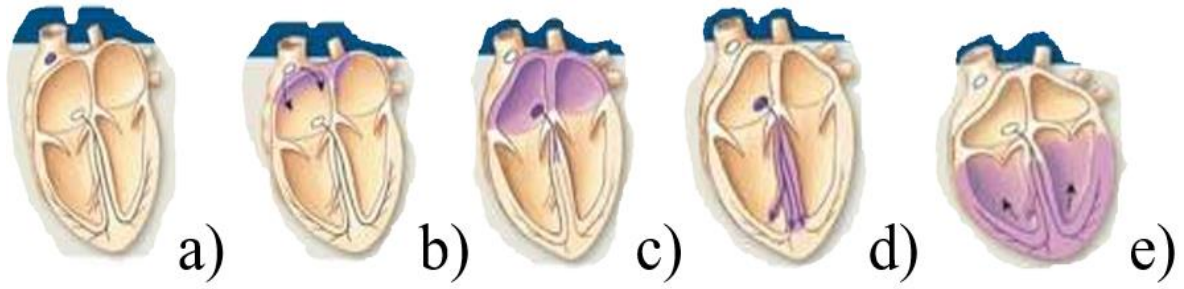

Figure 2-10: Normal spread of electrical activity. Electrical impulse (a) at SA node, pacemaker potential generation starts, (b) at AV node, atrial activation, (c) atrial contraction,(d) activation of ventricular myocardium, (e) ventricular contraction [14].

The pacemaker potential in SA node is formed by ion conductance and ionic flow through the cell membrane. In response to hyperpolarization, a type of channel opens and due to its permeability Na^+ ions enter in the cell and produce depolarization.

Cardiac pacemaker channels are also called HCN channels: hyperpolarization cyclic nucleotide channels. After the threshold voltage is passed, activation begins and the upward phase of the AP is reached by the inward diffusion of Ca^{2+} ions. Repolarization is produced by the opening of voltage-gated K^+ channels and the outward diffusion of K^+ ions [38].

Once neighboring myocardial cells have been simulated by AP, the cell also produces its own APs. According to the type and location of the cardiac cells, the AP also changes.

Different APs can be seen in Figure 2-11. Total electrical activity produces a few mV potential differences on the body surface, which can be measured non-invasively and recorded as an electrocardiogram (ECG) wave. ECG provides information on heart position, relative chamber size, heart rhythm, impulse origin, propagation and rhythm and conduction disturbances, severity

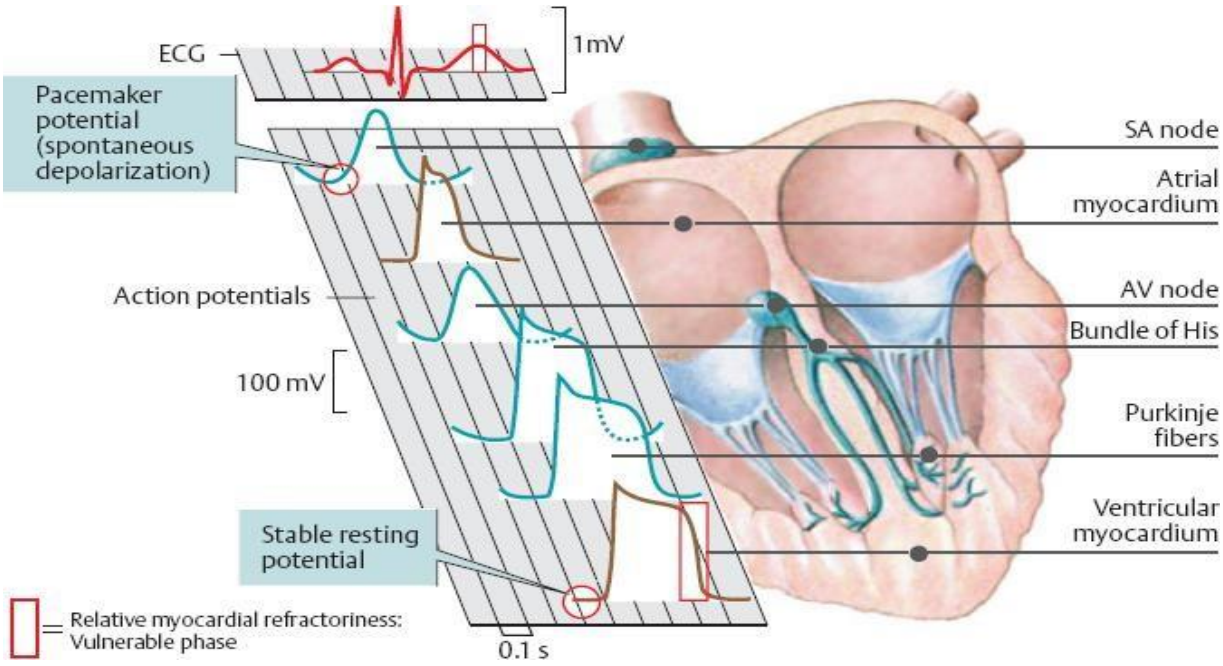

Figure 2-11:Myocardial excitation, action potentials of various myocytes [14].

and position of ischemic cardiac tissue, changes in electrolyte concentrations, and drug effects on the heart. However, it does not provide data on cardiac contraction or pumping function [14].

Duration of conduction, myocytic electrical propagation velocity on different cardiac locations as well as points activated ECG waves are shown in Table 2-2. The highest velocity of excitation propagation is in Purkinje fibers, which provides the simultaneous contraction of ventricles.

It can also be seen that the right side of the heart is excited earlier than the left side of the heart both in atria and the ventricles. While SA node conduction has the highest rate (60-100 per minute), no rate is seen in ventricular myocardium.

In a classical ECG, which measures the summation of cardiac action potentials, three main peaks are observed;

- P represents the atrial depolarization
- QRS interval represents the ventricular depolarization (also atrial repolarization occur at this interval but it is surpassed by ventricular depolarization)
- T represents the ventricular repolarization

Measurements of tissue from different regions show electrophysiological differences. These variations are due to different ion channel expressions influencing mainly the plateau and repolarization phase of AP and the development of tension. The excitation velocity in ventricular myocardium is given as 1 m/s. However, this value is absolute in fiber direction. Electrical activation propagates also in other directions with a decrease in velocity; for perpendicular direction to the fiber angle, the velocity is 1/3 of normal and propagation on other sheets decreases even more to 1/5 of normal [60].

Table 2-2: Cardiac impulses conduction [14].

Normal activation sequence		**Time (ms)**	**ECG**	**Velocity ($m \cdot s^{-1}$)**	**Conduction Intrinsic Rate (min^{-1})**
SA node	Impulse generation	0	P	0.05	60-100
Right atrium	Arrival of impulse in the distal parts of atrium	50		0.8-1.0 In atrium	
Left atrium	Arrival of impulse in distal parts of atrium	85			
AV node	Arrival of impulses	50	P-Q	0.05	40-45
AV node	Relaying of impulses	125		0.05	
His bundle	Activated	130		1.0-1.5	

End of bundle branches	Activated	145	QRS	1.0-1.5	25-40
Purkinje fibers	Activated	150		3.0-3.5	
Inner myocardium	Right ventricle	175		1.0 In myocardium	None
Inner myocardium	Left ventricle	190			
Outer myocardium	Right ventricle	205			
Outer myocardium	Left ventricle	225			

Table 2-3: Myocardium Ionic changes in phases.

Phase 0	The quick Na^+ channels open and sodium inflow begins. Then depolarization occurs and membrane potential rises up to +20 mV.
Phase 1	Slower K^+ channels open and the outward flow of K^+ stops the rising potential due to Na^+.
Phase 2	Na^+ channels close while K^+ channels are still open.
Phase 3	Slow Ca^{++} channels open and stay open for approximately 20 sec which causes the plateau in membrane potential due to the inward flow of Ca^{++}.

Phase 4	Ca^{++} channels close and repolarization occur and membrane voltage returns its resting value -90 mV.

Ion changes in all those phases have effects on both the electrical and mechanical basis of the cardiac tissue response to excitation. Figure 2.12 shows the intra- and extracellular and ion changes and potential changes. The changes are shown by five separate phases [38] as indicated in Table 2-3.

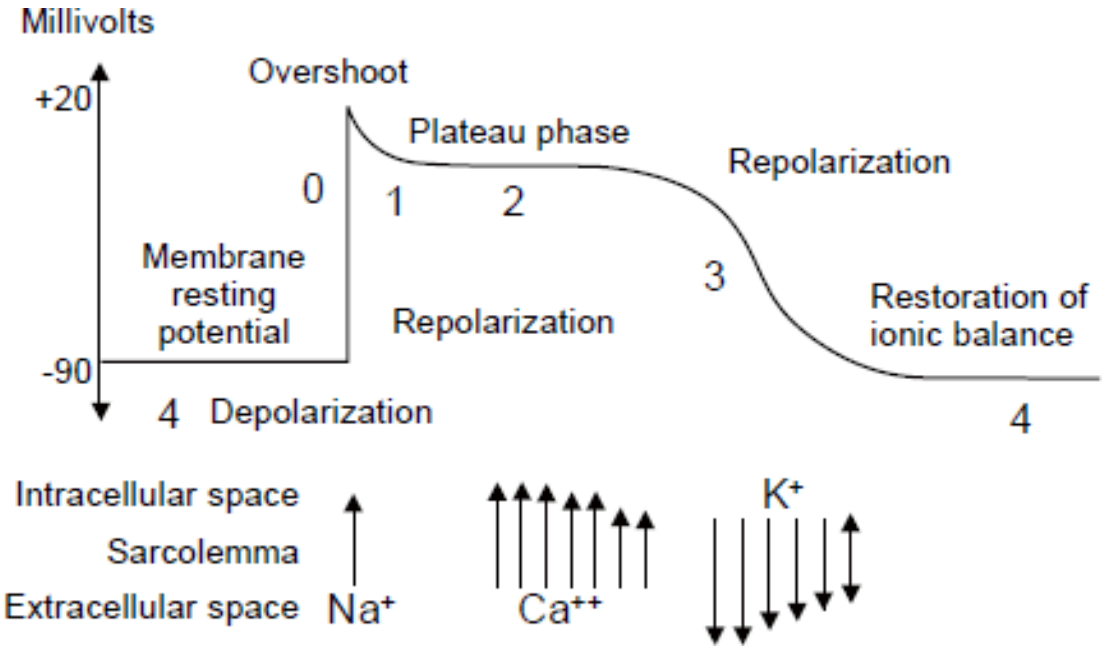

Figure 2-12: Transmembrane dynamics that leads action potential and an action potential in a myocyte from the ventricles [38].

2.7 Cardiac Mechanics

The tension development in the myocardium is initiated by an electrical impulse (action potential), via excitation-contraction coupling process. The electrical excitation of cardiac cells causes mechanical contraction controlled by intracellular calcium. The activity depends on tissue type and distribution, geometry of the heart, and heart rate.

The contractile response of cardiac muscle begins just after the start of depolarization and lasts about 1.5 times as long as the action potential. The timing and shape of electrical-mechanical coupling is shown in Figure 2-13. In the electrical wave, absolute refractory periods and relative refractory periods can be noted. In an absolute refractory period, no matter how big the excitation potential is, the cell cannot be stimulated. Nevertheless, in a relative refractory period, a cell can be stimulated if the exciting potential is big enough.

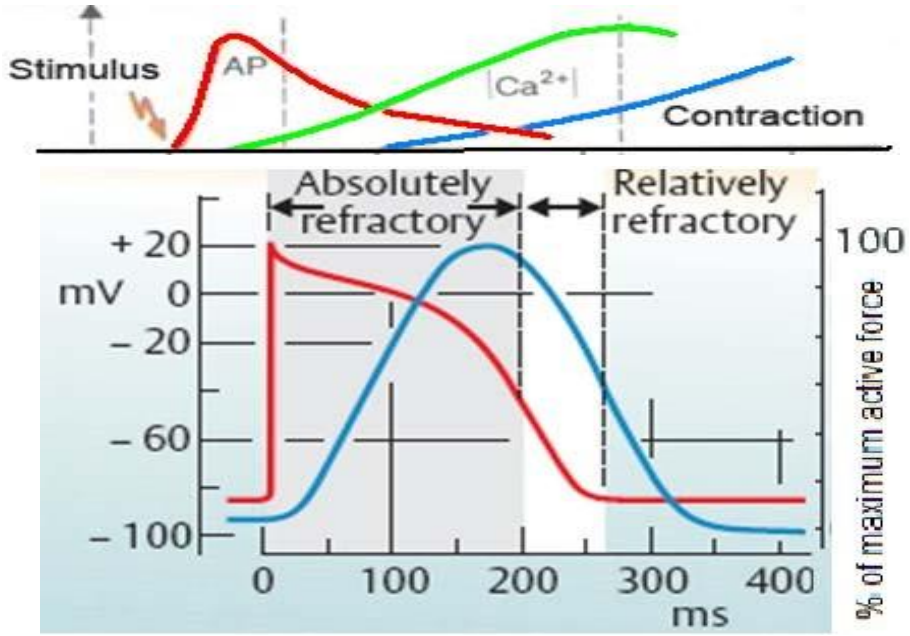

Figure 2-13: Action potential and contractile response of myocardium [3].

Response characters of the muscle are “all or none”, which means muscle fibers contract fully if they respond to the excitation. Since cardiac muscle is absolutely refractory during most of the action potential, the contractile response is more than half over by the time a second response can be initiated [14]. Therefore, the tetanus of the skeletal muscles cannot be seen in cardiac tissues.

It can be said that this property of the myocardium is a safety feature, because for any length of time, it would have lethal consequences. Ventricle muscle is said to be a vulnerable period just towards completion of an AP, because stimulation at this time will sometimes initiate ventricular fibrillation.

Myocardial muscle consists of contractile units called sarcomeres. Each sarcomere has characteristic proteins called actin, myosin, troponin, tropomyosin, whose lay out in the muscle fiber gives a striated appearance to the myocardium [61]. Figure 2-15 represents the three-dimensional structure of the sarcomere. Repeating units can be observed on the longitudinally oriented myofibrils. The excitation-contraction set up is contributed by calcium ions similarly to its role in skeletal muscle, except that Ca^{2+} entering from the extracellular fluid (ECF) as well as Ca^{2+} from the sarcoplasmic reticulum contributes to contraction [14]. The longitudinal section images taken with the electron microscopy and corresponding illustrations of sarcomere is given in Figure 2-14, for relaxation and contraction phases of the tissue.

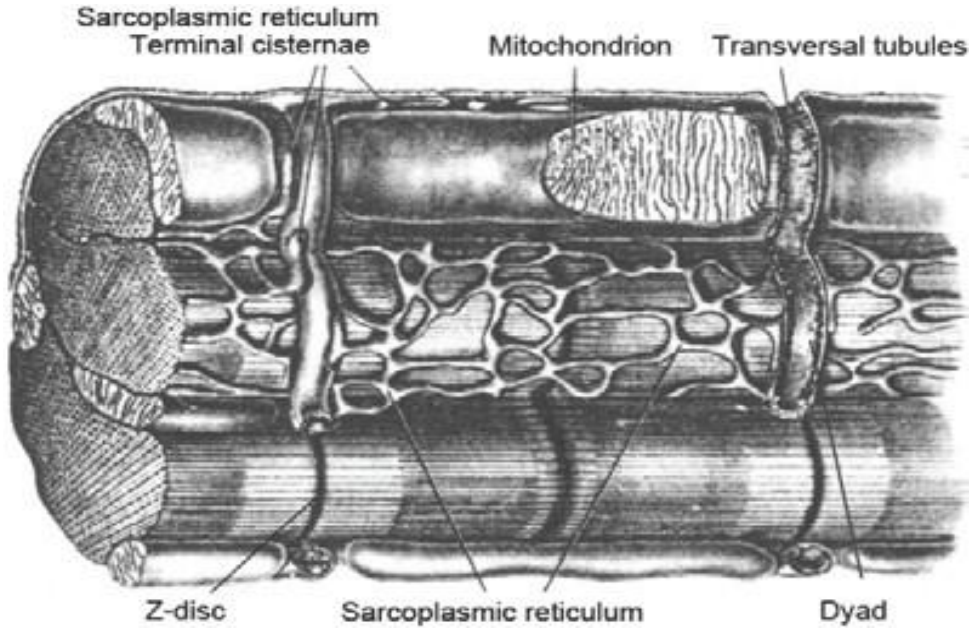

Figure 2-14: A myocardial cell or fiber reconstructed from electron micrographs[59]

In the illustrations (Figure 2-15), the sarcomere tension development is noted. Figure 2-15 (a) shows the thin actin (orange) and thick myosin (purple) filaments.

Description of the different colored sections:

Z lines: separate sarcomeres from one another, indicated as dark lines.

I band: lightly straining parts positioning outer ends.

A band: denser staining positioning in the I band.

H zone: positioned in the center of the A band.

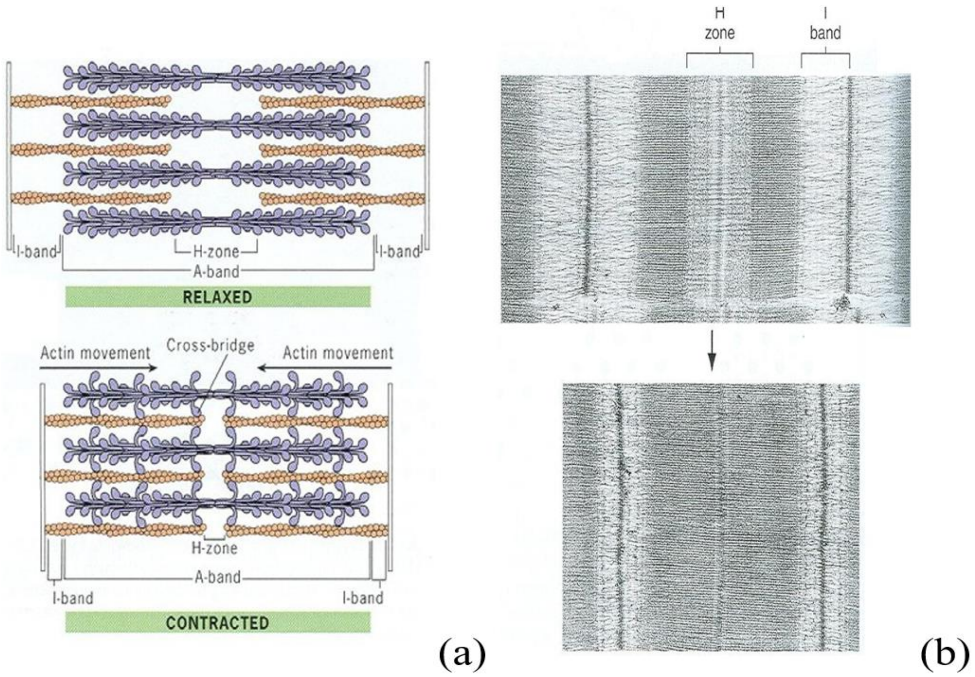

Figure 2-15 : Muscle contraction: shortening of the sarcomere, (a) schematic diagram, (b) electron micrographs of longitudinal sections [14].

When tension develops, muscle fibers shorten, the length of A band stands constant, while H and I bands decrease in width and then disappear together. As shortening progressed, the Z line of both ends of the sarcomere moves inward until they connect the outer end of the A band [38].

The length (L) and force (F) or "tension" of a muscle are closely related. The force-length relationship is illustrated in Figure 2-18. The total muscle force is the sum of its active force and its extension force at rest. Since the active force is determined by the magnitude of all potential actin-myosin interactions, it varies in accordance with the initial sarcomere length [62].

In Figure 2-16 sarcomere length in μm and corresponding tension percentage is given for systole and diastole, according to the cat papillary muscle experimental studies. Skeletal muscle can build maximum active (isometric) force (F_0) from its initial length (L_{max}; sarcomere length ca. 2 to 2.2 μm). When the sarcomeres get shortened ($L<L_{max}$), part of the thin filaments overlap, allowing only forces smaller than F_0 to develop.

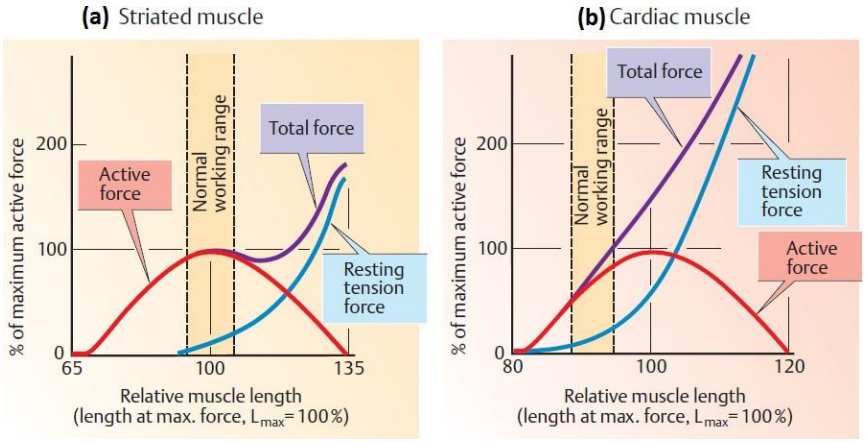

Figure 2-16: Length-force curve (a) for skeletal muscle, (b) for cardiac muscle [38]**.**

The length–force curve corresponds to the pressure–volume loop in the cardiac cycle, muscle length represents blood filling volume in the ventricles, and muscle force represents pressure in the ventricles. Cytosolic Ca^{2+} dynamics can cause modification in the pressure–volume loop due to contractility dynamics.

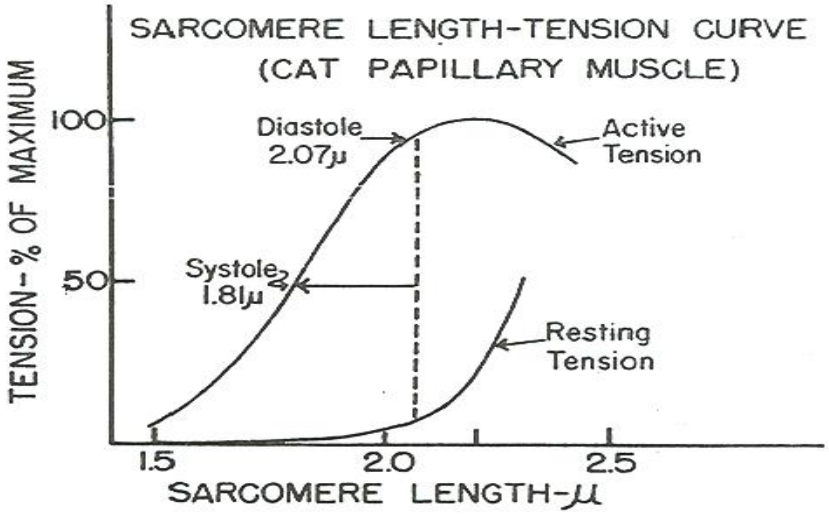

Figure 2-17: Length-Tension curve. Average sarcomere lengths in diastole and systole[63]

Since skeletal muscle is more extensible than the cardiac muscle, the passive extension force of cardiac muscle at rest is greater than that of skeletal muscle. Cardiac muscle often works in the ascending limb (below L_{max}) of its length–force curve without a plateau. As the filling loads rise

during diastole, the ventricular tension increases, which is called *Frank–Starling mechanism.* In the myocardium, troponin's sensitivity to Ca^{2+} is also affected by stretching leading into a steep rise in the curve.

The skeletal muscles have shorter action potential than those of cardiac muscles because of the increase in g_{Ca} and temporary decrease of g_K for 200-500ms after swift deactivation of Sodium channels. This results in a slow influx of calcium ions, causing a plateau in the action potential. Hence the refractory period is prolonged until the contraction has subsided. This explains tetanus in-occurrence in the cardiac muscles.

Cardiac muscles have no motor units unlike in the case of skeletal muscles, hence the electrical stimulus spreads across the myocardium from the atria to ventricles generating an all-or-none contraction of both the atria and, thereafter the ventricles.

In cardiac muscle but not in skeletal muscle, the duration of an action potential can change the force of contraction, which is controlled by the variable influx of Ca^{2+} into the cell. The greater the force (load) is, the lower the velocity of an (isotonic) contraction will be. Maximal force and a small rise in temperature will occur if shortening does not occur. The maximal velocity and high temperature rise will be developed in stress-free muscle. The lighter the loads the faster it can be taken up by the muscles. Isotonic contraction consumes greater energy during muscle work and delivers much heat compared to the work done during isometric contraction [63], [64].

2.8 Modeling the Electro-Mechanical Activity of the Heart

Modeling heart electromechanics provides knowledge of physiological and pathological phenomena. The model parameters are based on measurement data of protein, cell, tissue, or organ properties for the heart tissue. Detailed studies carried out for the cardiac tissue and physiological properties have been presented in the background information section of this thesis document. The human cardiac model provides a tool to investigate the dynamic behavior in a detailed way that cannot be achieved experimentally. Nevertheless, models are always simplified descriptions of the real process and thus the results need to be validated.

Different knowledge is needed to model coupled cardiac electromechanics which include anatomy, electrophysiology, conduction, force development and, shape change. The anatomical model builds the basis to describe the individual heart. The electrophysiological model reproduces the

electrical activity of macroscopic cardiac tissue. Models of the electrical current flow in tissue determine the conduction. The mechanical model describes the displacement process in the contractile unit.

The focus of the current thesis work is directed to mathematical modeling of the left ventricular anatomy, electrophysiology and contraction in the human heart. A main objective is to simulate atrioventricular block using human electromechanical inhomogeneity in an idealized anatomical model. The fiber orientation is inserted in the ventricular model using the software utilized.

Furthermore, several different pathological states of AVN were modeled to see the capacity of the models simulating cardiac dysfunction.

Mathematical modeling of cardiac electromechanical coupling has recently been a point of study focus. Numerous studies have been dedicated to formulate and derive governing equations describing only cardiac electrical activity [25], [65], [66], while limited studies have been dedicated to understanding cardiac mechanics and electromechanical coupling [67][68], and that makes cardiac electromechanical coupling modeling very challenging.

The first detailed study of electromechanical coupling model was proposed by R. Kaufmann et al. (1974), in a mammalian myocyte, based on transmembrane calcium movements, where this model behaviour is contrasted to that of a living myocardium [69].

More coupled electromechanical models were presented by P. Hunter et al. [29], [70] (1998). As reported by A. Panfilov and M. Nash [25], this model formed the background for modeling heart electromechanical systems, where passive and active parts of the stress tensor are decomposed and that is why approach based on active-stress is considered in this thesis. This method was adapted by a number of scholars. Some of the researchers focused on solving stability problems in coupling cardiac electromechanical models [22] but their major modeling obstacles were the computational issues despite the strides made by the researchers in solving stability problems. Researchers such as A. Panfilov and M. Nash [25], reported three variables coupled models of computational structure using the mechanic of active stress presented by P. Hunter et al. [29]. In 2005, A. Panfilov et al. [66] studied the effects of contraction on the dynamics of spiral waves and pacemakers, and in 2007, R. Keldermann et al. [31] found that deformation resulting from this contraction not only include pacemakers but has an effect on spatial organization.

Several experimental researches on myocardial mechanical behavior have reported nonlinearity, viscoelasticity and anisotropic property in its nature [9],[29],[71].

In 1972, Demiray et al. conducted the first study on myocardial mechanical behavior by using recorded experimental data to fit in the parameters for modeling the relationship between the strain and stress in the myocardium. Ever since then, strain energy density functions, viscoelastic properties of the myocardium, diastole and end-systole material descriptions, and anisotropy of the material were added to models for tissue properties. Fiber direction and residual stress were the determinants of the different ventricular myocardial parameterizations [8],[18]. The sarcomeres being the contractile units are used to describe the behavior of tissue at cellular level through modeling. Constitutive relationships are tried to be established and constitutive laws based on the Hill-Maxwell rheological law are used to simulate the relationship between force and displacement of the tissues [29]. Sliding filament theory defines the basic movement of the contractile proteins in activation. Also, Hill's model of three elements is commonly used mathematical models to explain the contraction of the cardiac cells [72]. Finite element method and finite difference approach are the main continuum approaches used in computational studies of organs, ventricular wall deformation and sarcomere. The myocardial twisting movements are induced by mechanical contraction following the electrical activation and therefore resulting into tangential displacement [27],[29]. This displacement can be restored by biomechanical volumetric modeling [28],[73].

A novel work can be dated to the previous work by P. Nardinocchi and L. Teresi [74] (2007) and C. Cherubini et al.[74] (2008), where decomposition of the deformation gradient into passive and active parts is multiplicatively solved and resulting into the foundation of models based on active-strain approach. The active-strain method was used by D. Ambrosi et al. [67] (2011) and F. Nobile et al. [67] (2011), where simulations were carried out in 1-dimensional and 2-dimensional geometry to demonstrate coupling models in the myocardium. In 2012, L. Mesin [75], adopted a similar idea started by C. Cherubini et al. [74], where he examined the impact of the myocardial electromechanical activities on spiral waves dynamics. In all of the publications above, myocardium was modeled as an isotropic material, although; the work completed has been improved to incorporate the myocardial anisotropic framework [76]. Recently, in 2013, a 3-D

mathematical modeling of myocardium demonstrating its anisotropic framework with inclusion of contraction as a result of calcium ions interaction was presented by A. Gizzi et al. [77].

The decision on preferred approach between the active-strain and active-stress is still debatable and proper experimental examination is needed by the researchers to come to the conclusion [78]. Even so, there are many other available approaches presented, different researchers document it in various ways due to the intricacy of the cardiac material [79]. Recently, in 2014, S. Goktepe et al. [80] demonstrated a combined approach in modeling 3D geometry as presented in the current thesis work.

Hill model treated the myocardium tissue as a hyper-elastic material with anisotropic framework. Later on (2015), this model has been used to investigate the effects of myocardial infarction on the electromechanically coupled behaviour of the heart [24], where the myocardial infarction is one of the leading causes of heart failures.

Three specific goals are presented in this thesis: first to represent the 3D-fiber orientation of the myocardium. Secondly, coupling the cardiac electrical activity to cardiac mechanics forming the cardiac electromechanical coupled models. Thirdly, we will investigate the AV block effect on the heart performance.

2.9 Kinematics and Fundamental Concepts.

Contraction of the heart causes deformation. For easy modeling, some of the authors made the assumption that myocardium deformation is small and hence considered it as a linear elastic structure during modeling [81]. However, during contraction the wall of the ventricle is thickened by almost 40 percent [61], accounting for the reported large deformation which will be further explained in the current work.

The two concepts in large deformation elasticity theory are the stress and the strain. The stress illustrates the force acting within the material per unit area, while the strain illustrates the length change of the material. The theory of elasticity is then composed of a set of equations which uniquely describe the state of stress, strain and deformation at each point within the elastic deformable body. Our aim is to develop the basic equations of nonlinear elasticity theory, and this requires us to first investigate the kinematics of material deformation.

2.9.1 Kinematic Relations

Kinematics deals with material movement acted upon by external forces. The original material state is called undeformed (no forces applied). The deformed state is achieved when the material is acted upon by some kind of force to reach the equilibrium state. Material particles need to be labelled since the movement of the particles demonstrates deformation.

We will define originally each material particle, **X**, by a set of rectangular cartesian coordinates, (X_1, X_2, X_3), in the undeformed region (or reference region) Ω_o. Then when the body moves and deforms due to applied loads, the particles reconfigure to **x**, with coordinates (x_1, x_2, x_3), reaching an equilibrium state (or current state) in region Ω_t.

The displacement, or deformation vector **u**, of a material particle is the transition from the

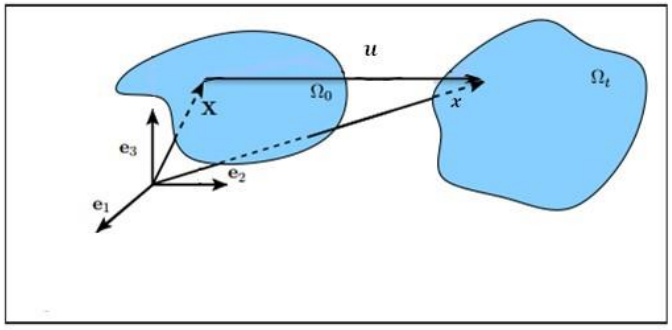

Figure 2-18: Motion from the reference configuration Ω_o *to the current configuration* Ω_t.

reference configuration to the current configuration. It is simply defined by the difference of the position vectors of a particle in both configurations:

$$u = x - X \tag{2.1}$$

Or in vector form it can be written as:

$$u = \begin{bmatrix} u_1 \\ u_2 \\ u_3 \end{bmatrix} = \begin{bmatrix} x_1 \\ x_2 \\ x_3 \end{bmatrix} - \begin{bmatrix} X_1 \\ X_2 \\ X_3 \end{bmatrix} = \begin{bmatrix} x_1 - X_1 \\ x_2 - X_2 \\ x_3 - X_3 \end{bmatrix} \tag{2.2}$$

This displacement vector tells us how a point moves from the reference to the deformed configuration when deformation happens. However, we would also like to know how a small piece of material behaves as a result of this deformation. Intuitively, we expect deformation to consist of a combination of rotation and stretching notions that we shall discuss using tensors in what follows.

Consider a line element $d\mathbf{X}$ coming out from position $\mathbf{X}$ in the original configuration (undeformed region) which becomes $d\mathbf{x}$ in the present configuration (deformed region), then using notations of J. Humphery et al. [82] we have the

following relation:

$$dx = \frac{\partial x}{\partial X} dX \tag{2.3}$$

Then we introduce the **deformation gradient tensor F**. It is the central ingredient needed for describing the deformation of an entire neighbourhood of a particle. This tensor maps line elements in the reference configuration $d\mathbf{X}$ into line elements in the deformed configuration $d\mathbf{x}$ in the following relation:

$$dx = FdX \tag{2.4}$$

Then using equation (2.3), the deformation gradient tensor will be given by:

$$F = \frac{\partial x}{\partial X} = \nabla x \tag{2.5}$$

Or in matrix form:

$$F = \begin{bmatrix} \frac{\partial x_1}{\partial X_1} & \frac{\partial x_1}{\partial X_2} & \frac{\partial x_1}{\partial X_3} \\ \frac{\partial x_2}{\partial X_1} & \frac{\partial x_2}{\partial X_2} & \frac{\partial x_2}{\partial X_3} \\ \frac{\partial x_3}{\partial X_1} & \frac{\partial x_3}{\partial X_2} & \frac{\partial x_3}{\partial X_3} \end{bmatrix}. \tag{2.6}$$

We need to introduce also the **inverse of the deformation gradient tensor $\mathbf{F}^{-1}$**, which represents the transformation from the current configuration to the reference configuration, and written as in [62] by:

$$F^{-1} = \frac{\partial X}{\partial x} \tag{2.7}$$

Or in matrix form using notations by A. Fortin and A. Garon [83]:

$$F^{-1} = \begin{bmatrix} \frac{\partial X_1}{\partial x_1} & \frac{\partial X_1}{\partial x_2} & \frac{\partial X_1}{\partial x_3} \\ \frac{\partial X_2}{\partial x_1} & \frac{\partial X_2}{\partial x_2} & \frac{\partial X_2}{\partial x_3} \\ \frac{\partial X_3}{\partial x_1} & \frac{\partial X_3}{\partial x_2} & \frac{\partial X_3}{\partial x_3} \end{bmatrix}, \tag{2.8}$$

where $\mathbf{F}\mathbf{F}^{-1} = \mathbf{F}^{-1}\mathbf{F} = \mathbf{I}$, the identity matrix.

Now we explore the relationship between the displacement, deformation gradient tensor, and inverse of deformation gradient tensor. Rearranging equation (2.1):

$$x = X + u \tag{2.9}$$

Then using equations (2.5) and (2.7), we conclude the following:

$$F = I + \nabla_x u, \tag{2.10}$$

$$F^{-1} = I - \nabla_x u \tag{2.11}$$

The deformation gradient tensor is responsible for the line element transformation between the reference and the current configurations whereas; the Jacobian of the deformation *J* is responsible for the volume transformation. The Jacobian is the measure of how the volume of a material element has changed with deformation, and for this reason it is often called the volume ratio. It is defined as the determinant of the deformation gradient tensor:

$$J = \det(F). \tag{2.12}$$

For an incompressible material, one for which the volume change is zero, the relation $J = \det(\mathbf{F}) = 1$ holds. The incompressibility constraint is therefore, $J - 1 = 0$. Another tensor important for large deformation is the **right Cauchy- Green strain tensor C**. It gives direct information about the body deformation, and measures how the angles and the line elements' length between line elements change between configurations. It is presented by:

$$C = F^T F \tag{2.13}$$

Whereas the right Cauchy-Green strain tensor gives information about rotation and stretch of line elements, the **Green-Lagrange strain tensor E** gives information about the change in the squared length of elements, defined by:

$$E = \tfrac{1}{2}(C - I) = \tfrac{1}{2}(F^T F - I). \tag{2.14}$$

After introducing some basic tensors, we are interested in relating them to the material and this can be done using **Strain Energy Density (W)** which is the measure of how much energy is

stored in small volume elements in the body due to deformation. It can be written in terms of the deformation gradient tensor, or Cauchy-Green strain tensor, or strain tensor as:

$$W = W(E) = W(C) = W(F). \tag{2.15}$$

Based on experimental observations of the material, the strain energy density changes. For instance, certain types of rubber exhibit almost isotropic behaviour and can be referred to Mooney-Rivlin materials. For this isotropic material, the strain energy density **W** is given by:

$$W = c_1(I_1 - 3) + c_2(I_2 - 3), \tag{2.16}$$

where c_1 and c_2 are material constants (mechanical properties) which must be estimated experimentally, I_1 and I_2 are invariants of the right Cauchy-Green strain tensor **C** given by:

$$I_1 = trC = tr(F^T F), \tag{2.17}$$

$$I_2 = \frac{1}{2}[(tr\mathbf{C})^2 - tr\mathbf{C}^2] \tag{2.18}$$

A subset of the Mooney-Rivlin materials are the Neo-Hookean materials, which are characterised by setting $c_2 = 0$ in equation (2.16):

$$W = c_1(I_1 - 3). \tag{2.19}$$

To ensure the incompressibility constraint $J - 1 = 0$ at each point of the tissue of a material by preserving the volume, a pressure function ***p,*** known as Lagrange Multiplier can be introduced, then the strain energy function **W** will be written in the form:

$$W = W(F) - p(J - 1) \tag{2.20}$$

There are much more forms for the strain energy density, other than Mooney-Rivlin and Neo-Hookean, available in the literature (see [29][76]), depending on the type of the material.

After establishing the kinematic framework for large deformation analysis, we are now interested in the governing force and equilibrium equations, which will be presented in the next section.

2.9.2 Stress Equilibrium

Equilibrium equations that consider deformed material follow from Newton's law of motion where in the absence of body forces, the equation of motion can read:

$$\nabla_x . \sigma = 0 \tag{2.21}$$

Or it can be written in matrix form as:

$$\nabla_x . \boldsymbol{\sigma} = \begin{bmatrix} \frac{\partial \sigma_{11}}{\partial x_1} + \frac{\partial \sigma_{12}}{\partial x_2} + \frac{\partial \sigma_{13}}{\partial x_3} \\ \frac{\partial \sigma_{21}}{\partial x_1} + \frac{\partial \sigma_{22}}{\partial x_2} + \frac{\partial \sigma_{23}}{\partial x_3} \\ \frac{\partial \sigma_{31}}{\partial x_1} + \frac{\partial \sigma_{32}}{\partial x_2} + \frac{\partial \sigma_{33}}{\partial x_3} \end{bmatrix} = \begin{bmatrix} 0 \\ 0 \\ 0 \end{bmatrix} \tag{2.22}$$

where σ is called the **Cauchy stress tensor**, and it represents the forces in the deformed configuration per unit area in the deformed configuration, defined by:

$$\sigma = \frac{df}{da}$$

where $d\mathbf{f}$ is a true force applied to a current area element and $d\mathbf{a}$ in the deformed region.

Since it is difficult to find the stresses in the deformed region, it will be convenient to transform the above equation to the undeformed region. This can be solved using Nanson's relation [76].

$$d\mathbf{a} = J\mathbf{F}^{-T} d\mathbf{A},$$

where $d\mathbf{a}$ is a current area subject (in the deformed configuration), and $d\mathbf{A}$ is a reference area subject (in the undeformed configuration).

Using the Cauchy stress tensor $\sigma = \frac{df}{da}$, the stress in the undeformed region reads:

$$\frac{df}{dA} = \sigma J F^{-T}$$

But this value constitutes the actual force applied to an area of element in the reference configuration, and it is represented by the **first Piola-Kirchhoff stress tensor P**:

$$P = \frac{df}{dA}$$

Thus, the first Piola-Kirchhoff stress tensor will be:

$$P = \sigma J F^{-T} \tag{2.23}$$

Rewriting the equation of motion (2.21) in the reference area, using Nanson's relation, we get:

$$\nabla_x \sigma = \nabla_x . (\sigma J F^{-T}) = \nabla_x . P = 0 \tag{2.24}$$

Thus, the equilibrium equation simply reads:

$$\nabla_x . P = 0 \tag{2.25}$$

where **P** can be derived using the strain energy density **W** that depends on the type of the material:

$$P = \frac{\partial W}{\partial F} \tag{2.26}$$

or for incompressible materials, it will read as:

$$P = \frac{\partial W}{\partial F} - JpF^{-T} \tag{2.27}$$

The material representation can be also considered independent of body motion. In this case, the first Piola-Kirchhoff stress tensor can be written as:

$$P = FT\,, \tag{2.28}$$

where **T** is the **second Piola-Kirchhoff stress tensor**, which relates the forces in the undeformed configuration with areas in the undeformed configuration.

Therefore, the governing equilibrium equation (2.25) will read:

$$\nabla_x.(FT) = 0\,. \tag{2.29}$$

Here we addressed the mechanics for any material in general. Now our aim is to discuss the mechanics that correspond to the cardiac in specific. Equations (2.25) and (2.29) can be considered for the cardiac mechanical modelling depending on the approaches used.

2.10 Cardiac Electromechanics

After deriving the mechanical equations that correspond to the two approaches, we are interested in the electrical activity of the cardiac tissues and its governing equations. Finally, we will couple the electrical and the mechanical equations to form models that correspond to the two approaches.

2.10.1 Cardiac Electrophysiology modeling

Cardiac electrophysiology is usually modeled by two classes: bidomain and monodomain. The book by J. Keener and J. Sneyd [84] is an excellent description in this respect. The first class called the bidomain model, proposed in 1978 by L. Tung and D. Geselowitz, is a system of two nonlinear partial differential equations coupled with one ordinary differential equation. This model gives an accurate representation of the electrophysiological wave in the cardiac tissues; however, it is computationally expensive. The bidomain model can be reduced to a monodomain model, which is the second class of electrophysiological representation. The monodomain model constitutes one nonlinear governing partial differential equation (PDE) for the transmembrane potential combined with equation for recovery variable which is an ordinary differential equation (ODE), and it expresses the changes of a general excitable myocardial tissue and the equations can be written in the form:

$$\frac{\partial V}{\partial t} = \nabla.(\mathbf{D}\nabla V) + f, \tag{2.49}$$

$$\frac{\partial w}{\partial t} = g, \tag{2.50}$$

where V is the transmembrane potential, w is the recovery variable, $\mathbf{D}$ is a diffusion tensor, and both f and g are functions depending on the ionic model.

There are many representations for the functions f and g; however, we restrict our attention to the simplified two-variable model called Aliev-Panfilov [25], where the two functions f and g have the form:

$$f(V, w) = -kV(V-\alpha)(V-1) - Vw,$$
$$g(V, w) = \left(\epsilon + \frac{\mu_1 w}{\mu_2 + V}\right)(-w - kV(V-\alpha-1)).$$

Thus, the Aliev-Panfilov monodomain model will read:

$$\frac{\partial V}{\partial t} = \nabla.(\mathbf{D}\nabla V) - kV(V-\alpha)(V-1) - Vw, \tag{2.51}$$

$$\frac{\partial w}{\partial t} = (\epsilon + \frac{\mu_1 w}{\mu_2 + V})(-w - kV(V-\alpha-1)), \tag{2.52}$$

where μ_1, μ_2, α, ϵ, and k are parameters used to modify the behaviour of the wave

based on observations [25]. Now these equations (2.51) and (2.52) should be coupled with the mechanical models presented previously.

2.11 Cardiac Electromechanical Coupling

In order to couple the electrical equations with the mechanical equations derived in the previous sections, we have to follow the two approaches mentioned before: active-strain approach and active-stress approach.

2.11.1 Active-strain approach.

First, following the active-strain approach (see work done in [67]), the electrical equations (2.51) and (2.52) in a material frame of reference after the mechanics is applied can be rewritten as:

$$\frac{\partial}{\partial t}(JV) = \nabla_x.(JF^{-1}DF^{-T}\nabla V) - kJV(V-\alpha)(V-1) - JVw\,, \tag{2.53}$$

$$\frac{\partial}{\partial t}(Jw) = J\left(\epsilon + \frac{\mu_1 w}{\mu_2 + V}\right)(-w - kV(V-\alpha-1)) \tag{2.54}$$

Thus, the general electromechanical cardiac coupled model reads:

$$\begin{cases} \dfrac{\partial}{\partial t}(JV) = \nabla_X.(JF^{-1}DF^{-T}\nabla V) - kJV(V-\alpha)(V-1) - JVw \\ \dfrac{\partial}{\partial t}(Jw) = J\left(\in + \dfrac{\mu_1 w}{\mu_2 + V}\right)(-w - kV(V-\alpha-1)), \\ \nabla_X(\mu J_0(I+\nabla_X u)F_0^{-1}F_0^{-T} - Jp(I+\nabla_X u)^{-T}) = 0 \end{cases} \tag{2.55}$$

This model includes the microscopic structure of the cardiac tissues since it dictates the fibers and includes them in the equations, and is considered as the final set of equations for the active-strain approach that will be used in the numerical simulations later.

2.11.2 Active-stress approach.

Next, following the active-stress approach (see work done in [25]), where isotropic material properties have been assumed, and anisotropic behaviour [29] have been neglected for simplicity. The general electromechanical cardiac coupled model then reads:

$$\begin{cases} \dfrac{\partial V}{\partial t} = \nabla.(D\nabla V) - kV(V-\alpha)(V-1) - Vw - I_g \\ \dfrac{\partial w}{\partial t} = \left(\in + \dfrac{\mu_1 w}{\mu_2 + V}\right)(-w - kV(V-\alpha-1)), \\ \dfrac{\partial T_a}{\partial t} = \in(V)(K_{T_a}V - T_a), \\ \nabla_x.((2c_1 + 2c_2 trC))F - 2c_2 FC + T_a FC^{-1}) = 0 \end{cases} \tag{2.56}$$

where **D** is the diffusion constant, and I_g is the stretch-activated current.

The main difference from the previous approach is that they introduced the active tension T_a to their equations, with the rate of change given by:

$$\frac{\partial T_a}{\partial t} = \epsilon(V)(K_{T_a}V - T_a), \tag{2.57}$$

where K_{Ta} is a parameter that controls the amplitude of T_a, V is the transmembrane potential, and T_a increases with V with a delay fixed by $\epsilon(V)$:

$$\in (V) = \begin{cases} 0.1, if V > a \\ 1, \quad if \quad V \leq a \end{cases}$$

System (2.56) is the final set of equations for the active-stress approach that will be used in the numerical simulations.

CHAPTER THREE

METHODLOGY

In this work, electromechanical coupling model was studied on a 3D idealized Left ventricular model and solved in COMSOL Multiphysics software version 5.4 .The formulation equations were based on phenomenological-type and data utilized in this thesis were adopted from the works of (Bakir et al.,2018 and Dokos et al.,2018) [85] documented in the Appendices.

3.1 Geometry Generation.

In generating the geometry of the left ventricle, many studies have different ways not excluding symmetric models generated from general LV dimensions and models generated from well detailed from medical imaging like MRI. However in this study, the Left ventricular geometry was built as a truncated 3D ellipsoid created in SOLIDWORKS and imported into COMSOL Multiphysics software as shown in figures 3-1and 3-2,with dimensions adopted from [86]. The boundaries of the mitral and aortic valves were constructed as semilunar and circular shapes respectively.

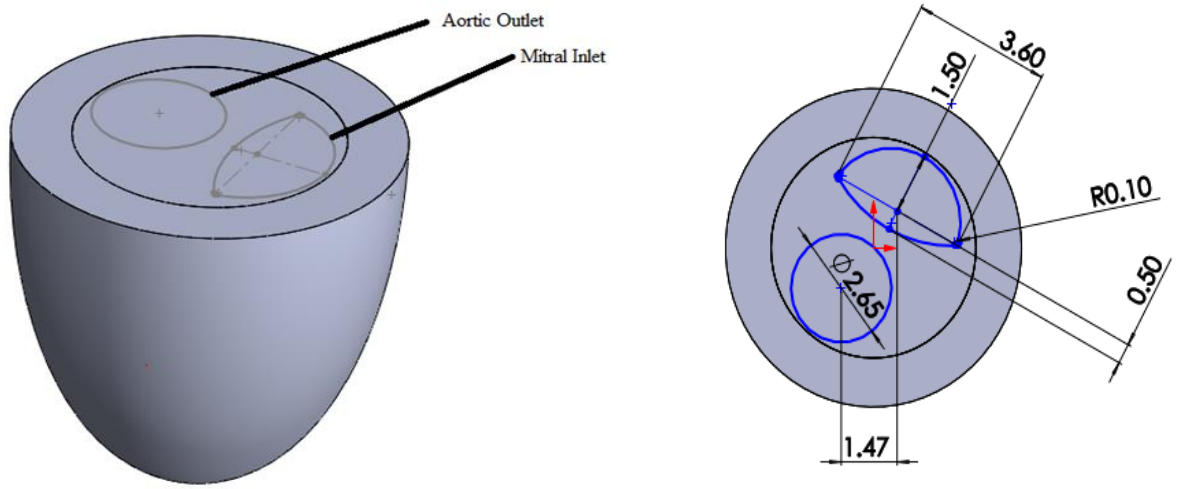

Figure 3-1: Truncated Ellipsoid.

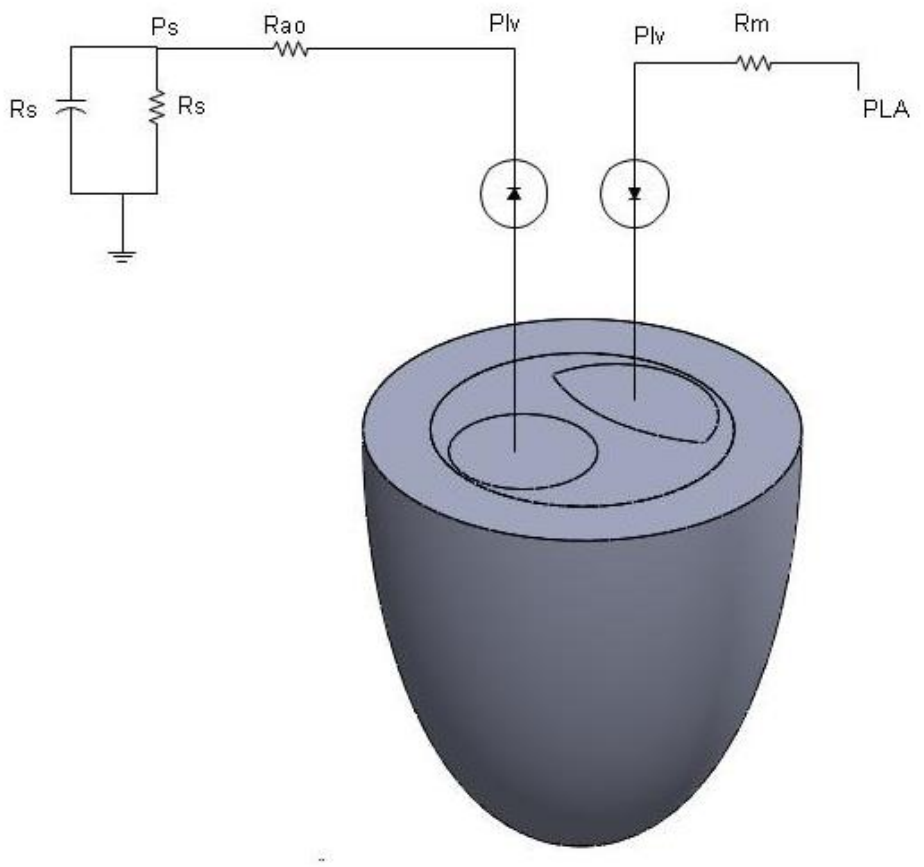

Figure 3-2: Left ventricular Element: Windekessel Model.

3.2 Microstructure

Based on the wall distance from each of the boundaries (epicardium and endocardium), a local fiber angle was assigned within the myocardium domain. Using the in-built wall distance tool in COMSOL, the distance of each position in the domain with respect to an origin boundary wall was determined.

COMSOL's wall distance tool utilized the method given by Fares and Schröder, (2002), based on modified Eikonal equations as in Equations (3.1) and (3.2).

$$\nabla G \bullet \nabla G + \sigma_w G\left(\nabla \bullet \nabla G\right) = \left(1 + 2\sigma_w\right) G^4 \tag{3.1}$$

$$D = \frac{1}{G} - \frac{2}{l_{ref}} \tag{3.2}$$

where *G* is the reciprocal of distance D to the origin wall. D was calculated for both endocardium and epicardium, D_{endo} and D_{epi}. D_{endo} was calculated with the endocardium set as the origin wall, whilst D_{epi} was calculated with the epicardium set as the origin wall. The smoothing parameter, σ_w was set to 0.2. At the origin wall, G was set as $2\,l_{ref}$, where l_{ref} was set to 0.07 m.

This setting gives us a sufficiently accurate measure of distance to the origin wall for distances greater than l_{ref} or 0.07 m.

A transmural index, γ was defined equal to 1 at the epicardium and 0 at the endocardium. The difference of the two wall distance variables, $d = D_{endo} - D_{epi}$ produced a linear relation with respect to the wall distance. Variable in Equation (3.3) was calculated using $\bar{d}_{endo}$ and $\bar{d}_{epi}$ which are the average of d at the endocardial and epicardial surfaces respectively.

$$\gamma = \frac{d}{\bar{d}_{epi}} - \frac{\bar{d}_{endo}}{\bar{d}_{endo}} \tag{3.3}$$

The fiber angle, α_f, can be assigned within the myocardium in accordance with Equation (3.4).

$$\alpha_f = (1-\gamma)\alpha_{f,endo} - \gamma\alpha_{f,epi} \tag{3.4}$$

where $\alpha_{f,epi}$ is - 60° and $\alpha_{f,endo}$ is 60°. The fiber and sheet orientations were defined based on the local boundary tangent bases vectors, ($\vec{e}_1$; $\vec{e}_2$; $\vec{e}_3$) similar to the approach of Eriksson et al. (2013). Tangent bases vectors of the ellipsoid were organized such that the first basis vector, $\vec{e}_1$ was aligned along the long-axis direction of the ellipsoid and the second basis, $\vec{e}_2$ aligned along the circumferential direction. Normal to $\vec{e}_1$ and $\vec{e}_2$ is the third basis vector, $\vec{e}_3$. By default, in COMSOL, these tangent basis vectors are defined only at the boundary. To define the base vectors within the myocardial wall, these local boundary tangent vectors at the endocardium and epicardium were defined in the myocardium by using COMSOL's Curvilinear coordinate system.

3.3 Electrophysiology Formulation

The formulation Equations (3.5)-(3.7) of the cardiac muscles action potential were adopted from the phenomenological Nash and Panfilov (2004) model, redesigned to include parameters into the initially dimensionless form. Variable V represents myocardial membrane potential, whilst R is a variable auxiliary recovery element for the myocardium. Parameter *a* in Equations (3.6) and (3.7) was chosen to vary linearly such that a_{epi} is 0.12 and a_{endo} is 0.07 to allow the cardiac tissue to relax in a direction opposite to its activation [88].

$$\frac{\partial V_m}{\partial t} = \nabla . \underbrace{\left(\sigma \nabla V_m \frac{1}{\beta C_m} \right)}_{-\Gamma} - \underbrace{\frac{1}{C_m}\left(I_{ion} - I_s \right)}_{f} \tag{3.5}$$

And presented in General form PDE in COMSOL Multiphysics:

Where: u = V_m, e_a =0, d_a =1.

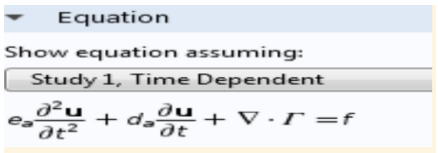

$$\frac{\partial R}{\partial t} = \left(\varepsilon_0 + \frac{\mu_1 R}{\left[\frac{V-B}{A} \right] + \mu_2} \right) * \left(-R - k_1 \left[\frac{V-B}{A} \right] \left(\left[\frac{V-B}{A} \right] - a - 1 \right) \right) \tag{3.6}$$

$$i_{ion} = \frac{I_{ion}}{C_m} \tag{3.7}$$

Equation (3.5) represents the myocardial action potential propagation and dynamics of membrane potential, Equation (3.7) governs the current flow from transmembrane ions while Equation (3.6) governs recovery of the AP in the myocardium.

The electrical conductivity tensor, σ, was set to exhibit anisotropy such that the largest conductivity was in the fibre direction (σf), followed by sheet direction (σs) and normal to sheet direction (σn). The ratio of σf : σs : σn was 4: 2: 1, in accordance with Hooks et al. (2007).

3.4 Solid Mechanics

The LV fibre varied continuously across the myocardium, oriented from +60° at the epicardium to −60° at the endocardium, and the sheet angle was from −45° to 45°. These fibre angles were defined based on the local circumferential direction.

A hyper elastic isotropic formulation of Holzapfel and Ogden (2009), was adopted to represent the myocardium as shown by Equations (3.8)-(3.11),which can use four units to simulate the response of the myocardium to the biaxial tension. The volumetric strain energy function, ψvol, was utilized to incorporate the nearly-incompressible constraint nature of the myocardium as in Equation (3.11) demonstrated by Doll and Schweizerhof (2000) formulation:

$$\psi = \psi_{isotropic} + \psi_{fiber} + \psi_{vol} \tag{3.8}$$

$$\Psi_{isotropic} = \frac{a_i}{2b_i}\exp(b_i(I_1 - 3)) \tag{3.9}$$

$$\Psi_{fiber} = \frac{a_f}{2b_f}\exp(\mathrm{b_f}\ (\mathrm{I_4f} - 1)^2 - 1) \tag{3.10}$$

$$\Psi_{vol} = \frac{K(J-1)\ln(J)}{2} \tag{3.11}$$

I_1 in Equation (3.9) denotes the first invariant of the isochoric elastic right Cauchy-Green tensor, **C**, while I_4f = **F** · (**CF**). J in Equation (3.11) represents the determinant of the deformation gradient tensor, **F**. In order to ensure material stability, I_4f was set to zero when $I_4f < 0$, assuming that myocardial fibers do not contribute significantly to passive mechanics during compression following Holzapfel and Ogden (2009). The strain energy function at the cardiac apex was only given by $\psi_{isotropic}$ due to the isotropic assumption in the apex.

3.4.1 Active stress

The simplified form of active stress proposed by Nash and Panfilov (2004), and further modified by Göktepe and Kuhl (2010), was chosen to generate mechanical contraction triggered by the action potential. Active stress, Ta, was represented by the phenomenological ordinary differential equation (ODE) as:

$$\frac{\partial Ta}{\partial t} = \varepsilon(V)\left(k_{Ta} * \frac{V - B}{A} - Ta\right) \tag{3.12}$$

where kTa controls the maximum magnitude of Ta. A, and B are fixed parameters introduced here to give units to the originally dimensionless formulation. The delay function, $\varepsilon(V)$ was given by Göktepe and Kuhl (2010) as follows:

$$\varepsilon(V) = \varepsilon_0 + (\varepsilon_\infty - \varepsilon_0)\exp\left(-\exp\left(-\xi\left(\frac{V-B}{A} - V_{th}\right)\right)\right) \tag{3.13}$$

where ε_0, ε_∞, ξ and $V_{threshold}$ are also fixed parameters. The active stress was set such that the myocardial membrane potential triggers active stress generation.

The deformation of the myocardium is governed by the equation of motion as indicated in equation (3.14):

$$\rho_s \frac{\partial^2 u_s}{\partial t^2} + \alpha\rho_s \frac{\partial u_s}{\partial t} = \nabla \bullet \left(FT + \beta \frac{\partial FT}{\partial t}\right) \tag{3.14}$$

And presented in COMSOL Multiphysics as;

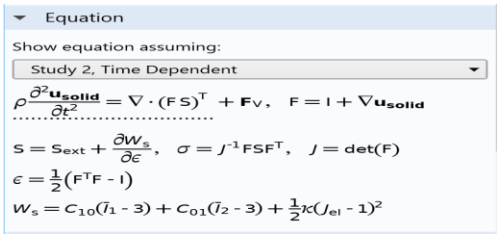

where $\vec{u}_s$ is the myocardial displacement, Equation (3.14) also contains Rayleigh damping, demonstrated by the first order time derivative of displacement and stress, to exclude non-physiological oscillations during fluid loading. Rayleigh damping factors were adapted from Fritz et al. (2014) such that $\alpha = 100\ s^{-1}$ and $\beta = 0.01$ s.

An active stress, Ta, was coupled with the hyper elastic model to generate active myocardial contraction. The active stress was obtained using the single ODE (3.12). The Ta, was summed with the second Piola Kirchhoff stress function, along the sheet, fibre, and normal to sheet directions, to combine the electrical and mechanical formulations where the Ta along sheet and normal to sheet directions was 40% of fibre direction equation (3.15).

$$T = \frac{\partial \Psi}{\partial E} + Ta(\hat{F} \otimes \hat{F}) + 0.4Ta(\hat{S} \otimes \hat{S}) + 0.4Ta(\hat{N} \otimes \hat{N}) \tag{3.15}$$

3.5 Fluid Interaction

The left ventricular fluid flow is demonstrated by the incompressible Navier-Stokes equations for the velocity field, v_f = (u, v, w), and the pressure, p, in the spatial (deformed) moving coordinate system:

$$\rho_f \frac{\partial \vec{v}_f}{\partial t} - \rho_f (\vec{v}_f \bullet \nabla)\vec{v}_f = \nabla \bullet (-pI + \mu_f (\nabla \vec{v}_f + (\nabla \vec{v}_f)^T) \tag{3.16}$$

$$\nabla \bullet \vec{v}_f = 0 \tag{3.17}$$

No-slip boundary conditions (in other words the velocity was set to zero) were specified at the basal surface(walls) of the left ventricle except at the outlet and inlet. Fluid structure interaction was implemented as a strongly coupled problem as follows [86].

(1) The specified endocardium and endocardial surface velocities are tuned to be equal as seen in Equation (3.18):

$$v_{fendo} = \frac{\partial u_s}{\partial t} \tag{3.18}$$

(2) The fluid total stress, **s**, a combination of viscous stress and pressure, was exerted along the normal of the endocardial surface, Equation (3.19):

$$s = n_{endo} \bullet (-pI + \mu_f (\nabla \vec{v}_f + (\nabla \vec{v}_f)^T) \tag{3.19}$$

The flow rates through the mitral and aortic valves were defined as:

$$Qin = \begin{cases} \dfrac{PLA - Plv}{R_m} & PLA > Plv \\ 0 & PLA < Plv \end{cases} \tag{3.20}$$

$$Qout = \begin{cases} \frac{P_{lv} - P_s}{R_{ao}} & P_{lv} > P_s \\ 0 & P_{lv} < P_s \end{cases} \quad (3.21)$$

3.6 Simulation Protocol

To start our simulation, the Windkessel circuit was disconnected from the outlet and the ventricle was subjected to a pressure until an end diastolic pressure of 8 mmHg is reached [93].

The Windkessel circuit was reconnected to the filled LV and the model was solved using the initial Windkessel volumes 50ml. The model was run for a steady cycle. A pulse stimulus of 2ms duration at 60 beats per minute (bpm) was applied at the endocardium of the ventricle. The simulations were performed on an Intel Core i7-970 processor workstation with 16 GB of RAM.

3.7 Material properties.

The left ventricular mechanical properties reported in vivo studies were used to determine the material property to be used for the myocardium. This thesis focused on the electromechanical behavior of the LV. The myocardium of the left ventricle is composed of muscle fibers. These fibrous tissues respond differently to different factors like strain, stress in different directions making its behavior to be complex. The myocardium has been experimentally reported to be a soft biological tissue and considered as an incompressible material. This was established in a study where hydrostatic stress of various quantities was applied to the tissue specimens [62].

The myocardium also demonstrates a viscoelastic behavior [94] which was neglected in this thesis study since the viscoelastic response time is long compared to diastole. For this reason, few studies and data have been reported on myocardial viscoelasticity.

In this study the strain energy density function was used to represent the LV myocardial material properties and furthermore, the strain energy function was related to the deformation gradient of the material. Hyper elastic model materials were used in this study since LV myocardium undergoes large deformation.

3.8 Finite Element Implementation.

COMSOL Multiphysics finite element (FE) software was used to simulate LV myocardial electromechanical behavior with and without the presence of AVN block. The simulations were constructed to demonstrate effects of the block on the LV performance. It was expected the study

results would be influenced by parameters with direct physiological impacts. For example, the general mitral valve behavior at the left ventricular base was taken to define the boundary condition imposed during simulation on the base of the LV. These parameters were implemented in COMSOL Multiphysics while other simulation parameters were related to the FE analysis. The mesh and solver properties are non-physiological parameters which affect the LV simulations.

3.8.1 Coordinate System.

The LV material model used during this electromechanical simulation was an isotropic necessitating the need to define the local model coordinate system. The LV muscle tissue is known to have fiber orientation varying transmurally. Due to the convoluted behavior of variation of fiber direction, a constant fiber direction was used to simplify FE analysis during simulation, hence the study was used to analyze the effect of AVN block than variations in fiber orientation. This allowed easy implementation of fiber structure in the simulation. COMSOL Multiphysics allowed user defined coordinate systems based on the model geometry. The LV myocardial fiber direction was defined by a diffusion method in the software. A scalar potential was automatically created by COMSOL Multiphysics forming the first base vector in defined direction following the curvature of the model geometry. This method was selected for its computational efficiency and implementation simplicity.

For simplicity, two orthogonal planes were manually chosen within COMSOL Multiphysics to define the first two vectors of the coordinate system. Vector one of the LV moved from the endocardium to the epicardium and was defined as radial direction. The second vector moved basial apically from the LV and was defined in longitudinal direction. The final vector coordinate direction was selected as orthogonal to the first two already defined directions and moved helically labeled as fiber direction. These three mentioned orthogonal vectors illustrated a local coordinate system which varied at every point in the Left ventricular muscle tissue.

The variables assigned by COMSOL Multiphysics to the three were represented as e_1, e_2, e_3 corresponding to the radial, longitudinal and fiber directions respectively.

3.8.2 Mesh Generation.

Mesh generation presented a crucial section of the simulation in FE analysis as poor mesh resulted into error-prone solutions. Automated and user-defined tools were implemented to build the mesh

of the LV with a solution based on quality, element size, distribution, refinement and convergence considerations.

COMSOL Multiphysics provided a user-controlled mesh interface with freedom of element size, element growth rate, curvature factor and resolution of small areas to be defined manually. It also provided various mesh density settings which were predefined. A tetrahedral element mode was used to capture the LV complexity in geometry while adhering to appropriate element quality. Model convergence had to be tested before Left ventricular mesh refinement using the symmetric model. The LV simulation was then completed by assigning a lesser density mesh.

COMSOL Multiphysics has the ability to generate statistical analysis of the mesh produced like mesh quality and size among other values as shown below in Table 3-1.

Table 3-1:User-defined mesh parameters from COMSOL Multiphysics V.5.4.

Parameter	Value
Maximum element size	0.0082 m
Minimum element size	0.0015 m
Maximum element growth rate	0.6
Curvature factor	0.5
Resolution of narrowing regions	1.5

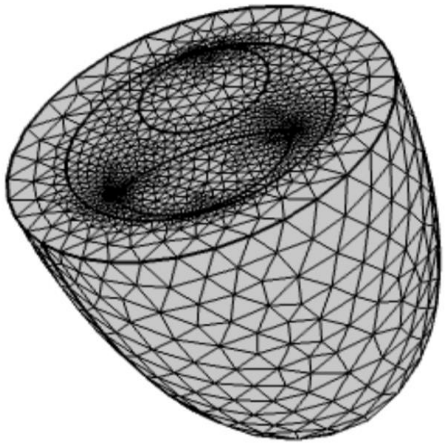

Figure 3-3: View of Left ventricular model with mesh.

The mesh near the sharp edges of the LV geometry along the outer top of the model in figure 3-3 were not refined. The edges were constraint to prevent movements and unrealistic artifacts were expected in the region. CM provided a statistical analysis of the generated mesh, giving values corresponding to mesh quality and size. The element quality parameter for the mesh was related to aspect ratio of the elements. The general distribution of the element quality was considered when refining the mesh.

3.8.3 Grid independence test.

A convergence test was performed at a point on the symmetric model to determine the reliability of the model in COMSOL Multiphysics for our simulation results. This involved a series of mesh refinements. The simulation value characteristics were recorded and were expected to be closer as the mesh was refinements were adjusted.

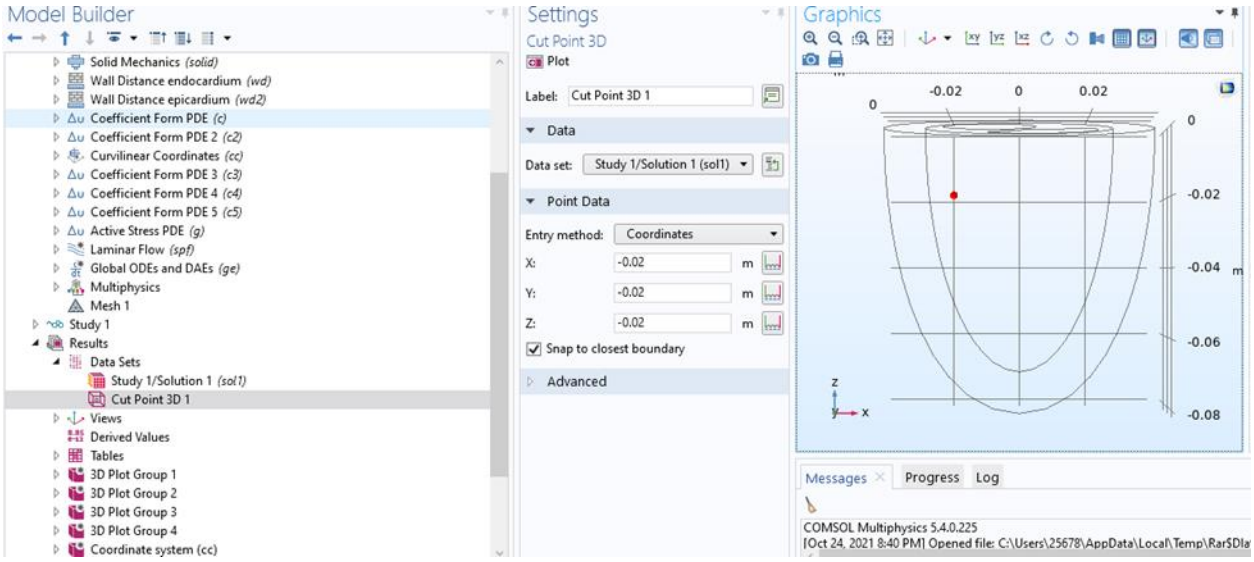

Figure 3-4: Point used for grid independent test.

Point coordinates x=-0.02, y=-0.02, z=-0.02

Table 3-2: Characteristic of the three meshes used Grid independence test for the symmetrical model

Mesh type	Number of elements	Number of degrees of freedom	Maximum action potential value
Fine	47791	3.2752E5	0.01884231216131727
Normal	21883	1.7003E5	0.01884298513416207
Coarser	8311	7.3261E4	0.01884087879391164

3.8.4 Boundary Conditions.

The boundary conditions were selected to approximate the free body constraints and loading conditions experienced by the LV. In cardiac modeling fixed base translational constraints are commonly used [92]. When examining realistic medical imaging, the Left ventricular base shows both the radial and translational expansion hence was considered during boundary condition setting. This research study considered a fixed base constraint and free LV apex and walls to expand during diastole with little anatomical constraints surrounding the heart. A pressure 8 mmHg was applied to the endocardium.

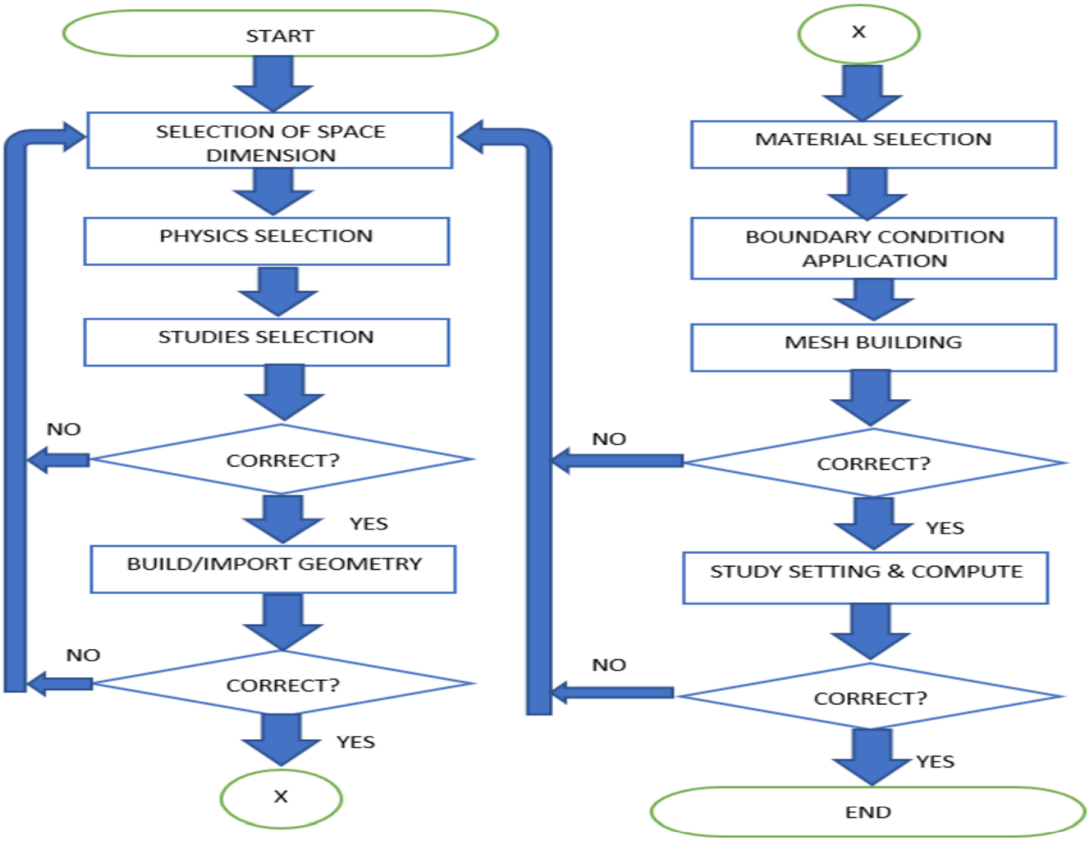

Figure 3-5: The Generic Algorithm of Modelling and simulation in COMSOL Multiphysics.

The modelling and simulation process in COMSOL follow a standard approach ranging from selection of space dimension to final computation based on the governing PDEs. The general flowchart of the modeling and simulation in COMSOL Multiphysics is presented in Figure 3-3.

CHAPTER FOUR

RESULTS AND DISCUSSION

In this chapter, the results obtained from the simulation are presented and discussed accordingly.

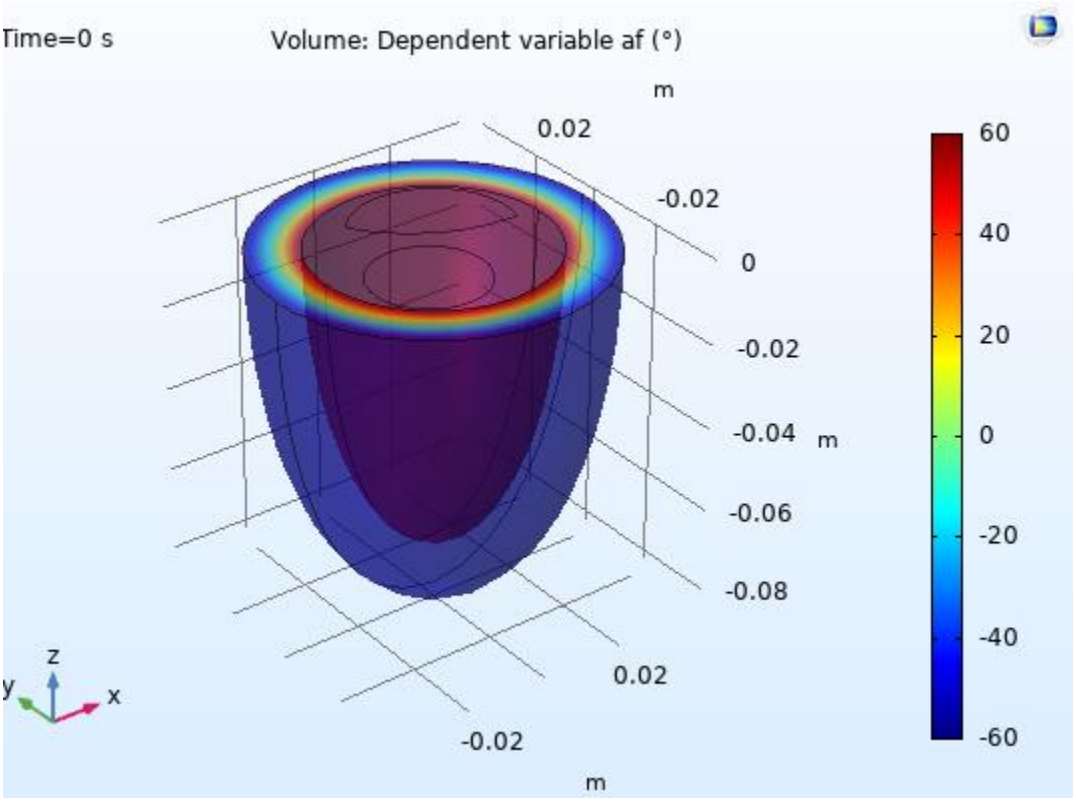

Figure 4-1: Output of simulated Left ventricle geometry.

Figure 4-1 illustrates the simulated output of the Left ventricle at initial activation showing the electrical stimulus starting from the superior section of the LV through the endocardium and propagates to the pericardium and the rest of the LV to cause contraction of the ventricle. The contraction of the LV is preceded by electrical stimulus when the threshold value for action potential is reached. It's worth noticing that every LV myocardial contraction begins with electrical initiation. If the ventricle is already excited, the action potential begins and it cannot be excited again until its resting state is regained.

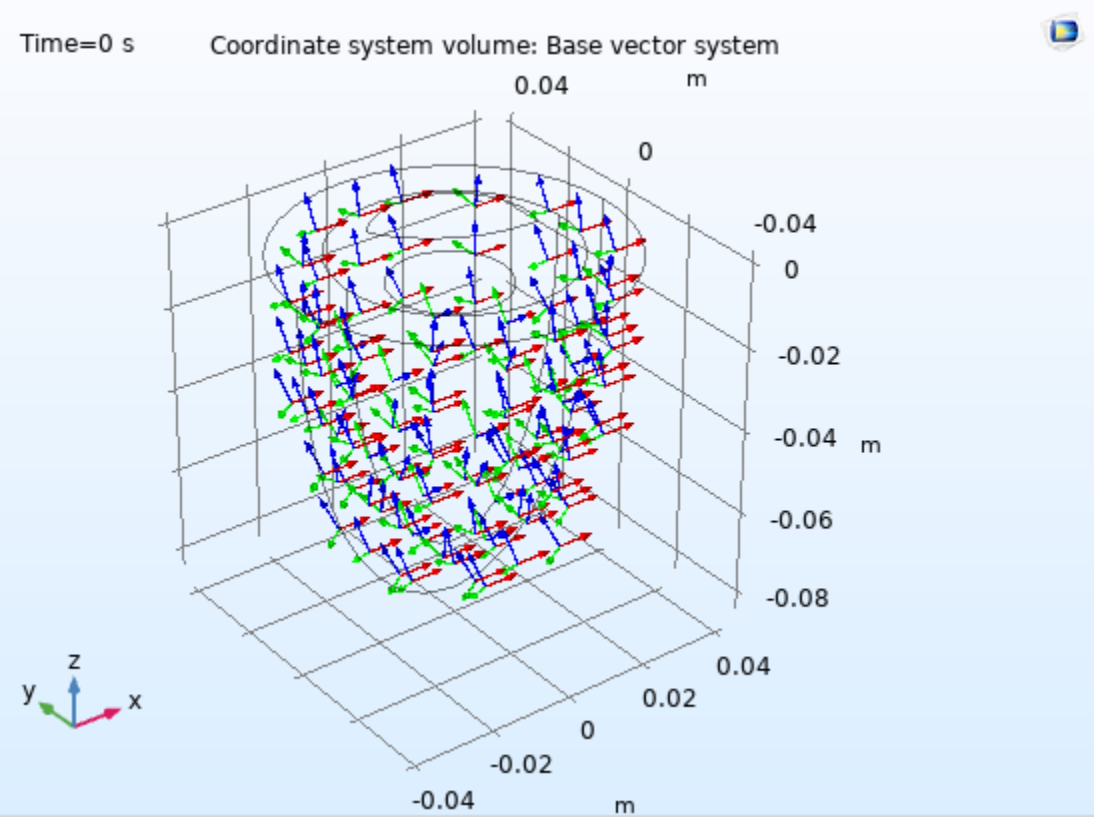

Figure 4-2: Left ventricular model local coordinate system.

(Corresponding direction: Red for radial, blue for longitudinal and green for fiber directions).

The local coordinates system demonstrates a simple way of representing the fiber structure as a vector following the curvature of the geometry in a defined direction.

The first vector (red) moves from the inner surface to the outer surface of the LV. This coordinate direction is defined as the radial direction. The second vector (blue) moves from base of the LV to the apex. This coordinate direction is defined as the longitudinal direction. The final coordinate direction is chosen as orthogonal to the first two defined directions. This vector (green) is labelled as the fiber direction and moves helically around the LV. The three orthogonal vectors represent a local coordinate system which varies at every point in the myocardium of the LV. Figure 4-2 and 4-3 give a visual representation of the defined local coordinate system [70]

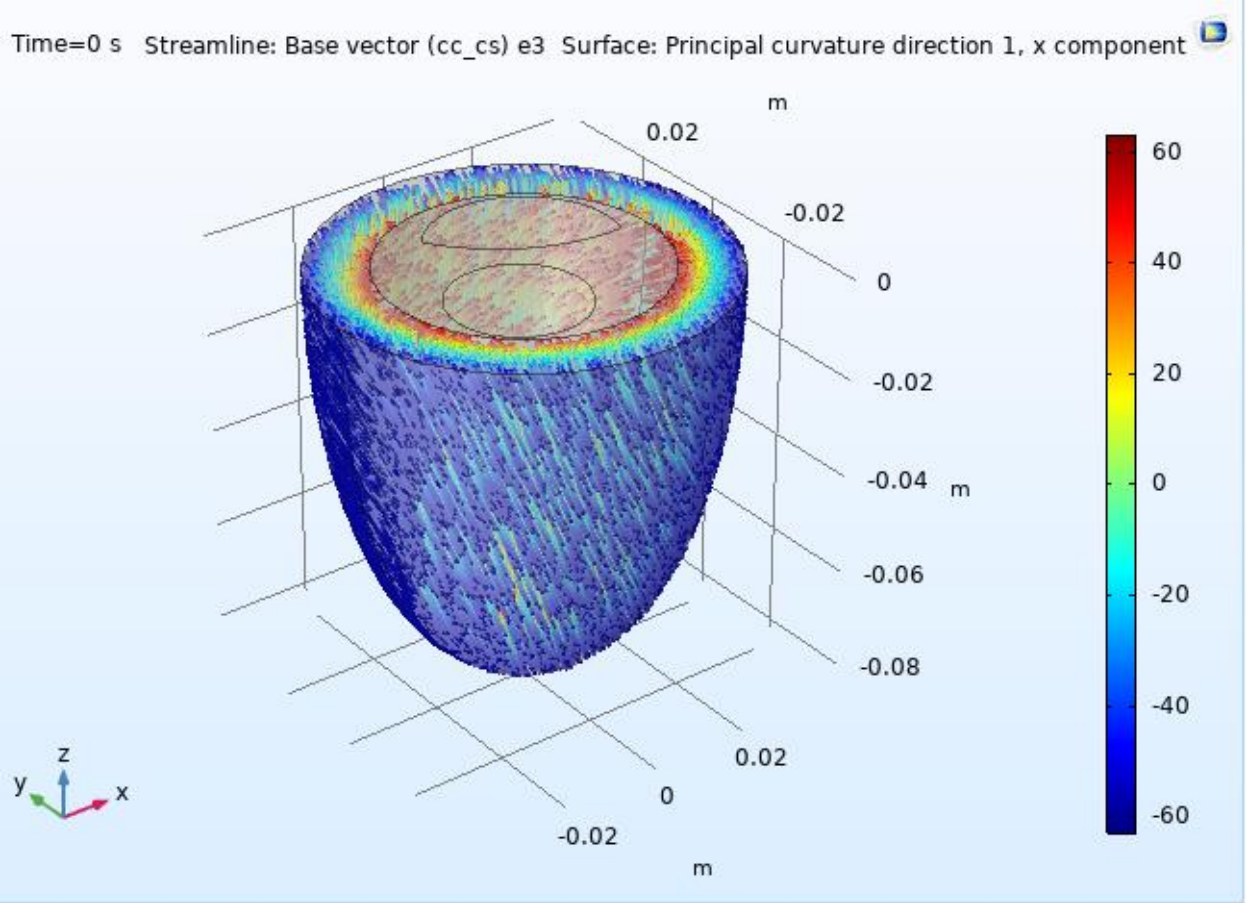

Figure 4-3: Output fiber angle orientations, overlaid on streamlines representing in the fiber, radial and longitudinal directions.

Description of cardiac fiber orientation is of great importance in analysing myocardial electrical and mechanical properties. Several works have been done in previous decades to inspect the myocardial fiber field focused on angle measurements of the myocardial wall fiber orientation [95],[96]. The fibers of myocardium are arranged in laminar sheets and oriented in a well-organized anisotropic manner as reported by Le Grice et.al, 1995 [70]. Considering through the myocardial wall thickness from the outer layer (epicardium) to the inner layer (endocardium) of the left ventricle the myocardial orientation of the fiber changes depending on the cubic function, with variation of the angle from 60 degrees to – 60 degrees and from about 45 degrees to – 45 degrees with respect to the fiber direction transmurally. A coordinate system is often adopted to demonstrate the myocardial microstructure, a universally adopted coordinate system for ventricular position and data transfer description was proposed [97]. Orthogonal sets of material

axes at every point can be locally defined. The orthogonal directions are mutually associated to the identified planes and the distinct material responses.

The results above verify that the myocardial fiber orientation is correlated highly in transmural depth with angle variation from epicardium to endocardium as demonstrated [98], [99].

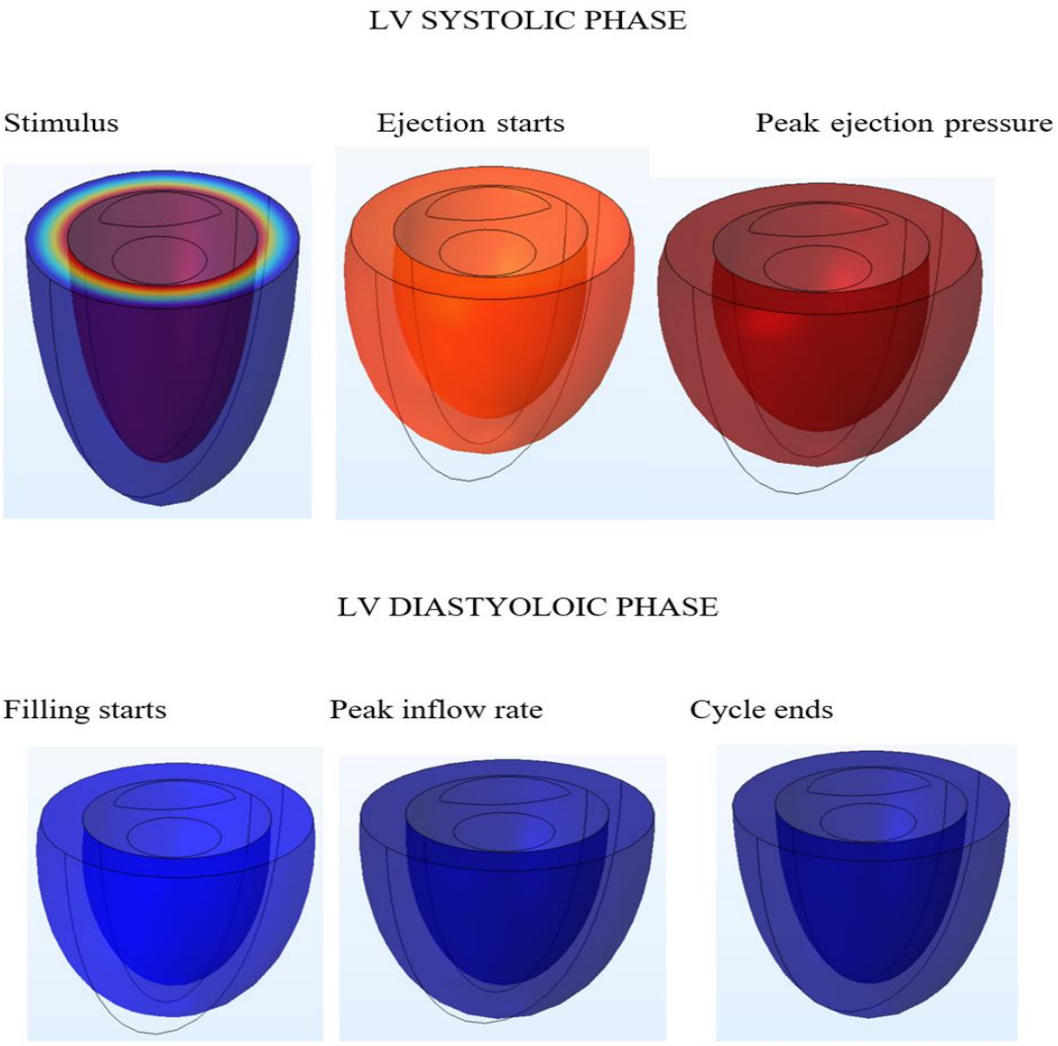

Figure 4-4: Snapshots of LV myocardial electrical activation, deformation, taken at different cycle phases.

The snapshots of electrical activation coupled with myocardial movements during systolic and diastolic phases are represented in Figure 4-4. The results show how the myocardium of the LV deforms with electrical stimulation. As the electrical impulses spread across the myocardium, there

is observable displacement of the LV from the apex to the base during contraction and displacement back to normal position during relaxation.

The initiation of electrical activation in various myocardial studies have been reported to begin at certain region of the myocardium or over the entire inner surface of the myocardium(endocardium) using Multiphysics models to resemble the natural human sequence of activation [80], [92][100]. This helped to rule out the need to model the network of AV node and purkinje fiber which would necessitate a finer mesh resolution and hence higher computational cost. The challenge with this set-up is that it limits the interaction effects between the myocardium and the purkinje fiber especially during arrhythmias [101].

The results presented in figure 4-4 are extracted from the second cardiac cycle. Since this study did not embed the purkinje network into the Left ventricle model, the stimulus spread over the entire inner myocardial surface in a few milliseconds hence quickly activating the whole left ventricle [100].

The electrical stimulus produced a twist motion followed by a strong torsion of the left ventricle at every initiation due to the myocardial fiber orientation in helical form [97]. Consequently, the distance between the apex and base is shortened due to the ape-basial contraction resulting into decrease in the volume of the LV causing blood to be pushed out during systole, while in diastole(relaxation) the vortices were created near the base and moved towards the apex as shown in the Figure 4-4 as obtained in a study done by Dokos et al.,2017.

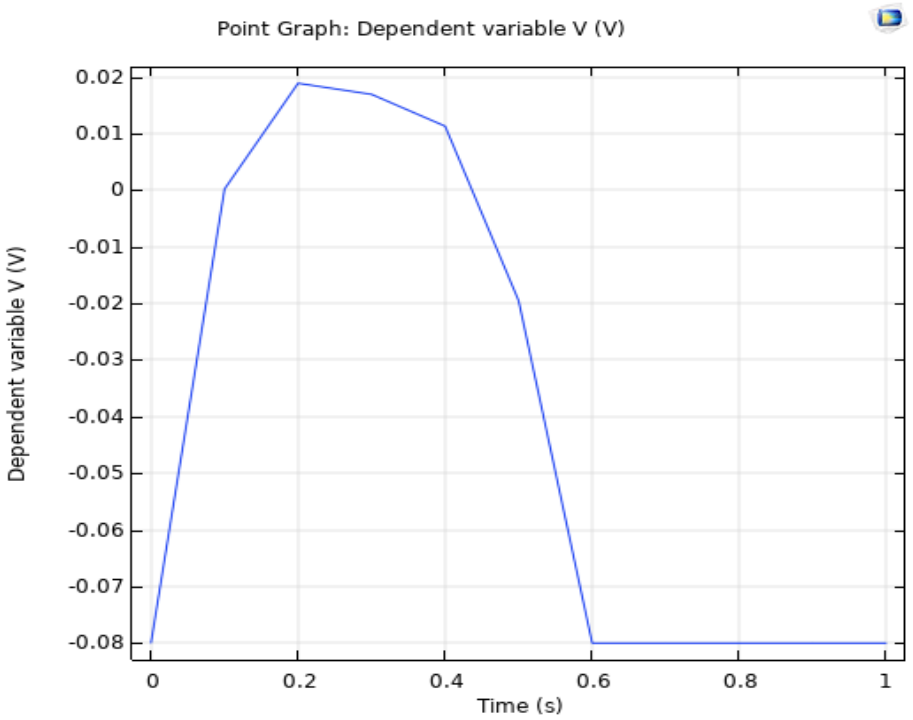

Figure 4-5: Generic Action potential trace taken of the left ventricle.

Figure 4-5 illustrates the result obtained by simulating generic action potential graph using the model proposed in this thesis on COMSOL and it's in agreement with reported data[102].

Microelectrodes are often used to record transmembrane potential of the heart. Myocardial ventricular resting potential is typically -80 to -90 millivolts relative to extracellular fluid. Cardiac action potential shape is quite distinctive due to its long duration of about 200-500 milliseconds [103]. Action potential duration (APD) is very important aspect of this thesis study since it's affected by the electric conduction through the ventricle hence, we used it in our AVN block simulation model. When the LV is stimulated before the normal heart beat excitation, the ventricle will complete its AP, and it will not answer to the normal conductivity since the it's already busy. Thus, the asynchrony in electrical wave propagation will be observed. In our model, absolute refractory period was taken as the whole AP duration.

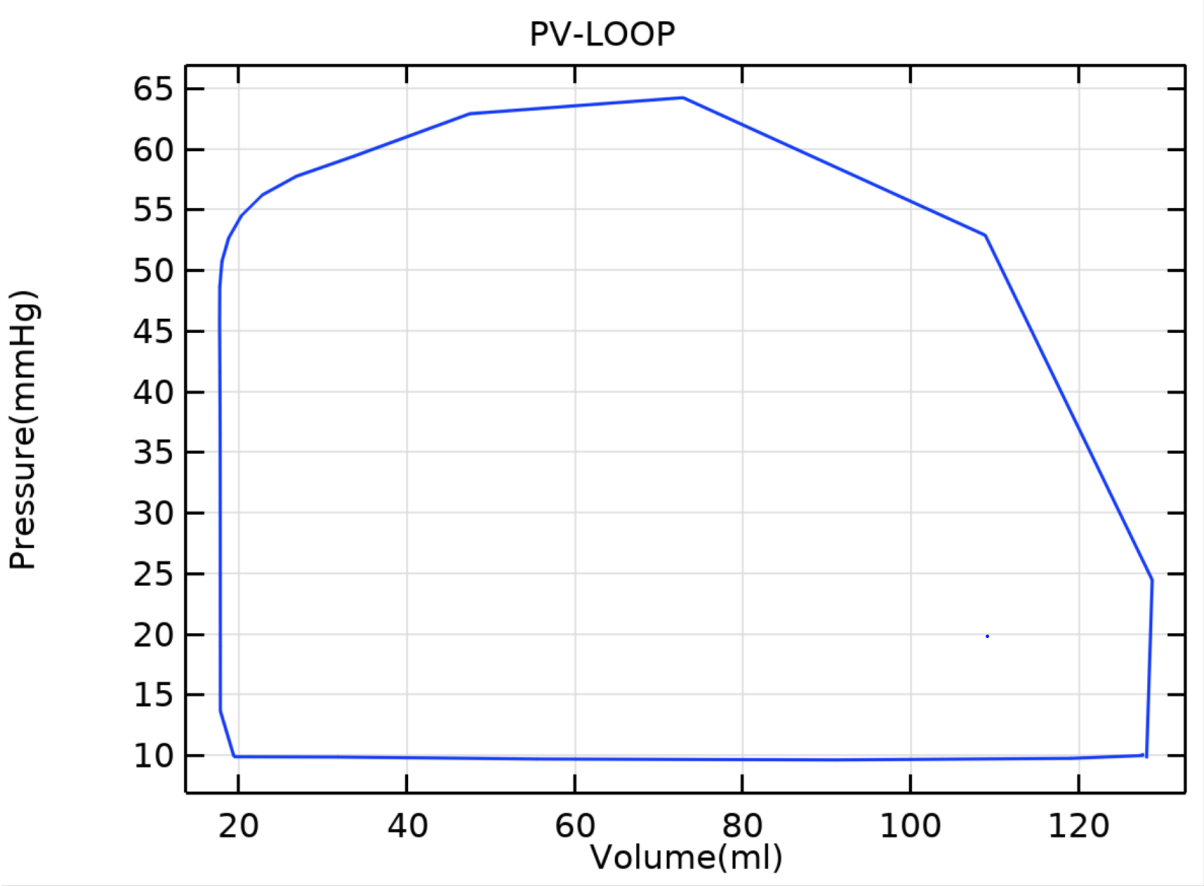

Figure 4-6: Generic simulated Left ventricular pressure- volume loop.

The proposed model was able to replicate a generic pressure-volume loop for the left ventricular haemodynamic nature, this further validates our results since it correlates with findings in various electromechanical models [86].

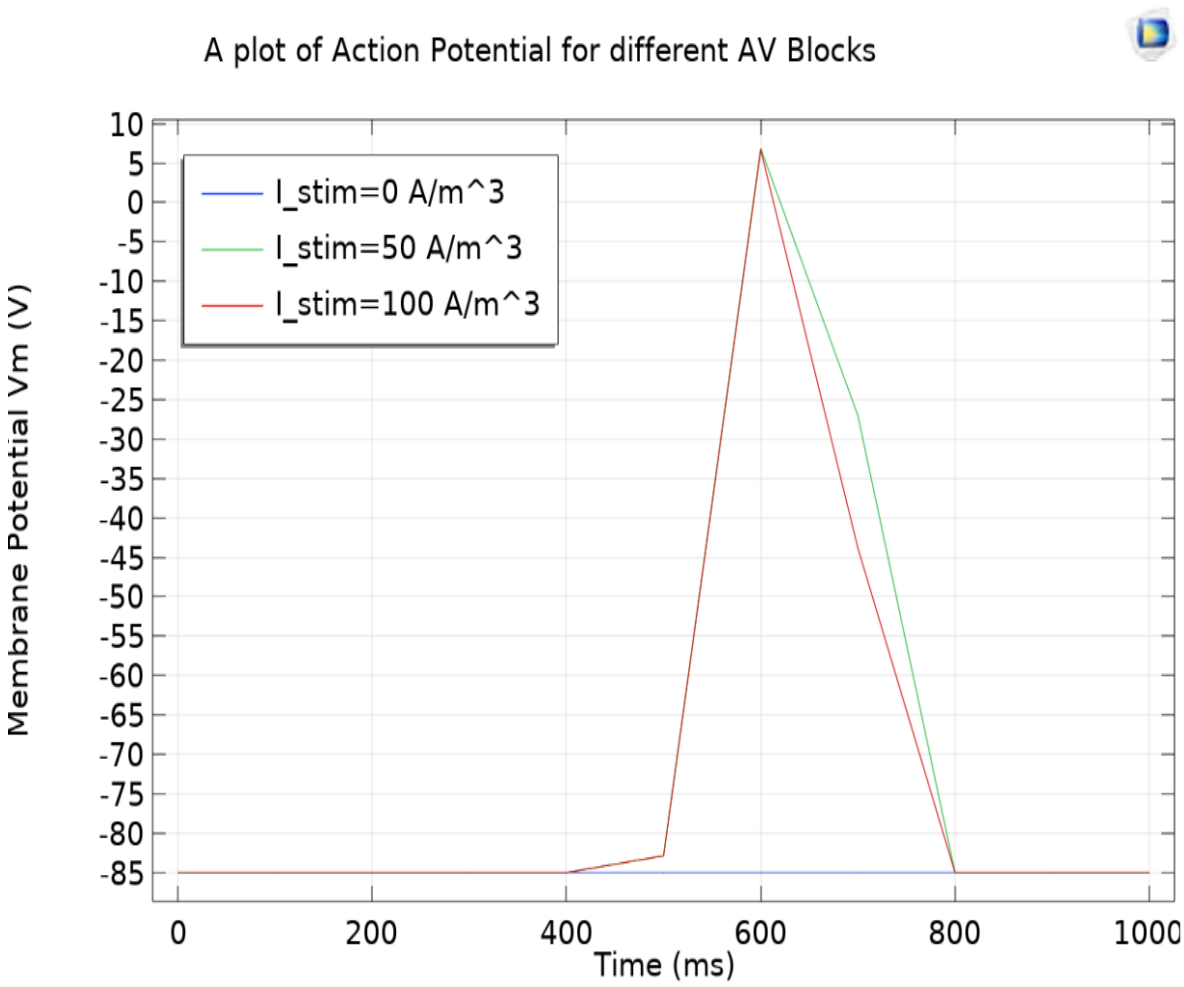

Figure 4-7: Simulated result of Action potential with different LV Atrioventricular block degrees.

From the observable results in Figure 4-7, important changes in myocardium electromechanics can be noted with stimulus variations. The electrophysiological simulation resulted in APD prolongation in agreement with experimental and clinical data [104].

The AVN role is majorly to prevent excessive atrial rates reaching the ventricles especially in atrial fibrillation with atrial rates of about 600 beats per minute. The refractory period is the major responsive factor of ventricular rate to the high atrial rate. This is related to the AVN cells' electrophysiological nature which can produce delay in repolarization of the membrane potential opposite to the cells in atria [105].

Increasing atrial rate results in an initial increase in ventricular rate in ratio of 1:1 conduction. However, excessive increase in the atrial rate causes decrease in ventricular rate due to the Wenckebach effect [105].

The transmembrane voltage potential is dependent on various factors not limited to stimulus current *I_stim* as reported in model by Hodgkin and Huxley, (1951) [98] who experimented the mathematical description of electrical behavior in an excitable tissue and this study was further backed up by Beeler-Reuter model that demonstrated the effect of stimulus frequency on the shape and size of action potential. These two different studies are in accordance with this thesis simulations where the variation in AVN stimulus conduction affected the transmembrane potential as shown in Figure 4-7. When the block was simulated at 0 *I_stim* (complete block), the action potential was significantly plateaued hence resulting into no impulse in the LV or little impulse if any from backup heartbeat hence significantly causing no or little left ventricular contraction force to pump blood.

At a partial block, the stimulus can be passed to the left ventricle partially with delayed duration in refractory periods (action potential duration, APD) compared to the normal conduction scenario as shown in the simulated result. The Priebe-Beuckelmann model went further and studied a normal and failing myocytes where the results still showed prolonged action voltage duration in failing myocytes [106].

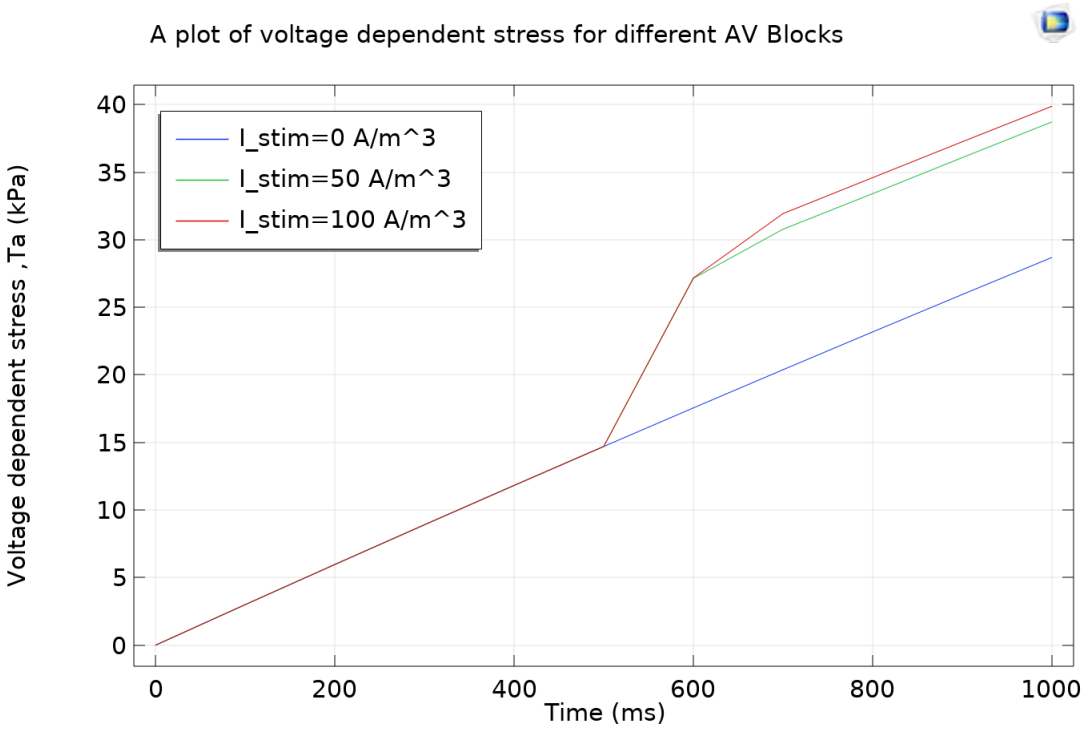

Figure 4-8: Simulated results of Voltage dependent stress with different AV block degrees.

From Figure 4-8, relationship of electrical impulse conduction and the myocardial stress is clearly illustrated. This demonstrates third objective of this thesis which is the effect of the AVN blockage on the left ventricular contraction.

The sarcomere tension development is provoked by an upstroke of cytoplasmic calcium concentration which is usually as a result of electrical excitation. This is reported in most excitation-contraction coupling studies [106], [107].

The increase in stimulus current causes the buildup in the left ventricular contraction force resulting in an increased blood pump out of the Left ventricle [108]. Our simulation in COMSOL Multiphysics shows the correlation between the myocardium stress and stimulus current through the AVN. The result shows that the contraction force increases with modulated increase in the excitation stimulus as simulated. The complete atrioventricular block (third-degree block) results in little contraction stress compared to the partial (second-degree block) and first-degree block respectively. Our output was in agreement with studies done by A.V. Hill et.al, 1938 [109].

Hence it can be concluded that progression of an electrical excitation influences the progression of the force development in the myocardium.

4.1 Model Validation

The challenges of model validation are not unique to the field of cardiac electrophysiology simulation. A limited number of measurable parameters, complicated geometries and the inability to validate all simulation results against experimental measurements make the task of validation even more cumbersome so in our model we were able to reproduce Left ventricular Action potential durations and Action potential morphologies as its validity. Models of action potential propagation can be validated against experimental studies in tissue where action potentials on the tissue surface are measured either with electrodes or by video imaging with a voltage sensitive fluorescent dye (Davidenko et al 199). However, in our studies we used a comparison method of validation where our monodomain model was validated against the spread of action potential wavefronts, such as APD restitution as conducted in experimental studies (Luo-Rudy et al 1994).

CHAPTER FIVE

CONCLUSION AND RECOMMENDATIONS

This chapter is divided into two components, those achieved by this study, and those that are proposed to be done by other researchers in future. Achievements summarize the study therein, while the future works propose what should be done as per the limitation of the study.

5.1 Conclusions.

The relationship between the electrical and mechanical activities are highly important. Electrical activation initiates the cardiac mechanical deformation through cytoplasmic calcium handling mechanism as well as activated-stretch (mechano-electric feedback) which was ignored in this study. Most of the detail literature on EMC are at cellular level hence limited data is available on electrical conduction and myocardial mechanics. This renders need for 3D model studies of EMC or other appropriate experimental approaches on the heart to analyze these physics interactions.

So, in this thesis study, a macroscopic level was considered using idealized 3D finite element Left ventricular model combining the myocardium fiber orientation and cardiac current stimulus sequences to investigate the effects of stimulus current (electrical conduction) blocks as it passes from the atria to the ventricles through the AVN hence the name AVN block on the left ventricular function. This was done through a Multiphysics coupling of the electrical activation to the mechanical contraction (deformation) of the left ventricle. The variations in the stimulus currents had significant effects on the myocardial voltage potential and tension development (stress) which is responsible for the deformation, thus pushing blood out of the left lower chamber of the heart to the rest of the body system.

This study was done in COMSOL Multiphysics software environment which is a Finite element (FE) analysis software and simplified phenomenological Ordinary differential equations were used. This helped to ease the computational tasks. The anisotropic representation of the left ventricle which was one of the objectives of this study was done using the COMSOL Multiphysics coordinate system. This study suggests the usefulness of electromechanical coupling models in assessing the mechanical function of the ventricles and to study various cardio pathological scenarios. Conclusively, from the modeling perspective, a detailed understanding of the electromechanical coupling is still needed and open to more discussion.

The simulation results obtained can be of significant importance in clinical setting with combination of ECG to detect and predict signs of heart failure in cardiac patients since the changes in the APDs give insight of how the action potential behaves with disturbance in the electrical conduction and this can be clearly depicted by the ECG wave especially for the second- and third-degree blocks. The block will eventually affect the QRS duration by increasing it to more than the normal 0.12s hence slowing the ventricular contraction. This aids in early diagnosis and treatment of cardiac patients. Being a non-invasive method of accessing Cardiac conditions it limits instances of noncompliance and pain among patients so with improved computational technology more information would be able to be captured.

5.2 Recommendations

It is recommended that future simulation work features more realistic materials and geometry to further investigate and identify other relevant parameters and anatomical structures which may offer performance close in performance as the anatomical and physiological model counterparts for the simulation. More so, actual electromechanical simulation of the heart is expected to consider appropriate clinical datasets.

Consideration should also be made for integrating the experimental, simulated data to the patient to improve clinical procedures in detecting the cardio pathological cases in clinical settings. This could be embedded into the computer system interface for patient's remote monitoring and data sharing.

Moreover, further calibration techniques such as the monte-Carlo simulation can be implemented to evaluate the robustness of the developed model and thus enhance the accuracy and performance. Variables such as ionic concentrations like calcium handling and mechano-electrical feedback which can temper with the left ventricular function were not considered.

A more holistic realistic microscopic integrated model may have impact on the results of the simulation. Hence, future studies should consider such variables and evaluate their impact on left ventricular performance to enhance the calibration of the cardiovascular system.

5.3 Limitations

This thesis did not use an anatomically realistic model as the main focus was to the ability of the idealized model to simulate Multiphysics scenarios of the Left ventricle. This reduces the computation work load and time considering the computer capacity used during the study. This study highlights future prospects for more personalized cardiac studies using the ever-evolving Imaging technologies like magnetic resonance imaging (MRI) and computed tomography (CT).

This has been a macroscopic level study where mechano-electric feedback parameters were not included like the stretch-activated currents which have been reported for initiating electrical activation via mechanical stretch [110]. Hence ignoring the stretch factors tend to reduce the non-linearity of the cardiac electrical component therefore altering simulation predictions of electromechanical interaction.

Nonetheless, the electrical model used that's phenomenological action potential and active stress is the simplest model to study the electrical excitation in the literature as it considered few variables to be solved compared to other complicated physiologically based models. Another macroscopic, tissue-based model can be used to simulate the electrical activation.

There is limited experimental data concerning the study of myocardium structure. More experimentation on myocardial electromechanical, and AVN block data would result in better LV tissue representation. This study neglected the detailed fluid-structure interaction which could have had more impact on the finite element model behaviour precisely on the endocardium.

REFERENCES

[1] S. Kaptoge *et al.*, "World Health Organization cardiovascular disease risk charts: revised models to estimate risk in 21 global regions," *Lancet Glob. Heal.*, vol. 7, no. 10, pp. e1332–e1345, 2019, doi: 10.1016/S2214-109X(19)30318-3.

[2] E. KESTERMANN, *Sudden cardiac death.*, vol. 11, no. 4. 195 7.

[3] P. W. Armstrong and J. T. Willerson, "Clinical cardiology: New frontiers," *Circulation*, vol. 97, no. 12, p. 1107, 1998.

[4] R. F. Gilmour, "The anatomy of an arrhythmia," *J. Clin. Invest.*, vol. 113, no. 5, pp. 662–664, 2004, doi: 10.1172/JCI200421223.

[5] G. A. Roth *et al.*, "Global Burden of Cardiovascular Diseases and Risk Factors, 1990–2019: Update From the GBD 2019 Study," *J. Am. Coll. Cardiol.*, vol. 76, no. 25, pp. 2982–3021, 2020, doi: 10.1016/j.jacc.2020.11.010.

[6] M. E. D. I. Cal, "B 1 Signal Analysis," *Eng. Med. Biol.*, pp. 1–2.

[7] A. D. Waller, "A Demonstration on Man of Electromotive Changes accompanying the Heart's Beat," *J. Physiol.*, vol. 8, no. 5, pp. 229–234, 1887, doi: 10.1113/jphysiol.1887.sp000257.

[8] "Understanding Heart Disease by Arthur Selzer (z-lib." .

[9] T. B. Ward, R. A. Finke, and S. M. Smith, "Printed book," vol. 2966, no. D, p. 45086, 1995.

[10] P. J. Hunter, A. J. Pullan, and B. H. Smaill, "Modeling total heart function," *Annu. Rev. Biomed. Eng.*, vol. 5, pp. 147–177, 2003, doi: 10.1146/annurev.bioeng.5.040202.121537.

[11] R. Schoeller, D. Andresen, P. Büttner, K. Oezcelik, G. Vey, and R. Schröder, "First- or second-degree atrioventricular block as a risk factor in idiopathic dilated cardiomyopathy," *Am. J. Cardiol.*, vol. 71, no. 8, pp. 720–726, 1993, doi: 10.1016/0002-9149(93)91017-C.

[12] W. Shamim *et al.*, "Intraventricular conduction delay: A prognostic marker in chronic heart failure," *Int. J. Cardiol.*, vol. 70, no. 2, pp. 171–178, 1999, doi: 10.1016/S0167-5273(99)00077-7.

[13] W. Shamim, M. Yousufuddin, M. Cicoria, D. G. Gibson, A. J. S. Coats, and M. Y. Henein,

"Incremental changes in QRS duration in serial ECGs over time identify high risk elderly patients with heart failure," *Heart*, vol. 88, no. 1, pp. 47–51, 2002, doi: 10.1136/heart.88.1.47.

[14] R. T. Sataloff, M. M. Johns, and K. M. Kost, *No 主観的健康感を中心とした在宅高齢者における 健康関連指標に関する共分散構造分析Title*. .

[15] G. Haywood, "Biventricular pacing in heart failure: Update on results from clinical trials," *Curr. Control. Trials Cardiovasc. Med.*, vol. 2, no. 6, pp. 292–297, 2001, doi: 10.1186/cvm-2-6-292.

[16] J. S. Meisner, D. M. McQueen, and Y. Ishida, "Effects of timing of atrial systole on LV filling and mitral valve closure: Computer and dog studies," *Am. J. Physiol. - Hear. Circ. Physiol.*, vol. 18, no. 3, 1985, doi: 10.1152/ajpheart.1985.249.3.h604.

[17] W. Illiam *et al.*, "The New England Journal of Medicine CARDIAC RESYNCHRONIZATION IN CHRONIC HEART FAILURE," *N Engl J Med*, vol. 346, no. 24, pp. 1845–1853, 2002, [Online]. Available: www.nejm.org.

[18] Z. I. Whinnett *et al.*, "Haemodynamic effects of changes in atrioventricular and interventricular delay in cardiac resynchronisation therapy show a consistent pattern: Analysis of shape, magnitude and relative importance of atrioventricular and interventricular delay," *Heart*, vol. 92, no. 11, pp. 1628–1634, 2006, doi: 10.1136/hrt.2005.080721.

[19] O. A. Breithardt *et al.*, "Acute effects of cardiac resynchronization therapy on left ventricular Doppler indices in patients with congestive heart failure," *Am. Heart J.*, vol. 143, no. 1, pp. 34–44, 2002, doi: 10.1067/mhj.2002.119616.

[20] D. Roose, *Computing the Electrical Activity in the Heart*, no. January. 2006.

[21] R. H. Clayton, "Computational models of normal and abnormal action potential propagation in cardiac tissue: Linking experimental and clinical cardiology," *Physiol. Meas.*, vol. 22, no. 3, 2001, doi: 10.1088/0967-3334/22/3/201.

[22] K. H. W. J. Ten Tusscher, D. Noble, P. J. Noble, and A. V. Panfilov, "A model for human ventricular tissue," *Am. J. Physiol. - Hear. Circ. Physiol.*, vol. 286, no. 4 55-4, pp. 1573–

1589, 2004, doi: 10.1152/ajpheart.00794.2003.

[23] R. C. P. Kerckhoffs, M. L. Neal, Q. Gu, J. B. Bassingthwaighte, J. H. Omens, and A. D. McCulloch, "Coupling of a 3D finite element model of cardiac ventricular mechanics to lumped systems models of the systemic and pulmonic circulation," *Ann. Biomed. Eng.*, vol. 35, no. 1, pp. 1–18, 2007, doi: 10.1007/s10439-006-9212-7.

[24] M. Sermesant *et al.*, "Simulation of cardiac pathologies using an electromechanical biventricular model and XMR interventional imaging," *Med. Image Anal.*, vol. 9, no. 5 SPEC. ISS., pp. 467–480, 2005, doi: 10.1016/j.media.2005.05.003.

[25] M. P. Nash and A. V. Panfilov, "Electromechanical model of excitable tissue to study reentrant cardiac arrhythmias," *Prog. Biophys. Mol. Biol.*, vol. 85, no. 2–3, pp. 501–522, 2004, doi: 10.1016/j.pbiomolbio.2004.01.016.

[26] I. R. Al'miev *et al.*, *Springer Proceedings in Physics*, vol. 115. 2007.

[27] L. Xia, J. H. Dou, Y. L. Gong, Y. Zhang, and D. D. Deng, "Simulation analysis of mechanical properties of the canine heart with bundle branch block based on a 3-D electromechanical model," *Comput. Cardiol.*, vol. 34, pp. 672–676, 2007, doi: 10.1109/CIC.2007.4745575.

[28] M. Sermesant, H. Delingette, and N. Ayache, "An Electromechanical Model of the Myocardium for Cardiac Image Analysis and Medical Simulation," 2004, [Online]. Available: file:///C:/Users/Vladimir/Desktop/148_17_electromechanicalModelOfTheMyocardium.pdf.

[29] M. P. Nash and P. J. Hunter, "Computational mechanics of the heart. From tissue structure to ventricular function," *J. Elast.*, vol. 61, no. 1–3, pp. 113–141, 2000, doi: 10.1023/A:1011084330767.

[30] L. Xia, M. Huo, Q. Wei, F. Liu, and S. Crozier, "Analysis of cardiac ventricular wall motion based on a three-dimensional electromechanical biventricular model," *Phys. Med. Biol.*, vol. 50, no. 8, pp. 1901–1917, 2005, doi: 10.1088/0031-9155/50/8/018.

[31] R. H. Keldermann, M. P. Nash, H. Gelderblom, V. Y. Wang, and A. V. Panfilov,

"Electromechanical wavebreak in a model of the human left ventricle," *Am. J. Physiol. - Hear. Circ. Physiol.*, vol. 299, no. 1, 2010, doi: 10.1152/ajpheart.00862.2009.

[32] J. Arumugam, J. Mojumder, G. Kassab, and L. C. Lee, "Model of Anisotropic Reverse Cardiac Growth in Mechanical Dyssynchrony," *Sci. Rep.*, vol. 9, no. 1, pp. 1–12, 2019, doi: 10.1038/s41598-019-48670-8.

[33] J. M. Guccione, L. K. Waldman, and A. D. McCulloch, "Mechanics of actiwe contraction in cardiac muscle: Part II—cylindrical models of the systolic left ventricle," *J. Biomech. Eng.*, vol. 115, no. 1, pp. 82–90, 1993, doi: 10.1115/1.2895474.

[34] A. R. Hosseinpoor *et al.*, "Socioeconomic inequalities in risk factors for non communicable diseases in low-income and middle-income countries: results from the World Health Survey.," *BMC Public Health*, vol. 12, no. 1, p. 912, 2012, doi: 10.1186/1471-2458-12-912.

[35] M. Rani, S. Nusrat, and L. H. Hawken, "A qualitative study of governance of evolving response to non-communicable diseases in low-and middle- income countries: Current status, risks and options," *BMC Public Health*, vol. 12, no. 1, p. 1, 2012, doi: 10.1186/1471-2458-12-877.

[36] G. A. Mensah *et al.*, "Mortality from cardiovascular diseases in sub-Saharan Africa, 1990-2013: A systematic analysis of data from the Global Burden of Disease Study 2013," *Cardiovasc. J. Afr.*, vol. 26, no. 2, pp. S6–S10, 2015, doi: 10.5830/CVJA-2015-036.

[37] R. L. Winslow, D. F. Scollan, A. Holmes, C. K. Yung, J. Zhang, and M. S. Jafri, "V ENTRICULAR F UNCTION : From Cell to Organ," *Annu. Rev. Biomed. Eng.*, vol. 02, pp. 119–155, 2000.

[38] G. J. Tortora and B. Derrickson, *anatomy & physiology*. .

[39] J. W. H. Fung, S. Garrigue, and C. M. Yu, "Optimization of Cardiac Resynchronization Therapy," *Card. Resynchronization Ther. Second Ed.*, vol. 4, pp. 356–373, 2009, doi: 10.1002/9781444300246.ch20.

[40] T. N. James, "Morphology of the human atrioventricular node, with remarks pertinent to its electrophysiology," *Am. Heart J.*, vol. 62, no. 6, pp. 756–771, 1961, doi: 10.1016/0002-8703(61)90664-0.

[41] G. K. MOE, J. B. PRESTON, and H. BURLINGTON, “Physiologic evidence for a dual A-V transmission system.,” *Circ. Res.*, vol. 4, no. 4, pp. 357–375, 1956, doi: 10.1161/01.RES.4.4.357.

[42] T. N. Mazgalev and P. J. Tchou, “Surface potentials from the region of the atrioventricular node and their relation to dual pathway electrophysiology,” *Circulation*, vol. 101, no. 17, pp. 2110–2117, 2000, doi: 10.1161/01.CIR.101.17.2110.

[43] F. L. Meijler and M. J. Janse, “Morphology and electrophysiology of the mammalian atrioventricular node,” *Physiol. Rev.*, vol. 68, no. 2, pp. 608–647, 1988, doi: 10.1152/physrev.1988.68.2.608.

[44] P. Coales, *Principles of Anatomy and Physiology*, vol. 86, no. 10. 2000.

[45] T. S. E. Eriksson, A. J. Prassl, G. Plank, and G. A. Holzapfel, “Influence of myocardial fiber/sheet orientations on left ventricular mechanical contraction,” *Math. Mech. Solids*, vol. 18, no. 6, pp. 592–606, 2013, doi: 10.1177/1081286513485779.

[46] G. D. Buckberg, A. Mahajan, B. Jung, M. Markl, J. Hennig, and M. Ballester-Rodes, “MRI myocardial motion and fiber tracking: a confirmation of knowledge from different imaging modalities,” *Eur. J. Cardio-thoracic Surg.*, vol. 29, no. SUPPL. 1, pp. 165–177, 2006, doi: 10.1016/j.ejcts.2006.02.064.

[47] G. J. Fahy *et al.*, “Mechanism of atrioventricular nodal facilitation in the rabbit heart: Role of the distal AV node,” *Am. J. Physiol. - Hear. Circ. Physiol.*, vol. 272, no. 6 41-6, 1997, doi: 10.1152/ajpheart.1997.272.6.h2815.

[48] J. Merideth, C. Mendez, W. J. Mueller, and G. K. Moe, “Electrical excitability of atrioventricular nodal cells.,” *Circ. Res.*, vol. 23, no. 1, pp. 69–85, 1968, doi: 10.1161/01.RES.23.1.69.

[49] A. J. Workman, K. A. Kane, and A. C. Rankin, “Rate-dependency of action potential duration and refractoriness in isolated myocytes from the rabbit AV node and atrium,” *J. Mol. Cell. Cardiol.*, vol. 32, no. 8, pp. 1525–1537, 2000, doi: 10.1006/jmcc.2000.1186.

[50] A. J. Workman, K. A. Kane, and A. C. Rankin, “Ionic basis of a differential effect of adenosine on refractoriness in rabbit AV nodal and atrial isolated myocytes,” *Cardiovasc.*

Res., vol. 43, no. 4, pp. 974–984, 1999, doi: 10.1016/S0008-6363(99)00166-2.

[51] Y. Rudy, "The ionic mechanisms of conduction in cardiac tissue," *J. Electrocardiol.*, vol. 34, no. SUPPL., pp. 65–68, 2001, doi: 10.1054/jelc.2001.28831.

[52] J. Li *et al.*, "Computer three-dimensional reconstruction of the atrioventricular node," *Circ. Res.*, vol. 102, no. 8, pp. 975–985, 2008, doi: 10.1161/CIRCRESAHA.108.172403.

[53] V. P. Nikolski, S. A. Jones, M. K. Lancaster, M. R. Boyett, and I. R. Efimov, "Cx43 and dual-pathway electrophysiology of the atrioventricular node and atrioventricular nodal reentry," *Circ. Res.*, vol. 92, no. 4, pp. 469–475, 2003, doi: 10.1161/01.RES.0000059304.97120.2F.

[54] G. Schram, M. Pourrier, P. Melnyk, and S. Nattel, "Differential distribution of cardiac ion channel expression as a basis for regional specialization in electrical function," *Circ. Res.*, vol. 90, no. 9, pp. 939–950, 2002, doi: 10.1161/01.RES.0000018627.89528.6F.

[55] S. Yoo *et al.*, "Localization of Na+ channel isoforms at the atrioventricular junction and atrioventricular node in the rat," *Circulation*, vol. 114, no. 13, pp. 1360–1371, 2006, doi: 10.1161/CIRCULATIONAHA.106.613182.

[56] J. P. Kucera, A. G. Kléber, and S. Rohr, "Slow conduction in cardiac tissue: Insights from optical mapping at the cellular level," *J. Electrocardiol.*, vol. 34, no. 4 SUPPL., pp. 57–64, 2001, doi: 10.1054/jelc.2001.28827.

[57] M. S. Spach and P. C. Dolber, "Relating extracellular potentials and their derivatives to anisotropic propagation at a microscopic level in human cardiac muscle: Evidence for electrical uncoupling of side-to-side fiber connections with increasing age," *Circ. Res.*, vol. 58, no. 3, pp. 356–371, 1986, doi: 10.1161/01.RES.58.3.356.

[58] M. Kobayashi, Y. Furukawa, and S. Chiba, "Positive chronotropic and inotropic effects of angiotension II in the dog heart," *Eur. J. Pharmacol.*, vol. 50, no. 1, pp. 17–25, 1978, doi: 10.1016/0014-2999(78)90249-2.

[59] S. Bound and P. Date, *Laboratory Atlas of Anatomy and Physiology.*, no. April 2003. 2004.

[60] M. Lorange and R. M. Gulrajani, "A computer heart model incorporating anisotropic propagation: I. Model construction and simulation of normal activation," *J. Electrocardiol.*,

vol. 26, no. 4, pp. 245–261, 1993, doi: https://doi.org/10.1016/0022-0736(93)90047-H.

[61] A. Quarteroni, T. Lassila, S. Rossi, and R. Ruiz-Baier, "Integrated Heart—Coupling multiscale and multiphysics models for the simulation of the cardiac function," *Comput. Methods Appl. Mech. Eng.*, vol. 314, pp. 345–407, 2017, doi: 10.1016/j.cma.2016.05.031.

[62] M. Y. Sheinin and M. D. Wang, "Twist-stretch coupling and phase transition during DNA supercoiling," *Phys. Chem. Chem. Phys.*, vol. 11, no. 24, pp. 4800–4803, 2009, doi: 10.1039/b901646e.

[63] E. H. Karam and G. Drzewiecki, "Modeling of cardiac growth and hypertrophy: Regulating factors," *Ann. Biomed. Eng.*, vol. 21, no. 3, pp. 309–309, 1993, doi: 10.1007/bf02368187.

[64] C. Chnafa, S. Mendez, R. Moreno, and F. Nicoud, *Modeling the Heart and the Circulatory System*, vol. 14, no. 1. 2015.

[65] S. Linge, J. Sundnes, M. Hanslien, G. T. Lines, and A. Tveito, "Numerical solution of the bidomain equations," *Philos. Trans. R. Soc. A Math. Phys. Eng. Sci.*, vol. 367, no. 1895, pp. 1931–1950, 2009, doi: 10.1098/rsta.2008.0306.

[66] M. Balakrishnan, V. Srinivasa Chakravarthy, and S. Guhathakurta, "Simulation of cardiac arrhythmias using a 2D heterogeneous whole heart model," *Front. Physiol.*, vol. 6, no. DEC, 2015, doi: 10.3389/fphys.2015.00374.

[67] D. Ambrosi, G. Arioli, F. Nobile, and A. Quarteroni, "Downloaded 12 / 31 / 12 to 132 . 206 . 27 . 25 . Redistribution subject to SIAM license or copyright ; see http://www.siam.org/journals/ojsa.php Copyright © by SIAM . Unauthorized reproduction of this article is prohibited . Copyright © by SIAM . Unauthor," vol. 71, no. 2, pp. 605–621, 2011.

[68] R. Chabiniok *et al.*, "Multiphysics and multiscale modelling, data–model fusion and integration of organ physiology in the clinic: Ventricular cardiac mechanics," *Interface Focus*, vol. 6, no. 2, 2016, doi: 10.1098/rsfs.2015.0083.

[69] N. A. Trayanova, "Whole-heart modeling : Applications to cardiac electrophysiology and electromechanics," *Circ. Res.*, vol. 108, no. 1, pp. 113–128, 2011, doi: 10.1161/CIRCRESAHA.110.223610.

[70] P. M. F. Nielsen, I. J. Le Grice, B. H. Smaill, and P. J. Hunter, “Mathematical model of geometry and fibrous structure of the heart,” *Am. J. Physiol. - Hear. Circ. Physiol.*, vol. 260, no. 4 29/4, 1991, doi: 10.1152/ajpheart.1991.260.4.h1365.

[71] F. B. Sachse, G. Seemann, M. B. Mohr, and A. V. Holden, “Mathematical modeling of cardiac electro-mechanics: From protein to organ,” *Int. J. Bifurcat. Chaos*, vol. 13, no. 12, pp. 3747–3755, 2003, doi: 10.1142/S0218127403008910.

[72] A. J. Brady, “The three element model of muscle mechanics: its applicability to cardiac muscle.,” *Physiologist*, vol. 10, no. 2, pp. 75–86, 1967.

[73] K. D. Costa, Y. Takayama, A. D. McCulloch, and J. W. Covell, “Laminar fiber architecture and three-dimensional systolic mechanics in canine ventricular myocardium,” *Am. J. Physiol. - Hear. Circ. Physiol.*, vol. 276, no. 2 45-2, pp. 595–607, 1999, doi: 10.1152/ajpheart.1999.276.2.h595.

[74] C. Cherubini, S. Filippi, P. Nardinocchi, and L. Teresi, “An electromechanical model of cardiac tissue: Constitutive issues and electrophysiological effects,” *Prog. Biophys. Mol. Biol.*, vol. 97, no. 2–3, pp. 562–573, 2008, doi: 10.1016/j.pbiomolbio.2008.02.001.

[75] O. Camara, T. Mansi, M. Pop, K. Rhode, M. Sermesant, and A. Young, “Statistical Atlases and Computational Models of the Heart: Imaging and Modelling Challenges: 5th International Workshop, STACOM 2014 Held in Conjunction with MICCAI 2014 Boston, MA, USA, September 18, 2014 Revised Selected Papers,” *Lect. Notes Comput. Sci. (including Subser. Lect. Notes Artif. Intell. Lect. Notes Bioinformatics)*, vol. 8896, pp. 63–73, 2015, doi: 10.1007/978-3-319-14678-2.

[76] R. Ruiz-baier, D. Ambrosi, S. Pezzuto, S. Rossi, and A. Quarteroni, “Computer Models in Biomechanics,” *Comput. Model. Biomech.*, pp. 189–201, 2013, doi: 10.1007/978-94-007-5464-5.

[77] C. Cherubini, S. Filippi, and A. Gizzi, “Diffusion Processes in Human Brain Using COMSOL Multiphysics,” Oct. 2006.

[78] N. A. Trayanova, J. Constantino, and V. Gurev, “Electromechanical models of the ventricles,” *Am. J. Physiol. - Hear. Circ. Physiol.*, vol. 301, no. 2, pp. 279–286, 2011, doi: 10.1152/ajpheart.00324.2011.

[79] L. Fan, J. Yao, C. Yang, Z. Wu, D. Xu, and D. Tang, “Material stiffness parameters as potential predictors of presence of left ventricle myocardial infarction: 3D echo-based computational modeling study,” *Biomed. Eng. Online*, vol. 15, no. 1, pp. 1–16, 2016, doi: 10.1186/s12938-016-0151-8.

[80] S. Göktepe and E. Kuhl, “Electromechanics of the heart: A unified approach to the strongly coupled excitation-contraction problem,” *Comput. Mech.*, vol. 45, no. 2–3, pp. 227–243, 2010, doi: 10.1007/s00466-009-0434-z.

[81] B. M. Rocha, E. M. Toledo, L. P. S. Barra, and R. W. Dos Santos, “An Electromechanical Left Ventricular Wedge Model to Study the Effects of Deformation on Repolarization during Heart Failure,” *Biomed Res. Int.*, vol. 2015, 2015, doi: 10.1155/2015/465014.

[82] J. D. Humphrey and M. Epstein, “Cardiovascular Solid Mechanics: Cells, Tissues, and Organs,” *Appl. Mech. Rev.*, vol. 55, no. 5, pp. B103–B104, Sep. 2002, doi: 10.1115/1.1497492.

[83] M. Fortin, “Old and new finite elements for incompressible flows,” *Int. J. Numer. Methods Fluids*, vol. 1, no. 4, pp. 347–364, 1981, doi: 10.1002/fld.1650010406.

[84] J. P. Keener and J. Sneyd, “Mathematical Physiology,” *Book*, p. 580, 2008, [Online]. Available: https://books.google.com/books?id=HIkZ3QHbpTQC&pgis=1.

[85] A. A. Bakir, A. Al Abed, M. C. Stevens, N. H. Lovell, and S. Dokos, “A multiphysics biventricular cardiac model: Simulations with a left-ventricular assist device,” *Front. Physiol.*, vol. 9, no. SEP, pp. 1–25, 2018, doi: 10.3389/fphys.2018.01259.

[86] A. A. Bakir, A. Al Abed, N. H. Lovell, and S. Dokos, “A generic cardiac biventricular fluid-electromechanics model,” no. 2, pp. 3680–3683, 2017.

[87] E. Fares and W. Schröder, “A differential equation for approximate wall distance,” *Int. J. Numer. Methods Fluids*, vol. 39, no. 8, pp. 743–762, 2002, doi: 10.1002/fld.348.

[88] A. V. Glukhov *et al.*, “Transmural dispersion of repolarization in failing and nonfailing human ventricle,” *Circ. Res.*, vol. 106, no. 5, pp. 981–991, 2010, doi: 10.1161/CIRCRESAHA.109.204891.

[89] D. A. Hooks, M. L. Trew, B. J. Caldwell, G. B. Sands, I. J. LeGrice, and B. H. Smaill,

"Laminar arrangement of ventricular myocytes influences electrical behavior of the heart," *Circ. Res.*, vol. 101, no. 10, pp. 103–113, 2007, doi: 10.1161/CIRCRESAHA.107.161075.

[90] G. A. Ho[1] G. A. Holzapfel and R. W. Ogden, "Constitutive modelling of passive myocardium: A structurally based framework for material characterization," Philos. Trans. R. Soc. A Math. Phys. Eng. Sci., vol. 367, no. 1902, pp. 3445–3475, 2009, doi: 10.1098/rsta and R. W. Ogden, "Constitutive modelling of passive myocardium: A structurally based framework for material characterization," *Philos. Trans. R. Soc. A Math. Phys. Eng. Sci.*, vol. 367, no. 1902, pp. 3445–3475, 2009, doi: 10.1098/rsta.2009.0091.

[91] S. Doll and K. Schweizerhof, "Volumetric Strain Energy," vol. 67, no. March, pp. 17–21, 2000.

[92] T. Fritz, C. Wieners, G. Seemann, H. Steen, and O. Dössel, "Simulation of the contraction of the ventricles in a human heart model including atria and pericardium: Finite element analysis of a frictionless contact problem," *Biomech. Model. Mechanobiol.*, vol. 13, no. 3, pp. 627–641, 2014, doi: 10.1007/s10237-013-0523-y.

[93] H. Gao, L. Feng, N. Qi, C. Berry, B. E. Griffith, and X. Luo, "A coupled mitral valve—left ventricle model with fluid–structure interaction," *Med. Eng. Phys.*, vol. 47, pp. 128–136, 2017, doi: 10.1016/j.medengphy.2017.06.042.

[94] T. C. Gasser and C. Forsell, "The numerical implementation of invariant-based viscoelastic formulations at finite strains. An anisotropic model for the passive myocardium," *Comput. Methods Appl. Mech. Eng.*, vol. 200, no. 49–52, pp. 3637–3645, 2011, doi: 10.1016/j.cma.2011.08.022.

[95] D. D. Streeter, H. M. Spotnitz, D. P. Patel, J. Ross, and E. H. Sonnenblick, "Fiber orientation in the canine left ventricle during diastole and systole.," *Circ. Res.*, vol. 24, no. 3, pp. 339–347, 1969, doi: 10.1161/01.RES.24.3.339.

[96] P. Clarysse *et al.*, "Human Atlas of the Cardiac Fiber Architecture: Study on a Healthy Population," *IEEE Trans. Med. Imaging*, vol. 31, no. 7, pp. 1436–1447, 2012.

[97] G. A. Holzapfel and R. W. Ogden, "Constitutive modelling of passive myocardium: A structurally based framework for material characterization," *Philos. Trans. R. Soc. A Math. Phys. Eng. Sci.*, vol. 367, no. 1902, pp. 3445–3475, 2009, doi: 10.1098/rsta.2009.0091.

[98] A. F. HUXLEY, “Muscle structure and theories of contraction.,” *Prog. Biophys. Biophys. Chem.*, vol. 7, pp. 255–318, 1957, doi: 10.1016/s0096-4174(18)30128-8.

[99] K. D. Costa, J. W. Holmes, and A. D. McCulloch, “Modelling cardiac mechanical properties,” *Philos. Trans. A. Math. Phys. Eng. Sci.*, vol. 359, no. 1783, pp. 1233–1250, 2001.

[100] H. Watanabe, S. Sugiura, H. Kafuku, and T. Hisada, “Multiphysics simulation of left ventricular filling dynamics using fluid-structure interaction finite element method,” *Biophys. J.*, vol. 87, no. 3, pp. 2074–2085, 2004, doi: 10.1529/biophysj.103.035840.

[101] E. J. Vigmond, M. Hughes, G. Plank, and L. J. Leon, “Computational Tools for Modeling Electrical Activity in Cardiac Tissue,” *J. Electrocardiol.*, vol. 36, no. SUPPL., pp. 69–74, 2003, doi: 10.1016/j.jelectrocard.2003.09.017.

[102] S. Krishnamoorthi *et al.*, “Simulation methods and validation criteria for modeling cardiac ventricular electrophysiology,” *PLoS One*, vol. 9, no. 12, pp. 1–29, 2014, doi: 10.1371/journal.pone.0114494.

[103] D. DiFrancesco and D. Noble, “A model of cardiac electrical activity incorporating ionic pumps and concentration changes.,” *Philos. Trans. R. Soc. Lond. B. Biol. Sci.*, vol. 307, no. 1133, pp. 353–398, 1985, doi: 10.1098/rstb.1985.0001.

[104] Y. Wang and J. A. Hill, “Electrophysiological remodeling in heart failure,” *J. Mol. Cell. Cardiol.*, vol. 48, no. 4, pp. 619–632, 2010, doi: 10.1016/j.yjmcc.2010.01.009.

[105] A. C. Rankin and A. J. Workman, “Rate control in atrial fibrillation: Role of atrial inputs to the AV node,” *Cardiovasc. Res.*, vol. 44, no. 2, pp. 249–251, 1999, doi: 10.1016/S0008-6363(99)00248-5.

[106] G. Goos, J. Hartmanis, and J. Leeuwen, *Lecture Notes in Computer Science*, vol. 1716. 1999.

[107] S. Elia, P. Lamberti, and V. Tucci, “A Finite Element Model for The Axon of Nervous Cells,” *COMSOL Eur. Conf.*, pp. 1–7, 2009, [Online]. Available: http://www.comsol.fi/papers/6735/download/Elia.pdf.

[108] Y. Saeki, S. Kurihara, K. Komukai, T. Ishikawa, and K. Takigiku, “Dynamic relations

among length, tension, and intracellular Ca2+ in activated ferret papillary muscles," *Am. J. Physiol. - Hear. Circ. Physiol.*, vol. 275, no. 6 44-6, pp. 1957–1962, 1998, doi: 10.1152/ajpheart.1998.275.6.h1957.

[109] L. O. F. Muscle, "The heat of shortening and the dynamic constants of muscle," *Proc. R. Soc. London. Ser. B - Biol. Sci.*, vol. 126, no. 843, pp. 136–195, 1938, doi: 10.1098/rspb.1938.0050.

[110] R. Avazmohammadi, J. S. Soares, D. S. Li, S. S. Raut, R. C. Gorman, and M. S. Sacks, "A Contemporary Look at Biomechanical Models of Myocardium," *Annu. Rev. Biomed. Eng.*, vol. 21, pp. 417–442, 2019, doi: 10.1146/annurev-bioeng-062117-121129.

Appendices

Table A1: Parameter and initial variable values for electrophysiology formulations.

Several parameters do not have physiological meaning as the formulations are merely phenomenological-type.

Parameter	Values	Description
Cm	0.01 F m^{-2}	Membrane capacitance
σ_f	2 S m^{-1}	Electrical conductivity along $\hat{F}$ direction. This is set to ensure that myocardial activation is within the limit of normal QRS duration (80-120 ms) (Guyton and Hall, 2006).
k_1	8	Based on Nash and Panfilov (2004)
k_2	1 F $m^{-2}s^{-1}$	Based on Nash and Panfilov (2004) for myocardium
A	0.1 V	Based on Nash and Panfilov (2004)
B	0.08 V	Based on Nash and Panfilov (2004)
a	0.12	At epicardium
	0.07	At endocardium
ε_0	0.2 s^{-1}	Based on Nash and Panfilov (2004)
μ_1	20 s^{-1}	Based on Nash and Panfilov (2004)
μ_2	0.3	Based on Nash and Panfilov (2004) for myocardium
T_on	500[ms]	
T_dur	2[ms]	
I_stim	100[A/m^{-3}]	
Initial values		
V	-0.08V	Membrane potential

R	0.02	Recovery variable

Table A2: Parameter and initial variable values for the active stress formulations. Several parameters do not have physiological meaning as the formulations are merely phenomenological-type.

Parameter	Value
ε_0	$28s^{-1}$
ε_∞	$5.7\ s^{-1}$
ξ	$7.6V^{-1}$
A	0.1V
B	-0.08V
$V_{Threshold}$	-0.03 V
k_{Ta}	135kPa
Initial Values	
Ta	0kPa

Table A3: Windekessel parameter.

Parameter	Values
R_o	$0.06[mmHg*s/cm^3]$
Cs	$2.75[cm^3/mmHg]$
Rs	$1[mmHg*s/cm^3]$
R_{in}	$0.001[mmHg*s/cm^3]$
Pr	10[mmHg]